UNIVERSITÀ
DI PAVIA

Dipartimento di Biologia e Biotecnologie

Dysfunctional mitochondria in CPVT: the path to a new treatment?

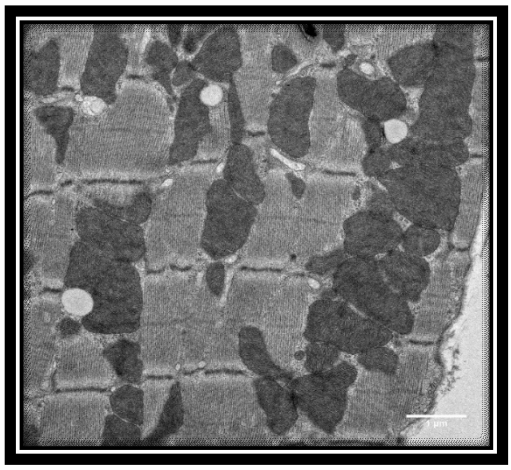

Francesca La Rosa

Dottorato di Ricerca in
Genetica, Biologia Molecolare e Cellulare
Ciclo XXXV – A.A. 2019-2022

UNIVERSITA' DEGLI STUDI DI PAVIA

Dipartimento di Biologia e Biotecnologie

"L. Spallanzani"

Dysfunctional mitochondria in CPVT: the path to a new treatment?

Francesca La Rosa

Supervised by

Prof. Silvia Giuliana Priori

Dottorato di Ricerca in

Genetica, Biologia Molecolare e Cellulare

XXXV Ciclo – A.A. 2019-2022

Table of Contents

ABSTRACT **1**

ABBREVIATIONS **5**

1. INTRODUCTION **11**

1.1 HEART **11**

1.2 CARDIAC MUSCLE CELLS **12**

1.3 **HEART'S BEHAVIOR AND EXCITATION-CONTRACTION COUPLING** **14**

1.4 THE CARDIAC CA^{2+}-RELEASE UNIT **15**

1.4.1 Ryanodine receptor (RyR) *15*

1.4.2 Calsequestrin (CASQ2) *18*

1.5 HEART MODULATION **19**

1.6 ABNORMAL ACTION POTENTIALS DRIVE PATHOLOGIC HEART BEHAVIOURS **21**

1.7 MITOCHONDRIAL STRUCTURE **23**

1.8 MITOCHONDRIA IN CARDIAC METABOLISM **26**

1.9 THE CARDIAC MITOCHONDRIAL CA^{2+} UNIT **27**

1.9.1 Voltage-Dependent Anion Channels (VDACs) *29*

1.9.2 Mitochondrial Ca^{2+} uniporter (MCU) *31*

1.10 MITOCHONDIAL INVOLVEMENT IN CPVT **34**

1.11 CATECHOLAMINERGIC POLYMORPHIC VENTRICULAR TACHYCARDIA (CPVT) **36**

1.11.1 Clinical features *39*

1.11.2 Therapy *41*

2. AIM **43**

3. MATERIAL AND METHODS 45

3.1 ANIMAL STUDIES 45

3.1.1 Animal model 45

3.1.2 Genotyping 45

3.1.3 Isolation of adult mice cardiomyocytes 46

3.1.4 Confocal ROS measurement 47

3.1.5 Mitochondrial free Ca^{2+} 47

3.1.6 Mitochondrial membrane potential measurement 48

3.1.7 Glycolysis measurement 48

3.1.8 ROS Citometry analysis 49

3.1.9 Mitotempo treatment 49

3.1.10 RyR2 immunoprecipitation and immunoblotting from isolated cardiomyocytes 49

3.1.11 Mitochodrial Isolation 50

3.1.12 Electron Transport Chain complexes activity measurement 50

3.1.13 Mitochondrial respiration 51

3.1.14 Fatty acid oxidation measurement 51

3.1.15 Measurement of total and soluble mitochondrial Ca2+ content 51

3.1.16 Telemetry implant and ECG monitoring 51

3.1.17 ATP content 52

3.2 MICROSCOPY 52

3.2.1 Electron Microscopy 52

3.2.2 Confocal Microscopy 53

3.3 CREATION OF RNA INTERFERENCE MOLECULES 53

3.3.1 election of target oligonucleotides 53

3.3.2 Annealing 53

3.3.3 Ligation 54

3.3.5 Bacterial strains and transformation 54

3.3.6 DNA extraction from bacterial cells 54

3.3.7 Miniprep DNA purification system 55

3.3.8 Midiprep DNA purification system 55

3.3.9 Megaprep DNA purification system 56

3.3.10 Analytic digestion 56

3.3.11 Agarose gel electrophoresis 56

3.3.12 Sequencing analysis 57

3.3.13 Plasmid insertion in pAAV 2.1 57

3.3.14 Growth and maintenance of C2C12 cell line 57

3.3.15 Transient transfection procedure 58

3.3.16 RNA processing 58

3.3.17 Protein processing 59

3.3.18 Statistical methods 63

4. RESULTS 65

4.1 CONFIRMATION OF STRUCTURAL ABNORMALITIES OF CPVT MITOCHONDRIA 65

4.2 MITOCHONDRIAL PHYSIOLOGY IN CPVT AND POTENTIAL RELATIONSHIP TO MITOCHONDRIAL STRESS AND STRUCTURAL ABNORMALITIES 70

4.2.1 Assessment of Ca^{2+} entry pathways and mitochondrial membrane potential. 70

4.2.2 Measure of mitochondrial free Ca^{2+} levels. 71

4.2.3 Measure of mitochondrial reactive oxygen species (ROS) levels. 75

4.2.4 Assessment of mitochondrial energetics: ATP production, mitochondrial respiration and complexes activities. 82

4.2.5 Evaluation of mitochondrial metabolism 85

4.3 IDENTIFICATION OF THE CHANNELS IMPLICATED IN MITOCHONDRIAL CALCIUM UPTAKE IN CPVT MICE 89

4.3.1 Generation of the miRNA molecule 90

4.3.2 Evaluation of in vitro RNA and proteins silencing by pcDNAmirVDAC2_544 on C2C12 cell line 91

4.3.3 Cloning in pAAV2.1 91

4.3.4 Evaluation of RNA and proteins silencing by pAAV2.1_CMV-GFP-mirVDAC2_544-TKpolyA on C2C12 cell line 92

4.3.5 In vivo screening results 92

4.3.6 Mitochondrial Ca^{2+} evaluation 95

4.3.7 Mitochondrial reactive oxygen species (ROS) levels in pAAV2.1_CMV-GFP-mirVDAC2_544-TKpolyA infected mice 97

5. DISCUSSION 100

REFERENCES 106

Abstract

Introduction: Catecholaminergic Polymorphic Ventricular Tachycardia (CPVT) is an inherited arrhythmogenic disease characterized by polymorphic ventricular tachycardia in a structurally intact heart induced by physical and/or emotional stress that may end up with syncope, seizures, and cardiovascular collapse [1] . Catecholaminergic polymorphic ventricular tachycardia belongs to a group of inheritable disorders referred to as ‘‘channelopathies’’, caused by mutations in genes coding for channel-proteins that regulate cardiac electrical function [2].
The average onset for CPVT is generally around the12th year of age. At basal state CPVT, patients do not show altered electrocardiogram records even though some authors reported a tendency of the heart to go under sinus bradycardia [3, 4]. The hallmark sign of CPVT, highly specific but not present in all patients, is a peculiar form of polymorphic VT, characterized by a 180° beat-to-beat rotation of the ectopic QRS complexes, that is therefore termed ‘‘bidirectional’’ [2] but more recent observations also evidenced as some patients also present irregular polymorphic VTs.

This disease is connected with non-physiological control of the coupling of Ca^{2+} release from the SR, activation of sarcomere contraction, and Ca^{2+} reuptake into the SR during relaxation [5]. The dominant form of CPVT is caused by mutations in the Ryanodine Receptor (*RYR2*) gene that encodes a large 560 KDa protein that forms a homotetrameric ion channel localized in the membrane of the junctional sarcoplasmic reticulum (jSR). RyR2 (Ryanodine Receptor type 2 protein) channels face the L-type Ca^{2+} channels (Cav1.2), which are positioned in specialized invaginations of the cellular membrane called transverse tubules (TT): influx of Ca^{2+} through these channels triggers RyR2-mediated Ca^{2+} release from the sarcoplasmic reticulum (SR), eliciting contraction of the heart. In normal myocytes, sympathetic activation promotes phosphorylation of RyR2 and increases Ca^{2+} release from the SR, whereas, in the presence of RYR2 gain-of-function mutations, in addition to the physiological response, adrenergic activation also elicits spontaneous diastolic Ca^{2+} release. In response to the increase in cytosolic Ca^{2+}, the Na^{+}/Ca^{2+} exchanger extrudes 1 Ca^{2+} ion for 3 Na^{+} ions; this electrogenic stoichiometry generates delayed afterdepolarizations (DADs) that depolarize cardiac cells and precipitate triggered arrhythmias.

Aim of The Work: The design of our study stems from the two studies performed on our CPVT mouse model carrying the gain-of-function mutation R4496C. Firstly, in 2017 [6] we showed that our model presents mitochondrial abnormalities and that RNA-interference that targets the mutant allele in CPVT mice, abolishes arrhythmias and blunts the development of mitochondrial abnormalities. Secondly, it was demonstrated that

pharmacological activation of mitochondrial Ca^{2+} uptake was successful in reducing the incidence of cardiac arrhythmias in our model [7]. These observations support our main hypothesis, which is that severe RyR2 mutations combined with exposure to environmental factors that increase cardiac workload may exacerbate Ca2+ release from SR, promote mitochondrial Ca2+uptake, which led to impaired mitochondrial function and contractile dysfunction. We therefore set out to extensively characterize the mitochondrial dysfunction and the molecular mechanisms underlying the damage and their contribution to the CPVT phenotype.

Materials and Methods: To evaluate mitochondrial physiology in our mouse model we subjected the R4496C mutant mice and their WT counterparts to two conditions prior to any experiment: (a) baseline condition or (b) the so-called "*adrenergic* a*ctivation*", obtained by delivering Norepinephrine and Caffeine since this is the standard approach to elicit arrhythmias in genetically modified mice with dominant CPVT. This pharmacologic challenge triggers abnormal diastolic calcium release from $RyR2^{R4496C/WT}$ mice but not from WT animals leading to arrhythmic events. In the experiments, mice were sacrificed 15 minutes post-administration of Norepinephrine and Caffeine.

Results: We first performed a more in-depth study of mitochondrial structure through the analysis of electron microscopy images and found that upon adrenergic stimulation there is a marked increase in mitochondrial fission in our model. These data are confirmed by Western Blot analysis of the major fusion/fission factors. We then corroborated our main hypothesis by proving that in our R4496C mice mitochondria uptake a greater quantity of the cytosolic calcium released by the "leaky" RyR2s both in baseline condition and upon adrenergic stimulation. Subsequently, we evaluated the changes in mitochondrial physiology that this increase in calcium might cause. We saw a reduction in mitochondrial respiration in the baseline condition, probably as an adaptation of the system to high calcium levels, which is overridden by acute and intense adrenergic activation. This decrease in respiration is accompanied by a hyperpolarization of the mitochondrial membrane potential and a greater reliance on glucose as a metabolic substrate. In the adrenergically activated condition, the catecholamine stimulus forces an increase in respiration and fatty acid beta-oxidation, as it is a more efficient process. This burst of mitochondrial activity however causes a greater release of ROS, which oxidize RyR2 channels making them more susceptible to activation and therefore "leakier". This creates a negative vicious proarrhythmic cycle in which mutated RyR2 releases extra calcium that induces ROS production, which themselves oxidize RyR2 further exacerbating the leak.

In order to prove that the event responsible for the mitochondrial alterations we observe is the excess in mitochondrial Ca^{2+} deriving from aberrant Ca^{2+} leak from the SR, we decided to create a silencing molecule targeting mitochondrial outer membrane channel VDAC2, which is responsible for Ca^{2+} uptake by mitochondria. We were able to document that VDAC2 is one of the main mediators, although not the only, of the buffering activity that mitochondria exert on cytosolic Ca^{2+} released in CPVT settings. Indeed, myocytes with VDAC2 knockdown presented lower mitochondrial Ca^{2+} levels (that returns to almost physiological levels) and lower mito-ROS production when compared to $RyR2^{R4496C/WT}$ non-treated animals.

Discussion: We were able to prove that in CPVT mitochondria act as a calcium buffer and that the forced uptake induces major changes in their structure and physiology. We also demonstrated the crucial role VDAC2 plays in mitochondrial calcium homeostasis and that its silencing in a CPVT context is able to partially restore mitochondrial physiology. Further studies are necessary to better elucidate the molecular pathways involved.

Abbreviations

3'UTR: 3' untranslated

3D: three-dimensional

AAV9: Adeno-associated viral vector serotype 9

AdV: Adenovirus

AP: Action potential

ATP: Adenosine triphosphate

AV: Aortic valve

BSA: Bovine serum albumin

bpm: Beats per minute

$Ca^{2+:}$ Calcium

CALM1: Calmodulin 1

CaMKII: Protein Kinase 2 Calmodulin-dependent

CASQ2: Calsequestrin 2

CICR: Calcium Induced Calcium Release

CMV: Cytomegalovirus

CPVT: Catecholaminergic polymorphic ventricular tachycardia

CRUs: Calcium release units

cryo-EM: Cryo-electron microscopy

CTD: C-terminal domain

DADs: Delayed afterdepolarization

DMSO: Dimethyl sulfoxide

Drp1: Dynamin-related Protein 1

ds: Double stranded

dsRNA: Double-stranded RNA

DTT: Dithiothreitol

EADs: Early afterdepolarizations

EC: Excitation-contraction

ECC: Excitation-contraction coupling

ER: endoplasmic reticulum

ETC: Electron transport chain

FKBP: Peptitdil-prolil isomerase FKBP 12.6 KDa

GAPDH: Glyceraldehyde 3-phosphate dehydrogenase

GFP: Green fluorescence protein

HD: Helical domain

HET: hetero

HK II: Hexokinase 2

ICD: Implantable cardioverter defibrillator

IMM: Inner mitochondrial membrane

IMS: Intermembrane space

IFM: Interfibrillar mitochondria

IF: Immunofluorescence

IP: intraperitoneal injection

IP3: Inositol 1,4,5-trisphosphate

ITRs: Inverted terminal repeats

IVF: Idiopathic ventricular fibrillation

JNT: Junctin

JSR: junctional Sarcoplasmic Reticulum

kDa: Kilodalton

MCU: Mitochondrial calcium uniporter

MEMMS: MCU-EMRE-MICU1-MICU2 supercomplex

MFN1: Mitofusin 1

MFN2: Mitofusin 2

MICU1: Mitochondrial Ca2+ Uptake 1

MICU2: Mitochondrial Ca2+ Uptake 2

MV: Mitral valve

NCLX: Sodium/calcium exchanger

NCX: Na+/Ca2+ exchanger

NS: not statistically significant

NTD: N-terminal domain

OCR: Oxygen consumption rate

OMM: Outer mitochondrial membrane

OP: Open Probability

Opa1: Mitochondrial dynamin like GTPase

OXPHOS: Oxidative phosphorylation

PBS: Phosphate-Buffered Saline

PCR: Polymerase chain reaction

pDNA: Plasmid DNA

PE: phosphatidylethanolamine

PKA: Protein kinase A

PP1: Phosphatase Protein1

PP2A: Phosphatase Protein 2A

PSNS: Parasympathetic nervous system

PV: Pulmonary valve

PVDF: Polyvinylidene difluoride

qPCR: Quantitative polymerase chain reaction

rAAV: Recombinant AAV

RIRR: ROS-induced ROS release

RISC: RNA-induced silencing complex

RNA Pol II: RNA polymerase II

RNAi: RNA interference

ROI: Region of Interest

ROS: Reactive oxygen species

RyR: Ryanodine Receptor

RyR1: Ryanodine Receptor type 1

RyR2: Ryanodine Receptor type 2

RyR3: Ryanodine Receptor type 3

SCD: Sudden cardiac death

SD: standard deviation

SERCA: Sarco/endoplasmic reticulum Ca2+-ATPase

shRNA: Short hairpin RNA

siRNA: Small interfering RNA

SOD: Superoxide dismutase

SOICR: Store overload¬ induced Ca2+ release

SR: Sarcoplasmic Reticulum

ss: Single stranded

SSM: Subsarcolemmal mitochondria

TBS-T: Tris buffered saline, 0.1% tween

TEM: Transmitted Electron Microscopy

TRDN: Triadin

TV: Tricuspid valve

VDAC: Voltage-dependent anion channel

VT: Ventricular tachycardia

WB: Western Blot

WT: Wild Type

ΔΨmt: Mitochondrial membrane potential

1. Introduction

1.1 Heart

The heart is a synchronized double pump crucial for the maintenance of blood circulation [8]. The organ is located at the center of the thorax and is divided into two portions, left and right: the left part pumps blood into the systemic circulation and the right one pumps blood into the pulmonary circuit. Each region is made up of two chambers: the atria (on top) receiving blood from the periphery, and the ventricles (below), that pump the blood out. The right atrium receives venous blood low in oxygen concentration that during diastole reaches the right ventricle, which, during systole, pumps it into the lungs to be oxygenated. Afterward, the oxygenated blood is collected in the left atrium, and then, during diastole, it moves from the left atrium to the left ventricle, from which is pumped to all body compartments. From this description of the heart's behavior and its role in circulation it is understandable how the heart's two sides work as two pumps in series in a closed circuit; meaning that they receive and pump the same amount of blood.

The heart is enclosed by the pericardium, a sac externally made of fibrous tissue and a layer of pericardial fat; while internally is made of two serous layers, the *parietal pericardium* and the *visceral pericardium,* both of which secrete the pericardial fluid that lubricates the heart during its mechanical movement. [9]. The heart itself is composed of three layers:

- Epicardium, covering the heart's external surface, is fused to the visceral pericardium

- Myocardium, representing the heart's muscular region

- Endocardium, covering the chambers' walls

The heart also contains four valves (two on each side) that enable blood circulation (Figure 1.1). On the right side, there is the tricuspid valve (TV) between the right atrium and the right ventricle and the pulmonary valve (PV) between the right ventricle and the pulmonary artery. While on the left side, there is the mitral valve (MV) between the left atrium and the left ventricle and the aortic valve (AV) between the left ventricle and the aorta.

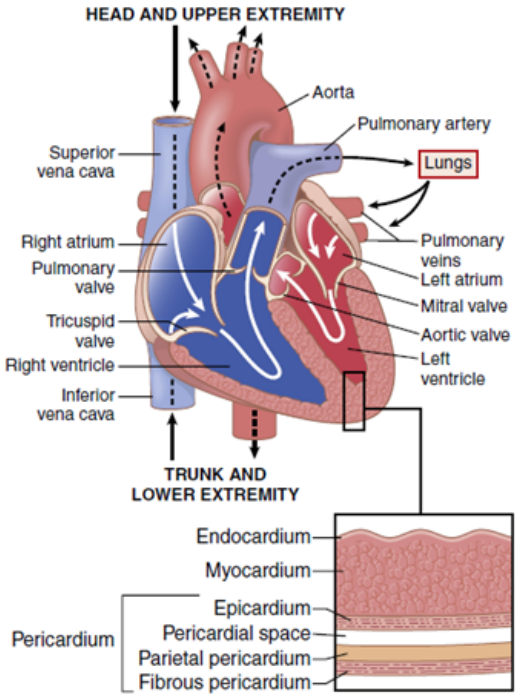

Figure. 1.1 Heart and cardiac cycle. Structure of the heart and course of blood flow through the heart's chambers and valves. The heart consists of multiple layers, including the inner endocardium, myocardium, and the epicardium and pericardium layers. [10]

1.2 Cardiac muscle cells

Cardiac muscle cells (cardiomyocytes) are specialized striated muscle cells making up the heart's myocardium. They are relatively short, branched fibers (10-20 µm of diameter and 50-100 µm in length), typically bi-nucleated cells, tightly in contact through the intercalated discs (specialized cell-cell junctions that form strong mechanical linkages) [11]. The components of the aforementioned cell-cell junctions are the desmosomes, which tightly join cells together, and the gap junctions, which are pores that reduce internal electrical resistance forming both mechanical and electrical (ionic) coupling [12],[13]. Cardiomyocytes comprise only approximately 25% of the total number of cells in the heart, but since their size is considerably greater than that of the intervening cells, they account for more than 90% of the myocardium's volume. Their cell membrane (sarcolemma) features deep invaginations called T-tubules that project into the cell, increasing the contact surface with the extra-cellular environment and thus facilitating

rapid conduction of calcium influx and contractile signals. Given their tremendous energy demands, cardiac muscle cells contain more mitochondria, both subsarcolemmal and interfibrillar, than skeletal muscle cells (approximately 23% of the cell volume vs. 2-10%), reflecting the almost complete dependence of cardiac muscle on aerobic metabolism.

Cardiac myocytes can be either pacemaker or non-pacemaker cells. The main feature of pacemaker cells is that they are able to generate regular spontaneous action potentials. Cells belonging to this class are the sinoatrial, the atrioventricular nodes, and the cells composing the first portion of His bundle [14]. These cells are responsible for the myogenicity of the tissue, in fact, the heartbeat is an intrinsic cellular characteristic, and no external signals are needed for its generation. Non-pacemaker cells (atria, ventricles and Purkinje cells) have a resting membrane potential of -90 mV and contrary to the pacemaker cells, in physiological conditions, these cells are not able to spontaneously depolarize [15]. In order to generate an action potential, they need to undergo an initial small depolarization that lowers the membrane potential to values around -70 mV and activates the sodium channels. This is normally ensured by the conduction of the spontaneous depolarizations that take place in the sinus node, from which they are conducted to the neighbouring atrial cells that develop action potential.

Basic cytological features of the cardiac muscle are similar to those of skeletal muscle cells and include an extensive myofibrillar structure made of parallel interdigitating thick and thin filaments: myosin and actin respectively (referred to as “contractile proteins”). These filaments are arranged in serial units called sarcomeres, which are responsible for the mechanical process of shortening and tension development. These contractile morphological and functional units are typically visualized as transverse striations: the I band, composed of solely thin filaments; the A band where both filaments are present; the H zone, made of only myosin fibers and lastly, the Z line, where the actin filaments are attached. The sliding of the thin filaments on the thick ones allows for the shortening of the sarcomere and therefore contraction. (Figure 1.2). Cardiac cells contain regions of the reticulum that are associated with the membrane, but they lack the terminal cisternae and central fenestrated cisternae, which are replaced by longitudinal tubes that, through extroversions that face the T-tubules, in the Z-lines area, form the so-called “dyads”. These portions are called the junctional sarcoplasmic reticulum [16].

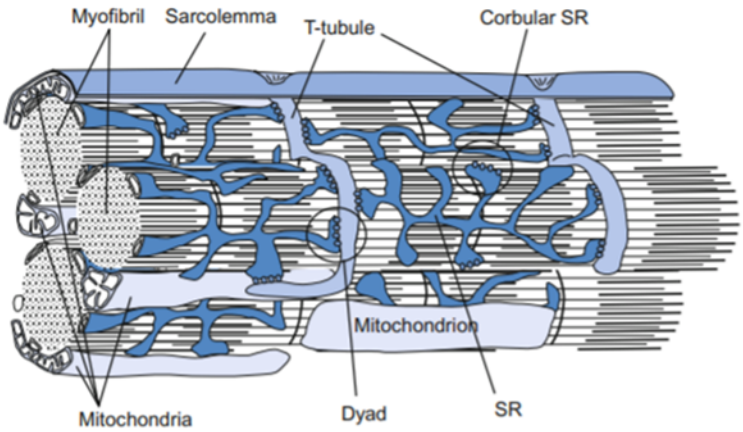

Figure. 1.2 Arrangement of T-tubules and SR in ventricular cardiomyocytes. The sarcolemma invaginates to form T-tubules at the level of the Z lines. The SR forms dyad junctions with the T-tubule. Cardiac SR also forms junctions with the peripheral sarcolemma and has regions called corbular SR that contain junctional proteins without forming a junction with the T-tubule or the sarcolemma. [17]

1.3 Heart's behavior and Excitation-Contraction coupling

The heart's physiological behavior of contraction relies on the process of excitation-contraction (EC) coupling, the mechanism of converting an electrical stimulus into a mechanical response. The fundamental process in muscle physiology of coupling between the electrical stimulus from the action potential and contraction of the cardiac fibers is made possible through the influx and efflux of calcium from the Sarcoplasmic Reticulum (SR). The SR is the dedicated intracellular storage site of Ca^{2+}in cardiac cells. In a general overview, the cell membrane depolarizes to generate an action potential which results in an increase of the cytosolic calcium, called "calcium transient" resulting in the activation of calcium-sensitive contractile proteins such as myosin and actin, which cause cell shortening (contraction) in an ATP-dependent manner.

E–C coupling depends on this close association between the SR network and t-tubule membranes. The junctional SR makes close contact with the t-tubule membrane so that RyRs on the SR are very closely opposed to L-type Ca^{2+} channels on the t-tubule, thus forming the cardiac "dyad", which is fundamental to the processes of initiating the systolic Ca^{2+} transient. The close association between the t-tubule and SR ensures the synchronous rise of Ca^{2+} during systole.[18]

A crucial dogma in the heart's physiology is that in the steady state the Ca^{2+} influx into the cell must be equal to the efflux and that the amount of Ca^{2+} released from the SR must equal the amount uptaken. The Ca^{2+} that activates cardiac contraction comes from two sources: the plasmalemmal voltage-dependent L-type Ca^{2+} channels, that allow the entrance of Ca^{2+} from the extracellular fluid, and the release of SR' Ca^{2+} through RyR2. The main participants in the removal of Ca^{2+} from the cytosol (a process required for muscle relaxation) are the Na^{+}- Ca^{2+} exchanger, a membrane anti-transporter that couples the influx of three sodium ions with the efflux of one calcium ion and is responsible for pumping out of the cell the free Ca^{2+}, and the Ca^{2+} -ATPase located in the SR membrane (SERCA2) responsible for Ca^{2+} reuptake into the SR. The extracellular Ca^{2+} entering through the L-type Ca^{2+} channels binds to and activates RyR2. Once RyR2s open, a greater amount of Ca^{2+} is released, leading to the activation of contractile proteins. This mechanism is known as Ca^{2+} -induced Ca^{2+} release (CICR) [19]. The free Ca^{2+} increased in the cytoplasm binds to troponin, opening the myosin binding sites on filamentous actin, and then force is produced.

1.4 The cardiac Ca^{2+}-release unit

Calcium release units (CRUs) are made of specialized junctional domains of the sarcoplasmic reticulum (jSR). The CRUs main components are the L-type channel of plasmalemma/T-tubules, the Ryanodine Receptor type 2 (RyR2) of the jSR, Triadin (TRDN), and Junctin (JCN), two components of the jSR membrane, Calsequestrin (CASQ), the internal calcium-binding protein, and SERCA Ca^{2+}-ATPase. Their involvement in the maintenance and functioning of the sarcoplasmic reticulum influences calcium sorting. Calcium release via RyRs from the SR of cardiac muscle is part of the excitation-contraction (EC) coupling process. Among the CRU proteins, RyR2, TRDN, JCN, and cardiac CASQ2 build a protein complex located at the junctional elements of the sarcoplasmic reticulum. Further, useful dissection of the system involves the concept of "couplon" [20];[21]. A couplon is the functional grouping of RyRs and L-type Ca^{2+} channels (and other junctional SR proteins), which may act in concert during EC coupling. According to this definition, dyads, the junctions between the jSR and T-tubules, are constituted of a single couplon. The junctions between jSR and plasmalemma/T-tubules function as discrete calcium release units and are sites at which calcium sparks are detected [22].

1.4.1 Ryanodine receptor (RyR)

The Ryanodine Receptor (RyR) is a protein channel localized in the SR membrane responsible for Ca^{2+} release. RyR belongs to a superfamily of ligand-gated intracellular cation channels, similarly to the evolutionarily and structurally related sequence homologous inositol 1,4,5-trisphosphate (IP3) receptor. RyR can be found either alone

(in skeletal and cardiac muscle) or associated with the IP3 receptors in the endoplasmic reticulum (ER) membrane of smooth muscle and non-muscle cells (including neurons and lymphocytes). The >2000 kDa RyR homotetramer is the largest ion channel protein identified to this day. The amino acids sequence composing the Ryanodine Receptor has been deduced in 1989 by cloning and sequencing its complementary DNA [23]. Three isoforms of RyR were identified and they differ mainly based on their location: Ryanodine Receptor type1 (RyR1) is mainly expressed at the skeletal muscle level, Ryanodine Receptor type2 (RyR2) is mainly expressed in the cardiac tissue and Ryanodine Receptor type3 (RyR3), the least studied isoform, is found in different cell types, such as neurons. There is a strong sequence and structural homology between the isoforms: 66% between RyR1 and RyR2; 67% between RyR1 and RyR3; 70% between RyR2 and RyR3 ([23]; [24]). RyR1's structure was resolved by cryo-electron microscopy (cryo-EM) with a resolution of 6.1 Å in 2014 [25].

The cardiac isoform is characterized by a high molecular weight of 565 KDa, is composed of 4967 amino acids, and is codified by a gene localized on chromosome 1 (1q42-q43) [26]. The functional channel is composed of four subunits, which form a homotetrameric complex of 2.2 MDa. In 2017 Dhinwal et al. determined the three-dimensional (3D) structure of rabbit RyR2 in complex with the regulatory protein FKPB12.6 in the closed state at 11.8 Å resolution by cryo-EM. Subsequently, they built an atomic model of the protein based on the cryo-EM atomic structure and fragments of both RyR1 and 2 obtained by x-ray crystallography [27].

The RyR2 N-terminal domain (NTD) is composed of three subdomains: NTDa, NTDb, and NTDc, following these, the protein folds into three homologous domains SPRY1, SPRY2, and SPRY3. There is a domain in this region called RyR repeat 1-2 (or P1) located between SPRY1 and SPRY2. After SPRY3 there are the Handle domain and two helical domains (HD1 and HD2). The second RyR repeat sequence, called RyR repeat 3-4 (or P2), is instead situated between HD1 and HD2. The latter is followed by two subdomains: the EF-hand and the U-motif. Next, the sequence forms the transmembrane region, made of six transmembrane helices, even if the structure of the transmembrane region was unresolved in this context, the VSC domain, and the inner helices were visible. Next to the six helices, the C-terminal region re-enters the cytoplasmic region forming a globular C-terminal domain (CTD). The overall structure of RyR2 could be divided into a three-tier structure: The N-terminus, which forms a large cytoplasmic scaffold, a central domain, and a C-terminus region that forms the channel domain spanning the membrane of the sarcoplasmic reticulum. RyR2 interacts with many accessory proteins, forming the RyR2 interactome, which globally constitutes two macromolecular complexes: one localized in the SR membrane at the C-terminal of the protein (Junctin, Triadin, Calsequestrin) and the second in RyR2 cytosolic portion, at the N-terminal of the protein (Calmodulin, Phosphatase Protein1, Phosphatase Protein 2, Protein Kinase A, Protein Kinase 2 Calmodulin-dependent, Calcineurin, and A and B isoform of Protein Kinase C)

[28] (Figure 1.3).

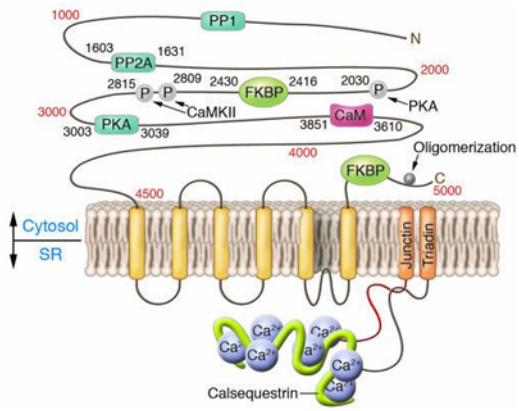

Figure 1.3. The structure of Ryanodine Receptor type 2 and its principal interactions. Calmodulin; PP1, Phosphatase Protein1; PP2A Phosphatase Protein 2A; PKA, Protein Kinase A; CaMKII, Protein Kinase 2 Calmodulin-dependent; FKBP, Peptitdil-prolil isomerase FKBP 12.6 [29].

RyR2 channels have a low "background" activity at rest, meaning during diastole, which leads to the Ca^{2+} "leak" from the SR at rest. This is influenced either by RyR2 associated proteins or covalent modifications, such as phosphorylation. A major effect of Ca^{2+} leak is the decrease of the SR Ca^{2+} content and hence the amplitude of the calcium transient. In previous studies, it has been discovered that in heart failure, there is an apparent sensitization of RyRs activation by luminal Ca^{2+} [30].

Some RyR2 accessory proteins have been particularly characterized, such as the Peptitdil-prolil isomerase FKBP 12.6 (or Calstabin 2), an endogenous high-affinity allosteric ligand, which binds to the cradle formed by the Handle domain, SPRY1, and SPRY3. The function of FKBP 12.6 is to stabilize the degree of the RyR2 closure, by reducing the flexibility of the HD2, preventing abnormal Ca^{2+} release ([27]; [31];[32]). RyR2 phosphorylation by protein kinase A (PKA) reduces the binding affinity for FKBp12.6, increasing RyR2 open state probability, thus amplifying its calcium release activity [33].

1.4.2 Calsequestrin (CASQ2)

A Ca^{2+}-binding protein associated with the sarcoplasmic reticulum (SR) was identified in the early 1970s [34]. Calsequestrin (CASQ) is present in cardiac, skeletal, and smooth muscle [35]. The "skeletal" isoform of Calsequestrin (CASQ1) is found in fast-twitch skeletal muscle, while the "cardiac" (CASQ2) is expressed in the heart and slow-twitch skeletal muscle; the two isoforms are encoded by two different genes [36].

In different animal species, there is considerable sequence homology between these isoforms, for instance, sequence alignment reveals a 98% homology among rabbit and human skeletal Calsequestrin, while the dog and human cardiac isoforms have 86% homology. This high homology indicates that functional studies on CASQ from one tissue can be extrapolated to other isoforms and other species. An insight into the role of Calsequestrin in cardiac muscle has been obtained from a murine animal model, in which overexpression of cardiac CASQ2 led to the development of severe hypertrophy and heart failure, characterized by impaired Ca^{2+} release from cardiac SR, and decreased Ca^{2+} spark frequency, despite increased Ca^{2+} loading [37]. The over-expression models revealed the integral role that the protein plays in the modulation of Ca^{2+} loading and Ca^{2+} release from the sarcoplasmic reticulum. CASQ is contained entirely within the terminal cisternae but is not itself membrane-associated. It forms a linear polymer as Ca^{2+} concentration increases [38] and electron-microscopic evidence suggests that is polymerized at physiological luminal Ca^{2+} concentrations, which are maintained at about 1mM. The protein undergoes a structural change upon Ca^{2+} binding and also changes its structure during excitation-contraction coupling, after t-tubule depolarization, and before Ca^{2+} release from the SR [39]. The luminal retention of ER proteins depends on the presence of a C-terminal sequence (Lys-Asp-Glu-Leu); however, this motif is absent from all isoforms of Calsequestrin, thus, some other targeting mechanism must exist. Studies suggest that the trafficking of cardiac Calsequestrin occurs with changes in glycosylation and phosphorylation of the protein [40]. CASQ2 has been crystallized and the structure determined with a resolution of 2.4 Å [38] and it was observed that this protein monomer has three identical domains: I, II, and III, each with a topology similar to thioredoxin, with four α-helices, two bordering either side of the core β-sheet structure. The folding and compaction of Calsequestrin depend both on Ca^{2+} presence and ionic strength and it occurs optimally in the presence of Ca^{2+} and K^{+} concentrations close to those in the lumen of the SR in vivo (about 1mM Ca^{2+} and 100mM K^{+}). High-capacity Ca^{2+} binding requires Calsequestrin to be compact, as does the interaction between it and the RyR/Triadin/Junctin complex. Data from CASQ crystals formed with 0.35M Na^{+} suggest that two types of dimers are likely to facilitate polymerization, the first is formed by a "back-to-back" interaction [38], where the C-terminal segments form a negatively charged pocket within the dimer that favors Ca^{2+} binding (Figure 1.5). The second type of dimer forms with "front-to-front" coupling which again generates a negatively charged pocket that supports Ca^{2+} binding and, like the back-to-back dimer, its formation is

thought to be favored by Ca^{2+} binding (Figure 1.4). Polymerization is thought to occur after the formation of the back-to-back dimer, when a further increase in Ca^{2+} induces front-to-front interactions, moreover, salt bridges and hydrophobic interactions between the monomers help stabilize the polymer. Evidence suggests that C-terminal residues (Glu354-Asp367) are responsible for Calsequestrin binding to Triadin. At a luminal Ca^{2+} concentration of 1mM, the polymer is stable and anchored to the SR membrane through Triadin and Junctin. A further increase in Ca^{2+} concentration to ≥10mM results in the dissociation of Calsequestrin from Triadin and Junctin [41].

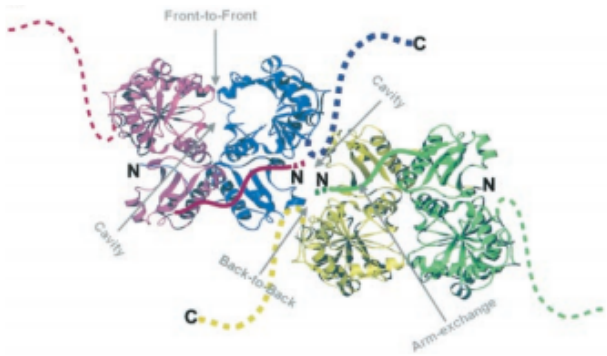

Figure 1.4 Crystal structure of Calsequestrin. Illustration of the interactions between four Calsequestrin molecules, each showing the crystal structure of Calsequestrin from rabbit skeletal muscle SR. Front-to-front interactions are shown between the red and the blue molecule and between the yellow and the green molecule. A back-to-back interaction is shown between the yellow and the blue molecule.

1.5 Heart modulation

Heart rate is the number of heartbeats per unit of time, typically expressed as beats per minute (bpm). The normal heart rate for an adult ranges from 60 to 100 bpm. This is modulated by both nervous and hormonal signals. Three major effects can be elicited from the heart:

- Dromotropic effect: it concerns the conduction speed in the atrioventricular node and subsequently the rate of electrical impulses in the heart [42];

- Chronotropic effect: (from *chrono-*, meaning time) it is related to the heart rate

- Inotropic effect: it is used in reference to the heart's contraction strength.

The sympathetic nervous system (SNS) and parasympathetic nervous system (PSNS) are two divisions of the autonomic nervous system. They can modulate various aspects of the performance of the heart (Figure 1.5). SNS acts positively on all three effects, whereas PSNS has a negative effect on them. However, these opposing influences are not algebraically additive; complicated interactions exist.

The parasympathetic nervous system is mostly distributed at the atrial level. Parasympathetic neurons release the acetylcholine neurotransmitter, which binds the muscarinic receptors on cardiomyocytes [43]. Thus, augmenting membrane permeabilization for potassium ions and decreasing calcium ions conductance. Indeed, the cell will hyperpolarize, the pacemaker potential will start from a more negative value and consequently, more time is needed to reach the threshold level.

SNS neurons are present prevalently in the ventricular myocardium but are also in contact with the sinoatrial node and His bundles. They are involved in catecholaminergic noradrenaline neurotransmitter release, which induces an ionic flow increase via the F-channels and Calcium-channels, through the binding to the β1 adrenergic receptors on the cardiomyocytes. Thus, SNS activation results in an increased heart rate.

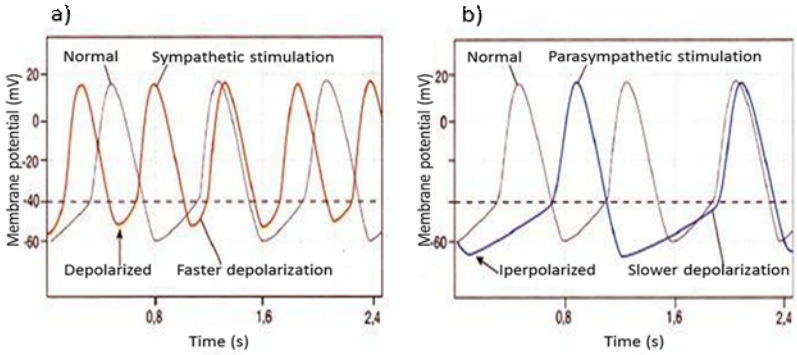

Figure 1.5 Heart rate modulation by the Autonomous Nervous System. a) Sympathetic stimulation (and the circulating adrenaline) depolarizes pacemaker cells increasing the depolarization speed, thus augmenting the heart rate. b) Parasympathetic stimulation hyperpolarizes the membrane potential of pacemaker cells decreasing the depolarization speed, thus lowering heart rate.

1.6 Abnormal action potentials drive pathologic heart behaviours

Normally, the cardiac action potential (AP) that allows the heart's contraction, originates in the sinoatrial node, thanks to pacemaker cardiomyocytes, and is conducted to the atria and ventricles through electrical synapses, the gap junctions. In general, the standard model used to understand the cardiac action potential is that of the ventricular myocyte. The cardiac AP is a hundred milliseconds long and has five distinct phases: from 0 to 4 (Figure 1.6). Phase 0 corresponds to the period of rapid depolarization from the diastolic membrane potential (resting potential). It is produced primarily by the activation of cardiac Na^+ channels with a contribution from cardiac Ca^{2+} channels. Phase 1 is produced by the termination of the depolarizing inward Na^+ current due to inactivation and the concomitant activation of the transient outward K^+ and Na^+/Ca^{2+} exchanger currents. This results in a transient repolarization period. Phase 2 is the long plateau phase of the action potential during which the membrane potential changes very little. This plateau is ensured by the balance of small, but non-inactivated, Na^+ and L-type Ca^{2+} current components and hyperpolarizing K+ currents. In phase 3, reductions of Ca^{2+} and Na^+ and the K^+ increase contribute to the repolarization of the myocyte. Phase 4, finally, corresponds to the diastolic membrane potential [44].

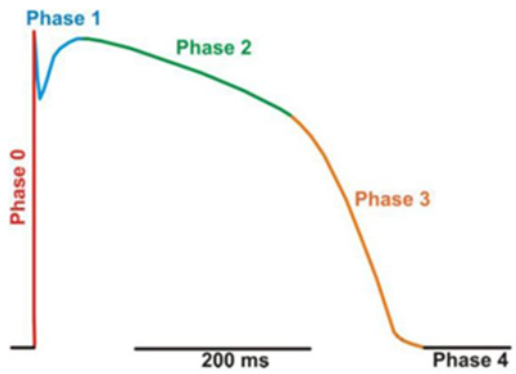

Figure 1.6 A typical action potential (AP) waveform of a healthy adult human ventricular myocyte.

Sometimes abnormal action potentials can occur, especially non -pacemaker cells may undergo spontaneous depolarization either during phase 3 or early in phase 4, triggering

irregular APs. These spontaneous depolarizations, termed afterdepolarization, if of sufficient magnitude, can trigger self-sustaining action potentials resulting in tachycardia. Early afterdepolarizations (EADs) occur during phase 3 and are more likely to do so when action potential durations are prolonged. Because these afterdepolarizations occur at a time when fast Na^+ channel are still inactivated, slow inward Ca^{2+} channels carry the depolarizing current. Delayed afterdepolarizations (DADs) are spontaneous small depolarizations that occur at the end of phase 3 or early in phase 4. They can activate sodium channels triggering action potentials (triggered activity) and cause tachycardia. DADs are associated with excessive accumulation of Ca^{2+} in the SR (Ca^{2+} overload). This overload causes releases of Ca^{2+} from the sarcoplasmic reticulum independently from an action potential (spontaneous Ca^{2+} release). Similarly to the systolic release, RyR2 mediates this spontaneous release. The increment in cytosolic Ca^{2+} produced by the spontaneous release activates the Na^+/Ca^{2+} exchanger that produces the depolarizing current responsible for the membrane depolarization [45]. DADs can occur during ischemia, digitalis toxicity and excessive catecholamine stimulation. Recent studies have demonstrated that DADs also occur in the absence of SR Ca^{2+} overload, in fact, this is what occurs in situations that alter RyR2 and/or CASQ2, such as catecholaminergic polymorphic ventricular tachycardia (CPVT). Alterations of Calsequestrin that lead to CPVT modify the capacity of the protein to buffer calcium in the SR. As consequence the latter is unable to retain Ca^{2+} and develops frequent episodes of spontaneous calcium release that result in DADs and arrhythmias. A condition where ventricular rate is greater than the atrial one, and therefore the frequency of QRS complexes is greater than the frequency of P waves, is termed ventricular tachycardia (100-200 beats/min). The most common causes of ventricular arrhythmias are reentry circuits caused by abnormal impulse conduction within the ventricles or rapidly firing ectopic pacemaker sites located in the ventricles (which may be caused by afterdepolarization). With ventricular arrhythmias, there is a complete dissociation between atrial and ventricular rate [46].

Ventricular fibrillation is seen in the electrocardiogram (ECG) as rapid, low-voltage, uncoordinated depolarization (having no discernible QRS complexes), which results in cardiac output going to zero (Figure 1.7). Another type of arrhythmia is the premature depolarization, which may occur within either the atria (premature atrial complex) or the ventricle (premature ventricular complex). They are usually caused by ectopic pacemaker sites situated in these cardiac regions and appear, in the electrocardiogram, as extra (and early) P waves or QRS-complexes. These premature depolarizations are often abnormally shaped, particularly in ventricles, because the impulse generated by the ectopic site are not conducted through normal pathways.

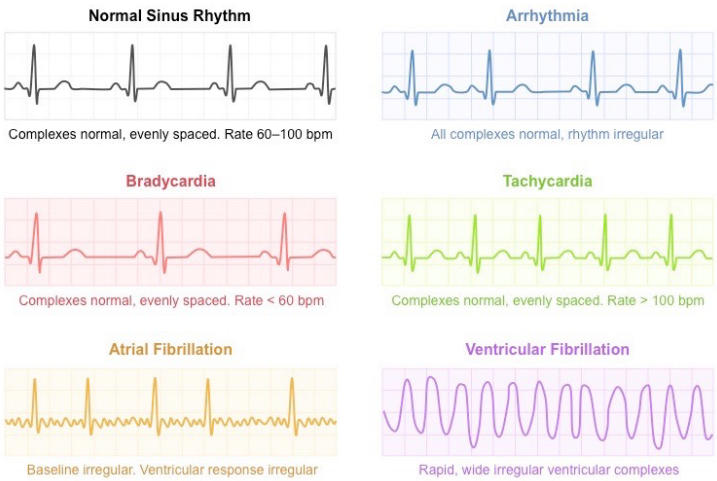

Figure 1.7 ECG examples of abnormal rhythms.

1.7 Mitochondrial structure

It is hypothesized that the mitochondrial formation traces back to an unlikely event over 1.5 billion years ago. To this day, there are two main hypotheses regarding their origin:

- The autogenous hypothesis states that mitochondria derive from a separation of a DNA portion from the nucleus of the eukaryotic cell and that this portion was then enclosed by membranes [47].

- The endosymbiotic hypothesis states that mitochondria were originally prokaryotic cells able to implement oxidative mechanisms. Over time, they became endosymbionts living inside the eukaryote cell [47].

The latter is the most widely accepted hypothesis, since these organelles share many features with bacteria, such as having their own DNA and an uncoupling of their replication from cell division.

The name "mitochondria" derives from two ancient Greek words, *mitos* (thread) and *chondrion* (granule). They appeared small and round (i.e., chondrion) while also being capable of arranging themselves in apparently interconnected threads (i.e., mitos).

Since these very early observations, it has become increasingly clear that mitochondria are in fact highly dynamic organelles that can constantly interchange their morphology. They can exist as either fragmented short mitochondrial rods or spheres or as an elongated and interconnected network.

Mitochondria are surrounded by a double-membrane system consisting of an inner (IMM) and an outer (OMM) mitochondrial membrane separated by an intermembrane space.

The inner membrane can be further divided into the inner boundary membrane and the cristae membrane. The latter is in continuous and close apposition to the outer membrane, with which it forms a kind of envelope. Cristae membranes are invaginations of the inner boundary membrane that protrude deeply into the matrix and enclose the crista space, on their membrane the proteins of the electron-transport chain are found. [48] (Figure. 1.8)

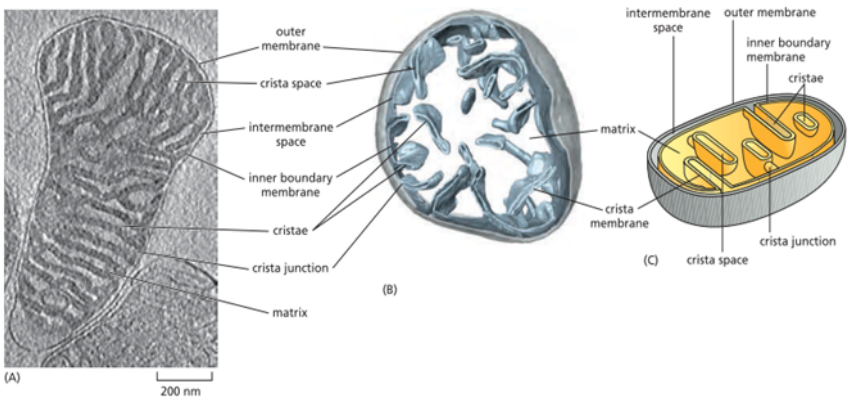

Figure. 1.8 Structure of a mitochondrion. (A) Tomographic slice through a three-dimensional map of a mouse heart mitochondrion determined by electron-microscope tomography. (B) Tomographic surface-rendered portion of a yeast mitochondrion. (C) Schematic drawing of a mitochondrion showing the outer membrane (gray), and the inner membrane (yellow) [49]

The outer mitochondrial membrane is freely permeable to ions and to small molecules (of up to 5000 Daltons) because it contains many porin molecules that create aqueous pores across the membrane. Therefore, the intermembrane space between the outer and inner membranes has the same pH and ionic composition as the cytoplasm, and there is no electrochemical gradient across the outer membrane.

Each of these components plays a distinct functional role, with the matrix and IMM representing the major working compartments of mitochondria. The matrix contains the mitochondrial DNA and the enzymes involved in the oxidative metabolism. The oxidative breakdown of glucose and fatty acids is the principal source of metabolic energy in animal cells.

The inner mitochondrial membrane is a diffusion barrier to ions and small molecules, just like the bacterial inner membrane. However, selected ions, like protons and phosphate, as well as essential metabolites such as ATP and ADP, can pass through it via specific transporter proteins.

The inner mitochondrial membrane is highly differentiated into functionally distinct regions with different protein compositions. The boundary membrane region is thought to contain the machinery necessary for protein import, new membrane insertion, and assembly of the respiratory chain complexes. The internal region, meaning the membranes of the cristae, which is continuous with the boundary membrane, contains the ATP synthase enzymes that produce most of the cell's ATP and the protein complexes of the mitochondrion's electron transport chain, the so-called respiratory chain.

Cristae membranes have one of the highest protein densities of all biological membranes, with a lipid content of 25% and a protein content of 75%. The folding of the inner membrane into cristae greatly increases the membrane's area that is available for oxidative phosphorylation. In highly active cardiac muscle cells, for example, the total area of cristae membranes can be up to 20 times larger than the area of the cell's plasma membrane [50].

Cardiomyocytes require a large and constant energy supply in order to accomplish the work required by the circulatory system; in fact, not surprisingly, mitochondria occupy up to 30% of the cardiac cell's volume and are essential for proper heart function.

Mitochondria provide the vast amounts of energy required for cellular functions, help maintain ion homeostasis, and are the initial site for the synthesis of many key substances such as steroids, iron-containing proteins, and porphyrins. However, they also possess the power to kill the cell. In response to stress they can shut off the energy supply upon which the cell relies, produce vast amounts of toxic oxygen species, and release a series of death-inducing proteins into the cellular environment.

Numerous studies have implicated changes in mitochondrial morphology with changes in cardiac development and heart failure. Other studies have suggested that mitochondrial morphology is interconnected with cardiac differentiation and that mitochondrial dynamics and intracellular calcium can coordinately regulate important developmental pathways [51]. Similarly, there is a growing interest in the role of mitochondrial dynamics in the progression of heart failure and other cardiac pathologies. [52]

1.8 Mitochondria in cardiac metabolism

Mitochondria generate energy in the form of ATP through the complexes of the electron transport chain (ETC). ATP molecules in a significantly minor quantity can also be produced in the cytosol by the process of glycolysis. Under normal physiological conditions, the heart's contraction consumes about 35 kg of ATP per day [53], but greater cardiac energy requirements need to be met under more strenuous conditions such as exercise or chronic stress. The heart mostly oxidizes exogenous substrates because its daily energy demands are greater than the amount of substrates it can store; however, in a lesser amount, it can also utilize internal stores of triglycerides [54]. The leading carbon sources used for energy production in the hart are fatty acids (FA) (~60%) and glucose (~40%). Biochemically, oxidation of glucose is more efficient than the oxidation of FA; however, the ATP yield deriving from FAs such as palmitate is greater than that deriving from glucose (~129 ATP vs. ~36ATP). For this reason, many more molecules of glucose should be oxidized in order to produce the same amount of ATP produced by oxidation of one molecule of palmitate. FA β-oxidation in the mitochondria generates acetyl-CoA (acetyl-CoA is also produced in the mitochondria from pyruvate deriving from glycolysis of glucose). In the mitochondrial matrix, acetyl-CoA enters the TCA cycle and results in the production of NADH and FADH2, which enter the electron transport chain (ETC) for oxidative phosphorylation (OXPHOS) (the ultimate process in mitochondrial respiration). During oxidative phosphorylation, oxygen is reduced to water through sequential redox reactions catalyzed by mitochondrial protein complexes I, II, III and IV.

These reactions generate an electrochemical gradient (ΔØm), which is required by complex V (ATP synthase) to generate ATP from ADP.[55]

As mentioned, in the adult heart, fatty acid oxidation (FAO) is the main fuel employed in the production of ATP. However, alterations in substrate metabolism can occur at different levels in the metabolic pathways, like at the substrate uptake level, during the TCA cycle and/or OXPHOS; they are however, interdependent on each other and involve complex feedback systems. The heart's metabolism is affected by different factors such as stress, availability of metabolites, dietary changes and different energy requirements of the organ itself [56–58]. For example, it was reported that in hypertrophic conditions the main source of energy switches from FA β-oxidation to glycolysis (a reversion to the fetal energy substrate preference pattern). This switch (from FA to carbohydrate metabolism) allows for an improved efficiency of the heart's functioning, as long as glucose is present [59]. Another example can be the complicated effect of adrenergic stimulation on the heart's metabolism, which was shown to both increase fatty acids metabolism and increase glucose uptake and use [60, 61].

1.9 The Cardiac mitochondrial Ca^{2+} unit

The first clear description of the ability of mitochondria to rapidly uptake calcium was reported in the early 1960s, by the work of Vasington, Murphy, De Luca, and Engstrom [62].

Ca^{2+} (intracellular calcium) is one of the most widely used signaling second messengers in living cells. Almost all events that contribute to changes in cell function, including fertilization, muscular contraction, secretion, protein folding, and energy metabolism, are mediated by changes in Ca^{2+} concentrations [63]. Ca^{2+} diffusion throughout the cell is substantially constrained by the complex cytosolic Ca^{2+} chelating apparatus. Furthermore, continuous Ca^{2+} extrusion to the extracellular environment or its uptake by intracellular reservoirs keeps cytosolic Ca^{2+} concentrations low in resting conditions, establishing a gradient for fast Ca^{2+} rise when specific channels are opened due to different stimuli. The creation of localized Ca^{2+} signals, which alter a target protein/organelle's activity with considerable spatiotemporal accuracy, is thereby enabled by this carefully regulated equilibrium.

Ca^{2+} must pass through both the OMM (permeable to ions) and the IMM (impermeable to ions) to enter the mitochondrial matrix. The expression and function of the voltage-dependent anion channel (VDAC) contribute to the OMM's high permeability, allowing the transfer of all energy-related metabolites and ions from the cytosol into the mitochondria. [64].

Ca^{2+} uptake through the IMM is an electrogenic process mediated by a Ca^{2+}-selective ion channel, the mitochondrial Ca^{2+} uniporter (MCU) which has a high affinity for Ca^{2+} and carries it along an electrochemical gradient [65].

In a physiological state, mitochondrial ion efflux must equal mitochondrial ion uptake. Mitochondrial Ca^{2+} efflux is primarily attributed to the function of the Na^{+}- Ca^{2+}-Li^{+} exchanger (NCLX). Studies in permeabilized cardiac myocytes also suggest that mitochondrial Na^{+} is lower than cytosolic Na^{+}. This Na^{+} gradient (lower in the matrix) is used as a driving force to extrude calcium from the matrix via the NCLX. The negative mitochondrial membrane potential (−150 to −180 mV), coupled with the inwardly directed Na^{+} gradients, provides a large driving force for extruding calcium from the mitochondrial matrix [66].

In addition to its roles in oxidative metabolism and ATP generation, mitochondrial Ca^{2+} has a role in cell death initiation and regulation. The intrinsic pathway, which is triggered by either internal cell damage, oxidative stress, or loss of protein homeostasis, and the extrinsic pathway, which is triggered by external cell death stimuli, are the two main routes that cause programmed cell death [67].

Mitochondrial dynamism is essential for healthy cardiac tissue. A shift toward mitochondrial fusion promotes the formation of interconnected and healthier mitochondria, and a shift toward mitochondrial fission could mediate the fragmentation and dysfunctions of mitochondria. It has been established that fission factor dynamin-related protein 1 (DRP1) and fusion factors Mitofusins (MFN1 and MFN2) are important regulators of mitochondrial dynamics [68].

It is generally accepted that when the cells experience oxidative stress, mitochondrial fusion helps repair small amounts of mitochondrial damage, facilitating the complementation among damaged mitochondria and healthier ones. On the other hand, mitochondrial fission could produce new mitochondria and separate the seriously damaged mitochondria that would be then eliminated. [68].

While Ca^{2+} controls mitochondrial fusion/fission and intracellular distribution, mitochondria also buffer local Ca^{2+} elevations and conduct Ca^{2+} currents across the cell. This allows different forms of signaling and the coordination of cellular functions through various metabolic activities. This aspect is especially critical for excitable cells and muscle fibers, which rely on whole-cell Ca^{2+} currents to perform their primary function (muscle contraction) [67].

The fundamental role of mitochondria in meeting changes in energy demand, such as an increased workload or hormonal stimulation, is linked to the close apposition of mitochondria and the major source of Ca^{2+} for contraction, the SR. [67].

1.9.1 Voltage-Dependent Anion Channels (VDACs)

Voltage-Dependent Anion Channels are the most abundant proteins of the OMM and are necessary to exchange solutes between the cytosol and mitochondria.

VDAC channels can be identified in the outer membranes of mitochondria from all eukaryotic kingdoms, yet there is some evidence that they may not be exclusive to the OMM [69]. Kayser et al. (1989) first showed evidence of their existence in the plasma membrane. Subsequently, a few groups supported their expression in plasma membrane while others refuted it [71].

VDACs represent a protein family consisting of three isoforms (VDAC1–3) with roughly a 70% sequence similarity, and a molecular weight of 30–35 kDa [72]. VDAC3 is the oldest isoform, and it is believed that VDAC2 diverged later, followed by VDAC1 [73]. Hence, VDAC2 acts as a bridge between the two isoforms.

The gene encoding the mouse VDAC2 (mVDAC2) isoform is located on chromosome 14 and, unlike VDAC1 or VDAC3, has 10 exons and an additional exon constituting part of the 5'-untranslated regions. VDAC2 spans approximately 14 kb and it encodes for a protein of 295 amino acids.

Schredelseker et al. (2014) were successful in crystallizing zebrafish's VDAC2 refolded in LDAO, a zwitterionic detergent, and they determined its structure at 2.8 Å resolution. The structure of mVDAC2 is similar to that of zebrafish VDAC2.

mVDAC2 forms a β-barrel composed of 19 β-strands with the N-terminal helical region located inside the pore (Figure. 1.9). All the strands exhibit an antiparallel pattern except for strands 1 and 19, which associate in a parallel manner to seal the barrel. The maximal height and width of the β-barrel are 35 and 40 Å, respectively.

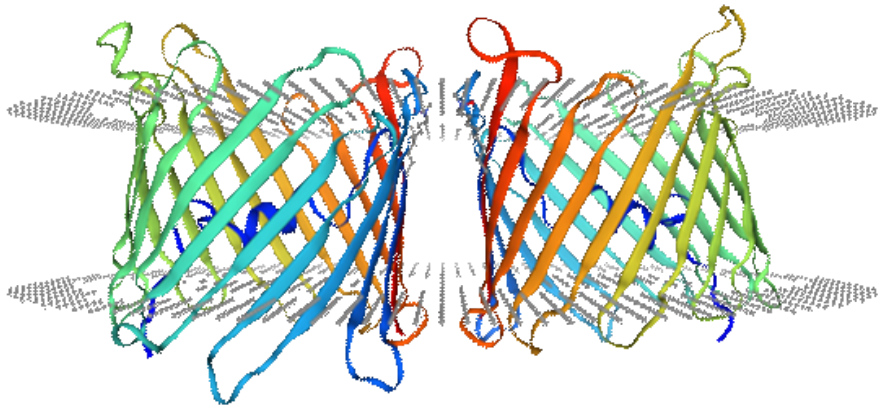

Figure. 1.9 Overall structure of VDAC2. Cartoon representations of VDAC2 dimer viewed perpendicular to the membrane plane. [74]

This channel has a relatively wide pore, with an internal diameter that is estimated to be about 4nm, and is capable of supporting the membrane transport of various substrates, metabolites, negatively and positively charged ions, and even larger molecules (up to 4–6 kDa) [74].

The VDAC channel has a conductance that varies with different voltages and specific ion selectivity, it is stable in a long-lived open state at low voltages (10 mV up to 2 h). When the transmembrane voltage surpasses 20–30 mV, the VDAC channel shifts into a closed state. With increasing voltage, closing events become more often, with some reported variability among the various VDAC isoforms. [75].

VDACs play a key role in calcium homeostasis, by transporting Ca^{2+} from the cytosol to the mitochondria, thus rapidly decreasing cytosolic Ca^{2+} levels. VDAC2 has also been shown to regulate Ca^{2+} homeostasis in cardiac cells [76].

Both the SR and mitochondria in the heart regulate the cytosolic Ca^{2+} transients. The two critical proteins for the functional interaction between the SR and mitochondria in the subsarcolemmal area are RyR2 and VDAC2 (Figure. 1.10). RyR2–VDAC2 interaction is critical for Ca^{2+} transport from the SR to mitochondria, as the SR creates high [Ca^{2+}] microdomains that are required for mitochondrial Ca^{2+} uptake [77].

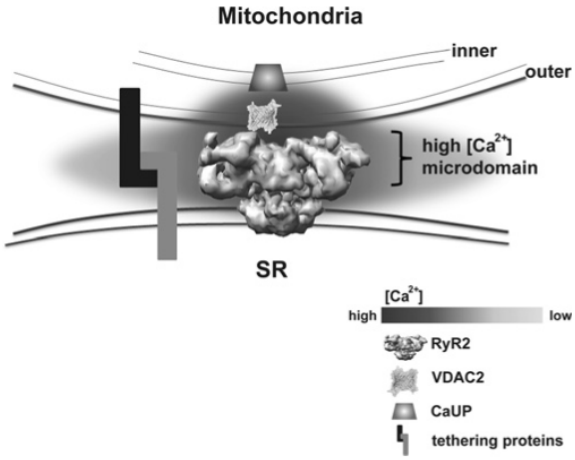

Figure 1.10 Schematic model for the molecular architecture involved in Ca^{2+} transfer from the SR to mitochondria. In cardiomyocytes, tethering molecules at the junction between the SR and mitochondria support the close apposition of the two sub cellular organelles. The physical association of RyR2 and VDAC2 provides the high [Ca^{2+}] microdomain at the junction and facilitates mitochondrial Ca^{2+} uptake. [77]

VDAC2 plays a role in shielding cells against oxidative stress and reactive oxygen species (ROS), either by moving them out of the mitochondria or by inducing apoptosis in oxidatively stressed cells. In reality, superoxide dismutases (SODs) residing in the mitochondrial intermembrane space can neutralize ROS created by the complexes of the electron transport chain inside the mitochondria. In other instances, ROS can be transferred to the cytoplasm and be neutralized by cytosolic SODs. Stress can cause an increase in ROS in mitochondria, affecting the redox state of cytosolic proteins and, as a result, their function. [76].

1.9.2 Mitochondrial Ca^{2+} uniporter (MCU)

Ca^{2+} in order to enter mitochondria must pass through both the OMM and the IMM. The electron transport chain translocates H^+ ions across the IMM, creating a concentration gradient that supplies the electrochemical driving force for Ca^{2+} buildup. Despite the uptake machinery's low Ca^{2+} affinity, cytosolic Ca^{2+} signals are promptly transduced into the mitochondrial matrix in physiological settings. The close proximity of mitochondria to Ca^{2+} hotspots accounts for the process's high efficiency.

Ca^{2+} uptake is mediated by a Ca^{2+} selective ion channel, the mitochondrial Ca^{2+} uniporter (MCU). The gene encoding mouse MCU (mMCU) is located on chromosome 10 and has 10 exons. MCU spans approximately 170 kb and it encodes for a protein of 350 amino acids.

MCU binds and transports Ca^{2+} following the electrochemical gradient, it does not perform its function by itself but cooperating with the mitochondrial Ca^{2+} uniporter complex, which is composed of: MCU; EMRE (Essential MCU Regulator) a regulatory protein; MICU1 and MICU2 (Mitochondrial Ca^{2+} Uptake) that are accessory proteins.

Zhuo et al.,) were successful in determining the structure of the MCU complex, or MEMMS (MCU-EMRE-MICU1-MICU2 supercomplex) as they called it, with a combination of a Titan Krios Cryo-EM and a K2 direct electron detector in super-resolution mode reaching a resolution of 3.3–3.7 Å.

The MCU subunit comprises three structural domains: the transmembrane domain (TMD), the coiled-coil domain (CCD), and the N-terminal domain (NTD). Each MCU domain constitutes two transmembrane helices, TM1 and TM2. The TMD is known to be responsible for the channel's Ca^{2+} selectivity and conduction. MCU's CCD and NTD are found within the mitochondrial matrix. The fundamental structures of MICU1 and MICU2 are quite similar (N-lobe and C-lobe) however, their N-terminal domains and C-terminal helices are distinct. MICU1 and MICU2 both have C-terminal helices that aid in MICU localization to the inner membrane. (Figure 1.11)

MCU tetramerizes in order to produce a Ca^{2+}-conducting pore with the regulatory EMRE proteins attached to the core with a symmetrical axis. MICU1 forms an extensive interacting surface with MCU to seal the pore's intermembrane space, while MICU2 binds to MICU1 from the side without making direct contact with MCU. As a result, the complex has an inverted L shape.

Fan et al., established the cryo-EM structure of the complex in presence of 2 mM Ca^{2+} to better understand how Ca^{2+} activates the channel. In a low Ca^{2+} environment, the O-shaped complex has a V-shaped dimer of MCU–EMRE tetramers with two MICU1–MICU2 heterodimers arching over the top, with the same subunit stoichiometry ratio.

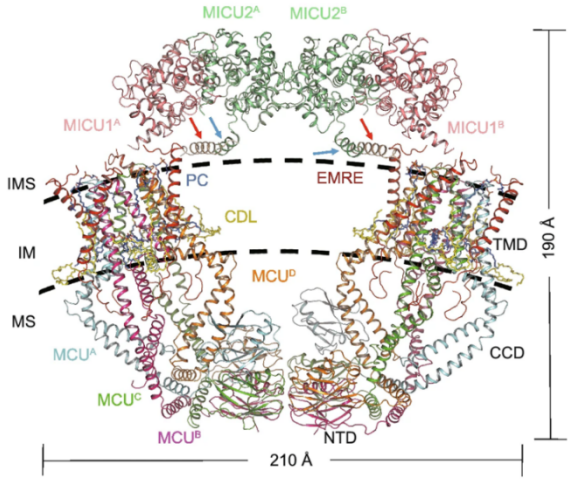

Figure 1.11 Structure of the MCU-EMRE-MICU1-MICU2 supercomplex. Atomic model of the MCU complex. The position of NTD, CCD and TMD of MCU are indicated. PCs, phosphatidylcholines, are shown in marine; CDLs, cardiolipins, are shown in yellow; subunits of MEMMS are differently colored. IMS, intermembrane space; IM, inner membrane; MS, matrix [78]

Fan et al., 2020 show that the MICU1–EMRE interaction helps keeping MICU1 in place in order to seal the MCU pore in low a Ca^{2+}environment. MICU2 does not directly block MCU but it prevents MICU1 dissociation from the complex when Ca^{2+} concentration increases. It is conceivable that EMRE's MICU1-tethering function might allow MICUs to stay close to the pore during Ca^{2+} stimulation in order to rapidly terminate the influx once the Ca^{2+} signal dissipates. (Figure. 1.12)

In this work, they also discovered that the uniporter could dimerize. Such dimerization is not required for the channel's basic function, but it might contribute to a biased uniporter distribution towards either inner- and outer-membrane contact sites, where nearby crista junctions could potentially provide favorable curvature to accommodate the V-shaped dimer.

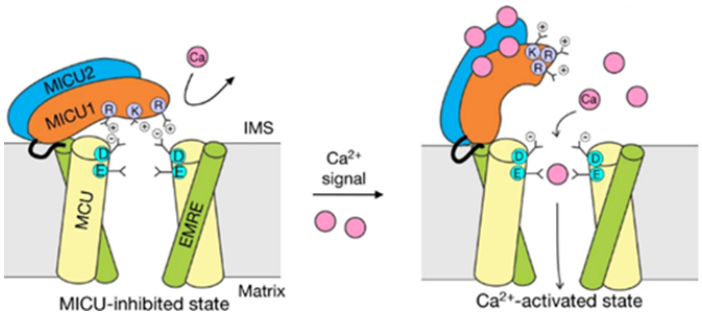

Figure. 1.12 Ca^{2+}-induced MICU conformational changes and the mechanism of complex activation. Molecular model of Ca^{2+} activation of the complex. Only two copies of MCU–EMRE in the tetramer are represented to reveal the Ca^{2+} pathway. Key amino acids are shown in single-letter code. [79]

1.10 Mitochondial involvement in CPVT

A coordinated electrical propagation throughout the heart is necessary for appropriate cardiac function. When such coordination in cardiac action potential fails, cardiac arrhythmias occur. Mitochondria in heart physiology do not contribute uniquely to the energy supply but are also able to modulate key electrophysiological and Ca^{2+} cycling properties, either directly through the activation of mitochondrial ion channels, or indirectly by modulating ATP levels or the redox state.

ATP production is made possible by mitochondrial membrane potential ($\Delta\Psi m$) that generates a proton motive force that liberates the energy necessary to phosphorylate ADP to ATP. This pathway is also one of the main sources of reactive oxygen species (ROS) in the cell. In physiological conditions, $\Delta\Psi m$ is highly regulated so that ATP production responds to the energy demand and ROS do not exceed cell-detoxifying capacity. Alterations of $\Delta\Psi m$ cause a reduction of ATP generation and an increase of ROS production that, once it exceeds the detoxifying capacity, leads to oxidative stress.

Mitochondrial dysfunction as result of Ca^{2+} overload suggests that these organelles can also contribute indirectly to arrhythmogenesis, through ROS production and $\Delta\Psi m$ collapse in response to high Ca^{2+} influx. In cardiac myocytes, mitochondria and SR are structurally and functionally related, co-localizing in the so-called mitochondrial microdomain; mitochondrial Ca^{2+} influx through MCU is tightly linked to SR Ca^{2+} release. Alterations of RyR2 on SR, and consequent increase of Ca^{2+} leak in the cytosol,

are among the causes of cardiac arrhythmias. Mitochondria, while not representing the primary cause, can strongly contribute to the arrhythmic phenotype, being a key component of the cycle.

The ability of ROS to affect mitochondrial membrane potential confers them a pro-arrhythmogenic role. Such arrhythmogenic effect of ROS depends on a complex and multifactorial response of cardiac mitochondria, named ROS-induced ROS release (RIRR). This is an autocatalytic process by which high levels of ROS induce further ROS release from mitochondria, therefore creating a vicious loop. RIRR is not yet fully understood; the most important evidence is that mitochondrial ion channels have a central role in the regulation of the electrophysiological equilibrium.

The functional role of mitochondria-dependent RIRR in arrhythmogenesis has already been demonstrated; in fact, the stimulation of the heart with H_2O_2 leads to a two-phase ROS production: the first amount of ROS is directly linked to H_2O_2 action, while the second amount corresponds to ROS of endogenous production derived by mitochondrial RIRR and is associated with arrhythmia. [80] (Figure. 1.13)

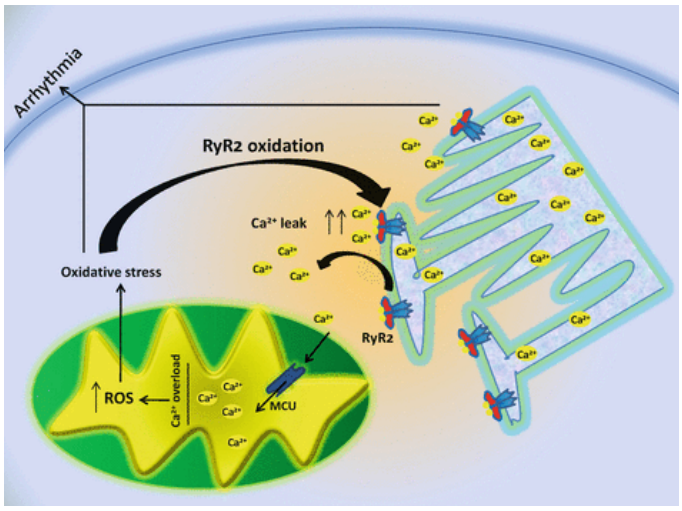

Figure. 1.13 Ca^{2+} dependent pathways and mitochondrial function in arrhythmogenesis. Alterations of Ca^{2+} release from the sarcoplasmic reticulum can induce mitochondrial dysfunction as consequence of mitochondrial Ca^{2+} overload. Mitochondrial dysfunction in turn, through means of oxidative stress, can mediate further alterations with increase of Ca^{2+} leak from SR. [80]

1.11 Catecholaminergic polymorphic ventricular tachycardia (CPVT)

Catecholaminergic Polymorphic Ventricular Tachycardia (CPVT) is an inherited arrhythmogenic disease characterized by polymorphic ventricular tachycardia (VT) in structurally intact heart induced by physical and/or emotional stress that may result in syncope, seizures and cardiovascular collapse. The first case of the disease was descripted in 1975 by Reid and was later characterized by Coumel in 1978. Catecholaminergic polymorphic ventricular tachycardia belongs to a group of inheritable disorders referred to as ‘‘channelopathies’’, caused by mutations in genes encoding for channel-proteins that regulate cardiac electrical function [81]. Subsequent studies allowed the discovery that this disease is related to the non-physiological control of the coupling of Ca^{2+} release from the SR, the activation of sarcomere contraction and the Ca^{2+} reuptake into the SR during relaxation [82]. In the early 2000s the identification of two main genetic variants explained the majority of genotype-positive cases.

The most frequent form of CPVT (about 60% of cases) was discovered by our group in a large pedigree with seven clinically affected family members in which the first mutation in the RYR2 gene was found to be related to the autosomal dominant form of CPVT [83]. The second variant of CPVT (less than 5% of cases) is related to autosomal recessive mutations in the CASQ2 gene encoding for cardiac Calsequestrin, a calcium-buffering protein situated within the SR that has inhibitory effects on RyR2’s activity [84]. CPVT’s genetic background has been characterized through linkage analysis in correlation with candidate gene approach. In 1999 Swan et al. described a correlation of the chromosomal locus 1q42- q43 in two large families with CPVT. While in 2001 [85] seven consanguineous Bedouin families were screened, and an autosomal recessive form of CPVT mapping at chromosomal locus 1q13-p21, at the level of the CASQ2 gene, was reported. Generally, mutations in both RYR2 and CASQ2 are point substitution of single bases causing substitution of a highly conservative amino acid. These mutations cause spontaneous leakage of calcium ions from the SR in diastole, particularly during intense adrenergic activation. The resultant calcium overload induces the development of DADs that can trigger supraventricular and ventricular extrasystoles, which have the potential to degenerate into sustained hyperkinetic arrhythmias [83]; [86].

Several *RYR2* mutations are localized in two regions of the protein, the C-terminus region and the central region, which are supposedly the domain containing the binding sites for FKBP12.6 and the protein region regulating channel sensitivity to the intracellular Ca^{2+} concentration. However, the N-terminus domain has been gaining attention in recent studies for its crucial role in RyR2 functionality. It contains the binding site for the protein phosphatase 1, which is known to reduce the CAMKII mediated phosphorylation of RyR2 and is therefore a key site in which mutations might induce the loss of the antiarrhythmic effect by attenuating the phosphorylation of RyR2 by CAMKII [31].

The majority of *RYR2* mutations identified in patients with CPVT cause a gain of function (increased calcium sensitivity). Different groups have studied the mechanism of this gain of function and reached three conflicting conclusions. These mechanisms are not mutually exclusive and, depending on the position of the mutation, could coexist [87]. Wehrens et al., in 2003, proposed that the leading mechanism by which RyR2 causes CPVT relies on the reduced binding affinity of RyR2 to the regulatory protein FKBP12.6 at basal state and even more so after beta-adrenergic stimulation (i.e., epinephrine and caffeine injection) since it causes RyR2 phosphorylation by PKA [31]. An alternative hypothesis to link RYR2 mutations and arrhythmogenesis in CPVT has been proposed by Chen and colleagues [88][89], who demonstrated that the majority of *RYR2* mutations change the properties of RyR2 so that the channel opens at reduced levels of luminal Ca^{2+}. The opening of RyR2 at reduced cytosolic Ca^{2+} levels is considered a gain of function feature that, by lowering the SR threshold, promotes spontaneous calcium release and facilitates the development of DADs. This mechanism is called store overload induced Ca^{2+} release (SOICR). On the other hand, in 2008 Yamamoto et al. have demonstrated that some RYR2 mutations cause severe disruption in the 3D conformation of this protein. They showed that the closed state of the channel is stabilized by tight contacts between the central and N-terminal regions of RyR2. The strength of these interactions was reduced by physiological or pharmacological stimulation, thus leading to channel instability. Reduced 'stickiness' of RyR2 domains is known as 'domain unzipping'. Two other studies have demonstrated that RYR2 mutations affecting the central domain of RyR2 result in domain unzipping and enhance Ca^{2+} sensitivity, thus facilitating spontaneous Ca^{2+} release [90].

Instead, in the *CASQ2* gene there may be deletions, null mutations and missense point mutations that can alter the quantity or function of the protein, causing the recessive form of CPVT. In particular, the most studied and characterized mutations are the missense point mutations R33Q, in which an arginine residue changed to glutamine at position 33, and the missense D307H mutation, in which an aspartic residue is changed to histidine at the position 307 [91]. All these mutations can cause an abnormal calcium release because, as already said, CASQ2 have inhibitory effect on RyR2 activity. Moreover, since its calcium buffering activity, is either mutated or absent Calsequestrin cause an arrhythmogenic event, the store-overload-induced Ca^{2+} release [92].

The induction of spontaneous calcium release from the sarcoplasmic reticulum is the final common pathway by which *RYR2* and *CASQ2* mutations induce CPVT. However, different mutations lead to this mechanism through different actions that may also depend on the specific amino acid change.

The result of all this abnormal calcium leakage is the generation of DADs which induce arrhythmias [93]. The mechanism of arrhythmogenesis in CPVT is summarized in Figure 1.14 [94].

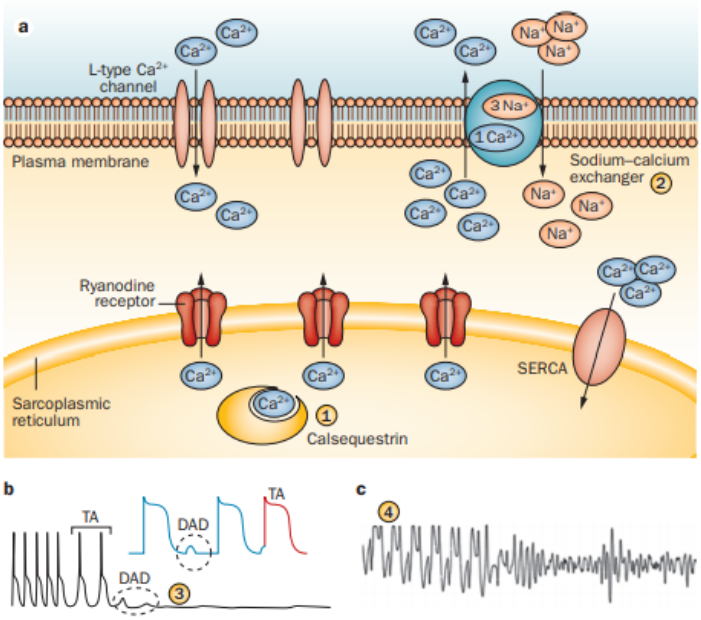

Figure 1.14 Schematic representation of the mechanisms of arrhythmogenesis in catecholaminergic polymorphic ventricular tachycardia. a. A mutation in Calsequestrin (1) causes a reduced threshold for calcium release and SOICR, which lead to calcium overload in the cytosol. Activation of the sodium–calcium exchanger (2) generates DADs (3). **b.** A schematic representation and an actual recording from a cardiac cell isolated from a *CASQ2* knock-out mouse. DADs (blue) and TA (red) are elicited by isoproterenol super fusion. **c.** These cellular abnormalities are the cause of the ventricular arrhythmias observed in the clinical setting (4). Abbreviations: DAD, delayed afterdepolarization; SERCA, sarcoplasmic/endoplasmic reticulum calcium ATPase; SOICR, store overload-induced calcium release; TA, triggered activity; VT, ventricular tachycardia[76].

Although RyR2 and CASQ2 are evidently major substrates for the disease, they do not account for all cases of CPVT. For this reason, other genes involved in the cardiac calcium release complex have also been investigated as potential candidates. Indeed, by performing a genome-wide linkage analysis in a large Swedish family with severe

dominantly inherited CPVT-like arrhythmias, Nyegaard et al. [96] identified *CALM1* as a new candidate gene for CPVT. Moreover, Roux-Buisson et al. [97] screened 97 probands and found three related variants in the *TRDN* gene, which encodes for a transmembrane protein located in the junctional SR that links RyR2 and CASQ2 in SR. In 2015, Rooryck et al. also found two new mutations in the *TRDN* gene, therefore providing further support of the role this protein plays in the disease. Interestingly, in a Triadin knockout mouse model, Cacheux et al., in 2019, discovered a significant reduction of CASQ2 protein quantity although the transcript level of this protein was unchanged. Complementarily, it was discovered that in a CASQ2 knockout mice model the protein level of TRDN was also downregulated [100]. These results point to a possible instability of the CASQ2 protein in the absence of TRDN, and vice versa, due to a possible inefficient mRNA translation or an increased protein degradation. Therefore, Triadin and Calsequestrin, both responsible for the recessive forms of CPVT, are intimately linked in the pathophysiological mechanisms leading to arrhythmias.

Other genes not involved in the cardiac calcium release complex, have been associated with CPVT; in particular the *KCNJ2* gene, that encodes the α-subunits that co-assemble to form the potassium inward rectifier channel Kir2.1. [101] Moreover, Devalla et al. [102] performed a whole-exome sequencing (WES) on patients from three different families that presented life-threatening arrhythmias and high risk of sudden cardiac death (SCD). Two probands carried identical homozygous rare variant in *TECRL* gene, which encodes the *trans*-2,3-enoyl-CoA reductase-like, an ER protein expressed preferentially in the heart. Mutation in these genes have been associated with arrhythmogenic events, comparable to those occurring in CPVT [103],[104].

1.11.1 Clinical features

The average onset of CPVT is generally around the 12th year of age [105];[106][107] ; patients typically resort to medical attention for the first time with either stress-induced syncope or cardiac arrest, thus making prevention of lethal events a difficult task.

At basal state CPVT patients do not show altered electrocardiogram records, even though some authors reported a tendency of bradycardia in some patients [86] [108]. Other scientists observed a high percentage of cases of U wave presence [109]; furthermore, a mild QT prolongation in some CPVT cases was reported [110]. Nonetheless, these characteristics are not constant features that are ubiquitously present in CPVT patients and therefore they cannot be considered a diagnostic criterion. According to current guidelines [111], the clinical diagnosis of CPVT is based on the documentation of polymorphic ventricular arrhythmias that are induced by adrenergic stimuli, such as an exercise stress test, in patients without any other structural or electrical cardiac abnormality [112]. This is mainly due to the highly reproducible pattern of arrhythmias

evoked during these tests or by isoproterenol infusion [113];[114]. However, in a subset of patients, rather than exercise, acute emotion represents a more powerful trigger. Hence, ECG-Holter monitoring and implantable loop recorders may be helpful for a diagnosis in those patients in whom emotional triggers (alone or in combination with exercise) are more arrhythmogenic than exercise alone [115].

The hallmark sign of CPVT, being highly specific and yet not present in all patients, is a peculiar form of polymorphic ventricular tachycardia (VT), characterized by a 180° beat-to-beat rotation of the ectopic QRS complexes that is therefore termed "bidirectional" [81] (Figure 1.15). Moreover, recent observations evidenced that some patients might also present irregular polymorphic VTs [116].

Figure 1.15 Electrocardiographic manifestations of CPVT. Different phases of an exercise stress test in a 27-year-old CPVT patient carrier of a RyR2 mutation. Panel A shows the baseline ECG characterized by sinus bradycardia (heart rate, HR, 33 bpm), normal atrio-ventricular and intraventricular conduction and normal QT interval (QTc 372ms). At 6:59 min of exercise and (HR of 71 bpm) isolated ventricular premature beats (VPB) appear (panel B), which become bigeminal at 10:04 min and the HR rises to 86 bpm (panel C). VPBs have a LBBB morphology with inferior axis (not shown), and a long coupling interval (ms), consistent with delayed after depolarization induced

triggered activity. Panel D shows a run of bidirectional VT arisen at the peak of the exercise and characterized by a 180° beat-to-beat rotation of the QRS complexes [81].

1.11.2 Therapy

The therapeutic approach toward CPVT includes changes in lifestyle, pharmacological measures, left ventricular denervation, and the use of implantable defibrillators. However, none of these options is fully effective and all of them have side effects; therefore, therapies should strive toward synergistic combinations [81].

Based on the clear evidence of the critical role of adrenergic stimulation as a trigger for arrhythmias in CPVT, beta-blockers were proposed as the primary pharmacologic CPVT therapy, since the first reports on this disease [117]. These drugs prevent DADs to reach the threshold value that induces the development of premature beats. One of the most used beta-blockers is nadolol for its daily dosing and non-selective effect. As a possible additional effect, patients could notice asymptomatic bradycardia that should not be considered an adverse effect but as an additional anti-arrhythmic benefit, along with the inhibition of sympathetic stimulation [118]. Since cardiac arrest may occur also in individuals who have never experienced symptoms like palpitations and syncope, these patients are considered silent carriers of pathogenic mutations and should receive prophylactic treatment with beta-blockers. Remarkably, even with appropriate use of beta-blockers, up to one-third of CPVT patients may experience recurrent arrhythmic events or display the persistence of complex arrhythmias during exercise stress tests. Furthermore, Priori et al. reported that 30% of patients treated with beta-blockers showed recurrences of syncopal episodes or sustained ventricular tachycardia [81]. Therefore, in parallel to beta-blockers treatment, implantation of an implantable cardioverter defibrillator (ICD) should be considered.

An ICD is a small battery-powered electrical impulse generator able to detect cardiac arrhythmias and correct them by delivering a jolt of electricity. In current models, the ability to revert ventricular fibrillation includes both atrial and ventricular arrhythmias as well as the ability to perform biventricular pacing in patients with congestive heart failure or bradycardia.

The incomplete protection afforded by beta-blockers calls for the need to identify new effective treatment options. Recently, it was demonstrated that a sodium channel blocker agent called flecainide is effective in preventing arrhythmias in CPVT patients. The mechanism for this unexpected antiarrhythmic action is related to the fact that the drug, by blocking sodium channels, renders less likely the induction of triggered beats by DADs [119]. Flecainide has proven its usefulness as a RyR blocker in CPVT, but it is known to be pro-arrhythmic following myocardial infarction. This effect is presumably

related to its Na^+ channel inhibition properties. Recent works highlight the potential for modifications of flecainide and the removal of its Na^+ channel inhibition feature. Other novel RyR inhibitors that have shown to be promising are the family of carvedilol derivates as well as the tetracaine derivates and dantrolene derivates. These drugs could open new avenues for more specific targeted pharmacotherapy [120].

Another option that is currently being explored is the use of calcium channel blockers, in particular verapamil, that have been recently studied in limited series of patients (Sumitomo et al., 2003); [122] evaluating the efficacy of a combined association between this drug and beta-blockers. A different more radical treatment of arrhythmias in CPVT, proposed by Wilde et al., is the Left Cardiac Sympathetic Denervation (LCSD) which is a surgical/endoscopic resection of a portion of the sympathetic chain that was shown to have long-term effectiveness [123].

2. Aim

The heart mainly relies on mitochondria for the production of the large amount of ATP required to sustain its contraction. Mitochondria are distributed throughout the cardiac myocyte to form inter-fibrillar clusters that run parallel to myofibrils to provide ATP to the sarcomeres more efficiently. Interestingly, in the proximity of Z lines, mitochondria also come in close contact (about 10 nm) with Ca^{2+} Release Units (CRUs), the intracellular junctions formed between the jSR (containing RyR2s) and transverse-tubules (TTs) (containing voltage-activated L-type Ca^{2+} channels). The proximity between mitochondria and CRUs, stabilized by specialized tethering structures is thought to create a microdomain that provides the bases for a functional cross-talk between the two intracellular organelles [124].
Due to the substantial driving force represented by the strongly negative inner membrane potential and the mitochondrial channels (voltage-dependent anion channel and the mitochondrial Ca^{2+} uniporter), mitochondria can rapidly and efficiently accumulate a large amount of Ca^{2+} in response to SR Ca^{2+} release.
Dominant catecholaminergic polymorphic ventricular tachycardia (CPVT) is an inherited disease that causes arrhythmic death in apparently healthy subjects and is caused by mutations in the ryanodine receptor gene (RyR2) that induce adrenergically mediated diastolic Ca2+ leak from the sarcoplasmic reticulum (SR). In 2017 we showed that our CPVT mouse model, R4496C, presents mitochondrial abnormalities and that RNA-interference that targets the mutant allele in CPVT mice carriers of the R4496C RyR2 mutation, abolishes arrhythmias and blunts the development of mitochondrial abnormalities [6]. Taken together, our observations support the view that the diastolic calcium released by the mutant RyR2 channels is uptaken by mitochondria and causes their degeneration.

It has been demonstrated how mutations in the skeletal muscle RyR (RyR1) cause Malignant Hyperthermia Susceptibility and that the leak of Ca^{2+} through the mutated RyR1 increases production of ROS by the nearby mitochondria [125]. This, in turn, increases RyR1 S-nitrosylation and oxidation, further enhancing SR Ca^{2+} leak in a dangerous feed-forward mechanism. It was also reported that these mice developed severe mitochondrial alterations compatible with increased redox stress and that these defects progressively lead to significant damage of mitochondria and formation of fiber cores.
Besides the evidence supporting the hypothesis that diastolic calcium leakage caused by RyR2 gain of function mutations may lead to a subclinical mitochondrial degeneration, it is interesting to explore whether environmental situations or particularly severe mutations may promote the development of a cardiomyopathic phenotype that has been reported in some carriers of RyR2 mutations. It was shown that R4496C mice present a failure to increase contractility in response to epinephrine, suggesting the presence of

concealed cardiomyopathy [126]. This, in turn, suggests that the majority of patients may present mitochondrial damage in isolation that causes only mild contractile impairment upon adrenergic activation (through a pathway of CAMKII activity enhancement, protein phosphorylation, and increase the diastolic calcium leakage from the sarcoplasmic reticulum).

We therefore hypothesize that severe RyR2 mutations combined with exposure to environmental factors that increase cardiac workload may exacerbate Ca2+ release from SR, promote mitochondrial Ca2+uptake, which leads to impaired mitochondrial function and contractile dysfunction.
Based on data from our laboratory and from evidence present in the literature, we set out to extensively characterize the mitochondrial dysfunction and the molecular mechanisms underlying the damage and their contribution to the CPVT phenotype in our R4496C-RyR2 model. We therefore planned to correlate the arrhythmic burden and contractile dysfunction with the ultrastructural and physiological changes of mitochondria by measuring mitochondrial Ca^{2+} uptake, energetics and the redox state. To further prove our hypothesis, we will selectively downregulate VDAC2, one of the key organelles specific Ca^{2+} channels, and therefore test the contribution of mitochondrial Ca^{2+} uptake to oxidative stress and CPVT phenotype.
The work that will be performed will set the framework that delineates the progressive involvement of mitochondria in CPVT pathogenesis.

3. Material and methods

3.1 Animal studies

3.1.1 Animal model

Animals were maintained and bred at the Charles River Laboratories in Calco (Italy) and transferred to Maugeri Foundation for the studies based on the characterization of the phenotype. Animals were maintained and studied according to the protocols approved by the Italian Ministry of Health.

Species: C57BL/6 mice.

Choice of strains: Knock-in heterozygous RyR2 R4496C/WT (Het) mice (previously developed by Prof. Priori's Scientific Group).

Sex: male and female.

Age: 3 months (12-15 weeks).

Body weight: 23 +/- 5 grams.

Identification: direct genotyping of each animal from tail DNA.

Procedure for euthanasia: Before any manipulation animals were anesthetized with Isoflurane (Isoflurane-Vet, Merial) using the apparatus (VisualSonics VevoTM Compact Anesthesia System). Animals were sacrificed by cervical dislocation.

3.1.2 Genotyping

Genotype was determined performing PCR with specific primers to assess mice genotype at RYR2 gene locus in DNA extracted from tail biopsies.

3.1.2.1 DNA extraction from tissue

Tail biopsies were cut from 1-month old mice by authorized technicians in Charles River Laboratories (Italy) and shipped to our laboratory in dry ice. The samples were then processed for the DNA extraction through KAPA Mouse Genotyping Kit (KAPA biosystems) according to the manufacturer's instructions. Mice tissues were digested in 10 ml of 10 KAPA Express Extract Buffer and 2 ml of KAPA Express Extract Enzyme

(500 U/ml) and 88 ml of H_2O and the reaction was performed with the Applied Biosystems 2720 Thermal Cycler.

The isolated DNA was stored at 4°C until being processed for the polymerase chain reaction (PCR).

3.1.2.2 Polymerase chain reaction (PCR)

The DNA samples corresponding to the tail biopsies were processed by PCR with specific primers in order to identify the correct genotype of the mice.

KAPA2G Fast Genotyping Mix (Merk) is a ready-to-use master mix containing all components for fast PCR, except the primers and the template. The ReadyMix™ also contains two inert dyes, allowing for the analysis of PCR reaction products by agarose gel electrophoresis without the need to add a DNA loading solution. PCR reactions were performed with the Applied Biosystems 2720 Thermal Cycler. Reaction mixture was composed of the genomic DNA, two specific oligonucleotide primers (complementary to the sense and anti-sense strand of the DNA to be amplified), the Master mix solution (2X KAPA2G Fast Genotyping Mix with dye) and 2µL of total genomic DNA

The PCR products were separated by 1% agarose gel electrophoresis and genotype was assessed through the analysis of the expected bands.

3.1.3 Isolation of adult mice cardiomyocytes

Ventricular myocytes were isolated using an enzymatic digestion method. Mice were treated with heparin, an anticoagulant, and sacrificed by cervical dislocation in order to open the thoracic cavity and chest with small scissors. After the heart's explant, the organ was immediately placed into a 30-mm dish containing 4 ml of perfusion buffer (in mM: 113 NaCl, 4.7 KCl, 0.6 KH_2PO_4, 0.6 Na_2HPO_4, 1.2 $MgSO_4$, 12 $NaHCO_3$, 10 $KHCO_3$, 10 HEPES, 30 Taurine, 10 2,3-Butanedione monoxime (BDM) and 5.5 Glucose) at room temperature. The aorta was cannulated and once it was stably positioned it was perfused for 4 min at 3 ml/min with perfusion buffer strictly maintained at 37°C. Subsequently, the heart was perfused with the digestion buffer (2 mg/ml Collagenase type II, 0.14 mg/ml Trypsin, 12.5 µM $CaCl_2$) for 8 min at 3 ml/min at 37°C in order to perform an enzymatic digestion. Consequently, it was cut off from the cannula just below the atria and mechanical digestion was performed cutting the heart into several small pieces. At this point the isolated cardiomyocytes were washed with 10 ml of room temperature Stopping buffer 1 (Stop 1: provided with 10% Fetal Bovine serum FBS and 12.5 µM $CaCl_2$). In the following step the pellet of cells was resuspended in Stopping buffer 2 (Stop 2: 5% Bovine calf serum BCS, 12.5 µM $CaCl_2$). Cells where stepwise then readapted to calcium,

with increasing concentrations of calcium chloride until reaching a final concentration of 1.71 mM.

All the following experiments were performed immediately after the isolation, since the isolated cells are not able to be keep their electrophysiological and molecular properties for more than 1 day.

3.1.4 Confocal ROS measurement

For the measurement of mitochondrial ROS, isolated cardiomyocytes were loaded with 5 µM MitoSOX™ Red reagent (Thermofisher) for 10 minutes at 37°C and then subsequently counterstained with 300 nM DAPI, used as a nuclear marker, for 5 minutes at room temperature. Images were collected with a Leica SP8 confocal microscope (Absorption/Emission: 510/580 nm).

For cellular ROS measurement, isolated cardiomyocytes were loaded with 5 µM cell-permeant 2',7'-dichlorodihydrofluorescein diacetate (H2DCFDA) (Thermofisher), a chemically reduced form of fluorescein, for 20 minutes at 37°C and then subsequently counterstained with 300 nM DAPI (used as a nuclear marker) for 5 minutes at room temperature.

Images were collected with a Leica SP8 confocal microscope (Absorption/Emission: 492–495 nm /517–527 nm).

3.1.5 Mitochondrial free Ca^{2+}

The important role that mitochondria play in the spatial buffering of cellular calcium makes the accurate monitoring of mitochondrial calcium critical. In these particular measurements performed in collaboration with Dr. Santiago, a senior member of our group, we relied on the complementary use of 2 techniques:

(1) Use of non-ratiometric calcium indicators (https://www.embl.de/eamnet/html/calcium/nonratio.htm) such as Fluo 4 (for cytosolic Ca^{2+}) and Rhod (for mitochondrial Ca^{2+})

Live cardiomyocytes were stained with 10 µM Rhod2 (Invitrogen) in 0.02% Pluronic, 75 min at 4° C. Through a subsequest step of Sapinin permeabilization of the cell's sarcolemmal membrane, the contaminant signals from cytosolic Rhod 2 are minimized. A solution of known composition permeates through the sarcolemmal pores, replacing the cytosol (the so-called "mock" cytosol) and offers experimental control of free Ca^{2+}, ATP, free Mg^{2+} and otherwise the overall experimental conditions. This maneuver

ensures the reproducibility of the intracellular conditions among cardiomyocytes from different hearts and phenotypes. The only downside is the partial loss of the cell's physiology (i.e., in this case, sarcolemma permeabilization obliterates the membrane potential found in cardiac myocytes [127]).

Rhod 2-loaded cardiac myocytes were permeabilized with saponin (0.1% for 45-60 s) in a mock cytosol containing: K-Asp 120 mM, K_2ATP 5 mM, NaPC 5 mM, HEPES 10 mM, EGTA 500 µM, Dextran 4%, Reduced Glutathione 10 mM, Free Mg 1 mM, Free Ca^{2+} 150 nM and Fluo 4 50 µM for cytosolic Ca^{2+} measurements.

Solutions were applied through a gravity driven perfusion system. All experiments were performed at room temperature (22-23.5 ºC).

(2) Confocal microscopy: This technique will be briefly discussed in section 3.2.2.

Ca^{2+} measurements were performed with a laser scanning confocal microscope. Fluo-4 was excited at 488 nm, while Rhod2 was excited at 568 nm. During our recordings, we minimized bleed-through (fluorescence detection from a neighboring channel [128]) with appropriate emission filters and sequential excitation of the fluorophores in order to separate the 2 signals. [128]

Images were acquired in 2-dimensional XY-mode (time coincides with the Y-dimension), with the scanned line oriented perpendicular to the longitudinal axis of the cell. This specific orientation ensures that the entire cell is scanned through time, so that a clear reading of all mitochondria in the focal plane can be obtained.

3.1.6 Mitochondrial membrane potential measurement

In collaboration with Dr. Santiago, we evaluated mitochondria membrane potential with the use of the JC-1 probe. Isolated cardiomyocytes were loaded with the ratiometric probe JC-1 (Thermofisher) at a concentration of 10µg/ml at 37°C for 30 min. Subsequent data acquisition was performed on a Leica SP8 confocal microscope. The ratio of densitometric values for red (590 nm) and green (510–527 nm) fluorescence was used as an indicator of Mitochondrial membrane potential.

3.1.7 Glycolysis measurement

Glycolysis measurement on isolated cardiomyocytes were performed using the Agilent Seahorse XF Glycolysis Stress Test Kit (Agilent Technologies). The Seahorse assay indirectly measures glycolytic activity by quantifying the extracellular acidification rate (ECAR). As lactate is secreted it is co-exported with a proton into the extracellular fluid

which reduces the media's pH and is measured as ECAR by the Seahorse XF. A Seahorse XF96 instrument (Agilent Technologies) was used in the experiment. Cardiomyocytes were plated on laminin (18mg/ml) coated cell culture microplates (Agilent Technologies) in Seahorse XF Base modified Medium (0mM glucose, pH 7.35, Agilent Technologies) at a density of 16000 cells per well. The Seahorse sensor cartridge was hydrated in a non-CO2 incubator overnight, prior to the experiment (Agilent Seahorse XF Calibrant). The day of the assay, culture medium was replaced stepwise with non- buffered XF assay medium (Agilent Seahorse) and the designated assay conditions were added. The cell microplate was placed in a 37°C incubator without CO2 for 45 minutes. The various assay compounds were loaded into the injector ports within the cartridge: Glucose (10mM) (substrate), (2µM) oligomycin (ATP synthase inhibitor), and the glycolytic inhibitor 2-desoxyglucose (2-DG) (100mM). The measurement of ECAR was performed during 2-min intervals for over 1 hour using the Seahorse XF96 analyzer. ECAR rates were indicated as PPR [pmol/min]. ECAR values were then imported into Microsoft Excel for normalization to cell number and technical replicates were then averaged.

3.1.8 ROS Citometry analysis

Isolated cariomyocytes were loaded with the probes Mitosox, H2DCFDA and DAPI as previously mentioned in section 3.1.4 of the methods chapter. Loaded cells were analyzed with the Canto 3L HTS flow cytometer. Raw data was exported as 3.0 fcs-files and analyzed using FlowJo software (Version 10; TreeStar Inc.)

3.1.9 Mitotempo treatment

Isolated cardiomyocytes were preincubated with specific mitochondrial superoxide scavenger mitoTEMPO (20 µmol/L; Millipore Sigma) for 50 min prior to further experiments.

3.1.10 RyR2 immunoprecipitation and immunoblotting from isolated cardiomyocytes

Freshly isolated mouse myocytes were immediately lysed in RIPA lysis buffer (25 mM Tris-HCl pH 7.6, 150 mM NaCl, 1% NP-40, 1% sodium deoxycholate, 0.1% SDS). RyR2 was immunoprecipitated from cell lysate using anti-RyR2 antibody (5 µL) in 0.5 mL of RIPA buffer at 4 ° overnight C. Samples were incubated with Protein A/G Plus-agarose beads (Santa Cruz) for 1 h at 4 °C and washed three times with RIPA buffer. To determine the oxidation status of RyR2, the Oxidized Protein Western Blot Kit was used, whereby carbonyl groups of immunoprecipitated RyR2 were derivatized to 2,4 dinitrophenylhydrazone (DNP) by reaction with 2,4 dinitrophenylhydrazine. As a control,

we used the kit-provided Derivatization Control Solution. The DNP-RyR2 protein samples were separated on 4–20% Mini-PROTEAN TGX gels (Bio-Rad Laboratories) and the DNP-associated signal was assessed by the kit-provided anti-DNP rabbit primary antibody and anti-RyR2, followed by HRP-conjugated anti-rabbit goat secondary antibody and anti-mouse lgG (H + L), HRP secondary antibody. Blots were developed with ECL (Bio-Rad Laboratories).

3.1.11 Mitochodrial Isolation

Heart mitochondria isolation was performed using the Mitochondrial Isolation Kit for tissue (ab110168; Abcam) according to the manufacturer's protocol. The heart tissue was washed and minced in Isolation Buffer and cells were disrupted using a Dounce tissue grinder pestle (Sigma). The homogenized tissue was then centrifuged at 1,000 g for 10 minutes at 4 °C and the supernatant was later centrifuged at 12,000 g for 15 minutes at 4 °C. This process yielded the enriched mitochondria and cytosol fractions in the pellet and the supernatant, respectively.

Both were then quantified using the Quick Start Bradford protein assay (Bio Rad) with a standard curve of a range of concentrations of bovine serum albumin (BSA). Absorbance at a wavelength of 595 nm was then collected using a microplate reader (ELx800, BioTek). Sample protein concentrations were then calculated using the equation generated from the linear line of the best fit through the readings from the standard curve.

3.1.12 Electron Transport Chain complexes activity measurement

In collaboration with Dr. Hernansanz, a senior member of our collaborators belonging to the José Antonio Enríquez group (CNIC), we performed the assessment of mitochondrial activity. Mitochondrial fractions underwent five freeze-thaw cycles in order to disrupt the mitochondrial membranes. The experiment's reaction cuvette contained the complex 1 buffer (containing 25 mmol/L monobasic potassium phosphate, 120 µl of 50 mmol/L dichlorophenolindophenol (DCIP), 100 µl of 1mmol/L Antimycin A, 400 µl of 17.5 mmol/L Decylubiquinone, made up to 100 ml with RO water), 50 µl of 70 g/L fatty acid free BSA and 30 µg of mitochondrial sample (all reagents sourced from Sigma). The volume of mitochondrial extract required to load 30ug was previously determined by Bradford assay. The cuvette was allowed to equilibrate at 37 degrees for 1 minute before the initiation of the reaction by the addition of 10 µl of 10 mmol/L stock of NADH (Sigma) after which the absorbance was recorded at 550nm every 30s for 2.5 minutes. The complex I inhibitor Rotenone (Sigma) at a concentration of 40 mmol/L was added to the reaction and the absorbance was recorded every 30s for a further 2.5 minutes. The overall activity reaction rate was determined by calculating enzyme activity following the addition of NADH (the slope of the reaction) minus the rotenone resistant activity.

3.1.13 Mitochondrial respiration

The Oxygraph-2k (O2k, OROBOROS Instruments, Innsbruck, Austria) was used for measurements of mitochondrial respiration in collaboration with Dr. Hernansanz. Experiments using isolated mitochondria from heart tissue homogenate were performed in MAITE buffer (10 mM Tris-HCl, pH 7.4, 25 mM sucrose, 75 mM sorbitol, 100 mM KCl, 10 mM K2HPO4, 0.05 mM EDTA, 5 mM MgCl2, and 1 mg/mL BSA). All experiments were performed at 37 °C. Isolated mitochondria from heart (50 µg) were resuspended in MAITE buffer. Substrates and inhibitors were then successively added: (5 mM) glutamate and (5 mM) malate, (1 µM) rotenone, (10 mM) succinate, (2.5 µg/mL) antimycin A, (10 mM) N,N,N',N'–tetramethyl–p-phenylenediamine and (10 mM) sodium azide. Measurement of the OCR was performed by calculating the slope after each treatment. Values for specific complex input were acquired from the subtraction of substrate-less-specific inhibitor rates.

3.1.14 Fatty acid oxidation measurement

In collaboration with Dr. Hernansanz, isolated mitochondria (50 µg) were resuspended in MAITE buffer and the the Oxygraph-2k instrument was used for measurements of fatty acid beta-oxidation induced respiration. All experiments were performed at 37 °C. Substrate additions were palmitoylcarnitine (25 µM), coenzyme-A (25 µM), and malate (2 mM) all together, followed by 5 mM ADP. Following consecutive injections were: Rotenone (1 µM), Antimicin (1µM), TMPD (2mM) and sodium ascorbate (10mM) and Sodium azide (10mM). Measurement of the OCR was performed by calculating the slope after each treatment with the substrate and the relative complexes inhibitors.

3.1.15 Measurement of total and soluble mitochondrial Ca2+ content

Mitochondrial insoluble Ca^{2+} content was measured by incubating isolated mitochondrial fractions from cardiomyocytes in a hypotonic buffer (either pH 6.8 for total Ca^{2+} or pH 7.5 for soluble Ca^{2+}) for 5 min. Then, the amount of Ca^{2+} was determined by Calcium Green (C3737, Thermo Fisher) fluorescence and calibrated with a $CaCl_2$ calibration curve set at the same pH of the measurement. Excitation/acquisition was performed three times with a 488/535 filter cube in a Fluoroskan Ascent fluorimeter (Thermo Labsystems).

3.1.16 Telemetry implant and ECG monitoring

Electrocardiography (ECG) of mice was detected by electrodes and recorded by a device external to the body. ECG radiotelemetry transmitters, PhysioTel® ETA-F20 (Data

Sciences International), were implanted subcutaneously under general anesthesia (Isoflurane (Isoflurane-Vet, Merial) to measure ECG data in mice.

After 72 h of recovery from surgery, phenotype characterization was performed. First, basal ECG was recorded for 10 minutes. Subsequently, mice were injected with norepinephrine (2 mg/kg) and caffeine (120 mg/kg) to induce ventricular arrhythmias under a controlled stimulus. All animals were freely moving in their cage while ECG recordings were performed. The analyses of the recorded files were processed using Ponemah® software (Data Sciences International, DSI).

3.1.17 ATP content

ATP content was measured by using the commercial ATP Assay Kit (Colorimetric/ Fluorometric) (ab83355) on heart tissue lysates. The assay is based on the phosphorylation of glycerol in order to generate a product that can be easily quantified colorimetrically (OD 570 nm) by Tecan microplate reading. Hearts were extracted and homogenized with the Kit's ATP Buffer. An ATP standard curve was prepared and for each sample two wells were prepared: one for the measurement and one was used as the sample's blank. Calculations to obtain the ATP content (nmol) were performed according to the kit's instructions.

3.2 Microscopy

3.2.1 Electron Microscopy

Electron Microscopy was performed at the Centro de Biología Molecular (CBO) Severo Ochoa in Madrid.

Hearts isolated from mice were fixed, ultrathin sections were cut in a Leica Ultracut R microtome (Leica Microsystem, Austria) using a Diatome diamond knife (Diatome Ltd. CH-2501 Biel, Switzerland) and double stained with uranyl acetate and lead citrate. All sections were examined with a JEM-1400 Flash (Jeol) electron microscope (JEOL Ltd., Tokio, Japan) equipped with CMOS Oneview camera (Gatan).

3.2.2 Confocal Microscopy

Confocal microscopy fluorescent images were acquired in Madrid with a Zeiss LSM 880 confocal laser scanning microscope, equipped with an oil immersion objective Plan Apochromat 40x (numerical aperture: 1.40). A laser source was used.

Images were exported and analyzed with ImageJ.

3.3 Creation of RNA interference molecules

3.3.1 election of target oligonucleotides

The double stranded (ds) oligo encoding the engineered miRNA was generated by annealing 2 single stranded (ss) oligos designed following the manufacturer's instructions and under the supervision of Dr. Bongianino, a senior member of our group.

The oligos utilized are:

- VDAC2 **544 top:**

  TGCTGATCAAAGTCAACATCACAGCCGTTTTGGCCACTGACTGACGG
  CTGTGATTGACTTTGAT

- VDAC2 **544 bottom:**

  CCTGATCAAAGTCAATCACAGCCGTCAGTCAGTGGCCAAAACGGCT
  GTGATGTTGACTTTGATC

3.3.2 Annealing

The BLOCK-iT^{TM} Pol II miR RNAi Expression Vector Kits facilitates the expression of microRNA (miRNA) for their use in RNA interference (RNAi) of a target gene in mammalian cells.

The annealing procedure was performed by incubating the annealing mix at 95° for 10 min and then cooling down the mix at room temperature for 5-10 min (ss oligos anneal during this time). Afterwards, part of the mixture was diluted with the Oligo Annealing Buffer in order to get the final concentration of 10 nM.

3.3.3 Ligation

The ultimate procedure to generate a recombinant plasmid is connecting the DNA insert (fragment of interest) into the vector backbone.

The ds oligo encoding for the pre-miRNA was ligated with the linearized pcDNA^{TM}6.2-GW/EmGFP-miR vector, that presents 4-nucleotide 5′- overhangs on each strand to facilitate directional cloning of the ds oligo. This vector allows the expression of the engineered miRNA under the control of the Pol II human CMV (cytomegalovirus) promoter and Herpes Simplex virus (HSV) thymidine kinase (TK) polyadenylation signal. It also permits visual or automated selection of cells expressing the miRNA through co-cistronic expression of EmGFP.

Ligation is performed by T4-DNA ligase (New England Biolabs), the reaction was performed at 16°C overnight. The enzyme inactivation was performed at 65°C, 10 min using the MJ Research Peltier Thermal Cycler 200.

3.3.5 Bacterial strains and transformation

One Shot® TOP10 E. coli (Invitrogen) chemically competent cells were used in all the cloning steps, their genotype is: F- mcr A Δ (mrr-hsdRSM-mcrBC) φ80lacZΔM15 ΔlacX74 recA1 araD139 Δ (ara-leu) 7697 galU galK rpsL (StrR) endA1 nupG λ-.

The purpose of the transformation is to introduce a foreign plasmid into bacteria in order to amplify the plasmid and obtain alarger amount of it. Transformation of TOP10 *E. coli* cells (Invitrogen) was performed following 'heat shock' protocol. A single aliquot of competent cells was thawed on ice, and then the DNA deriving from the ligation (500ng) was added. Consequently, after 30 min of incubation on ice, the heat shock step was performed for 30 sec at 42°C. Then, cells were grown in S.O.C. medium at 37°C for 1h while shaking horizontally at 225 rpm without the selective antibiotic. The transformed cells were seeded in sterile conditions on an agar plate supplied with the selective antibiotic at the working concentration of 10 mg/ml. Colonies were grown overnight at 37°C in aerobiosis.

3.3.6 DNA extraction from bacterial cells

Miniprep, Midiprep and Megaprep DNA purification systems were used. The plasmid purification protocols follow alkaline lysis procedure. The plasmid DNA binds an anion-exchange resin under specific salt and pH conditions. Impurities are washed away by a

salt medium. Plasmid DNA is eluted thanks to a high salt buffer and then ethanol or isopropanol are used for concentrating and desalting the plasmid.

3.3.7 Miniprep DNA purification system

Miniprep kit (Promega) allows the purification of 5-10 µg of low-copy number plasmid DNA from 3 ml of culture. The bacteria, once grown overnight, were centrifuged at 10500 rpm for 5 min at room temperature. 200 µl of Cell Resuspension Solution and 200 µl of Cell Lysis Solution were used to dissolve the pellet. After 5 min at room temperature, 200 µl of Neutralization solution was added to stop the lysis reaction. The lysate was centrifuged at 10500 rpm for 5 min at room temperature to extract the DNA. The supernatant was moved to a silica resin mini-column. The washing was performed by adding 2 ml of Column Wash Solution with ethanol and then centrifuging at 10500 rpm for 2 min at room temperature. Purified DNA was eluted with 50 µl of Nuclease-Free Water into the column after a centrifugation step at 10500 rpm for 1 min at room temperature. Quantification was obtained with the Nanodrop spectrophotometer (ND-1000; NanoDrop Technologies, Wilmington, DE, USA).

3.3.8 Midiprep DNA purification system

DNA from of *E. coli* in 100 ml LB was extracted thanks Midiprep kit (Qiagen). Bacteria were pelleted by centrifugation at 6000 rpm for 15 min at 4°C and once the supernatant was removed, they were suspended in 4 ml of P1 Buffer (RNase A is contained). Bacterial cells lysis was induced by adding 4 ml P2 buffer. After 5 min on ice, 4 ml of P3 Buffer was added to stop the lytic reaction. A centrifugation at 13000 rpm for 30 min at 4°C was performed first, and then other one at 13000 rpm for 15 min at 4°C. The supernatant containing the plasmid DNA, was moved to a silica resin column (QIAGEN-tip) which was previously activated with QBT buffer. 20 ml QC buffer were used to wash the column. Plasmid DNA was eluted with 5 ml QF Buffer, precipitation was performed with 3.5 ml isopropanol and centrifuged at 11000 rpm for 30 min at 4°C. The pellet was washed with 2 ml of 70% ethanol and centrifuged again at 11000 rpm for 10 min at 4°C. The pellet was air- dried and dissolved in 50 µl of TE buffer (10 mM Tris·Cl pH 8.0, 1 mM EDTA). Quantification was obtained with the Nanodrop spectrophotometer (ND-1000; NanoDrop Technologies, Wilmington, DE, USA).

3.3.9 Megaprep DNA purification system

DNA from of *E. coli* in 500 ml of LB was extracted thanks Megaprep kit (Qiagen). Bacteria were pelleted by centrifugation at 5500 rpm for 15 min at 4°C and once the supernatant was removed, they were resuspended in 50 ml of P1 Buffer (containing RNase A). Bacterial cells lysis was induced by adding 50 ml P2 buffer. After 5 minutes, 50 ml of P3 Buffer were added to stop the lysis process, and the mix was incubated for 30 min on ice. The lysate was poured into the QIAfilter Mega-Giga Cartridge and incubated at room temperature for 10 min. The vacuum source was switched on until all liquid has been pulled through. 50 ml of Buffer FWB2 was applied to the QIAfilter Cartridge and the precipitate was gently stirred using a sterile spatula until the liquid was pulled through completely.

The supernatant with the plasmid DNA, was moved to a silica resin column (QIAGEN-tip) previously activated with 35 ml of QBT buffer. 200 ml QC buffer were used to wash the column. Plasmid DNA was eluted with 35 ml QF Buffer, precipitation was performed by addition of 24,5 ml of isopropanol and centrifuged at 13000 rpm for 30 min at 4°C. The pellet was washed with 7 ml of 70% ethanol and centrifuged again at 13000 rpm for 10 min at 4°C. The pellet was air-dried and dissolved in 800 µl of TE buffer (10 mM Tris·Cl pH 8.0, 1 mM EDTA). Quantification was obtained with the Nanodrop spectrophotometer (ND-1000; NanoDrop Technologies, Wilmington, DE, USA).

3.3.10 Analytic digestion

Analytic digestion was performed to identify the correct plasmid. Endonuclease enzymes employed were chosen according to the position of their restriction site along the constructs, to obtain a predictable pattern of bands following enzymatic digestion (the enzyme used was MscI). The pattern of bands visualized on agarose gel electrophoresis allowed the identification of the clones carrying the right construct since they had the digestion pattern corresponding to the one predicted. All restriction enzymes were derived from New England Biolabs (NEB).

3.3.11 Agarose gel electrophoresis

The DNA molecules were visualized by addition in the gel of ethidium bromide (10 mg/ml), which intercalates into the major grooves of the DNA and fluoresces under UV light. The agarose gel electrophoresis was performed using a 1% W/L of purified agarose (Euroclone) in TAE buffer (EDTA-Na_2-$2H_2O$: 18.6 g/L 0,05M; Acetic acid glacial: 60.05 g/L 1M; Tris: 242.30 g/L 2M). The running was performed in TAE 1x at 110 V for 25 min at room temperature, later the gel was exposed to a standard transilluminators (Vilber

Lourmat), which uses wavelengths of 302/312-nm (UV-B), to visualize the DNA fragments.

3.3.12 Sequencing analysis

DNA sequencing was performed on all the cloned products to control the fidelity of the gene sequence and the effective presence of the induced mutation. The analysis was based on the Sanger sequencing method. All the sequencing reactions were performed on a Thermo Cyclers with the ABI Prism BigDye Terminator v1.1/ Sequencing Standard Kit 310/377/3100 Series Systems.

3.3.13 Plasmid insertion in pAAV 2.1

From the obtained plasmids, a fragment consisting in CMV promoter, EmGFP, pre-miRNA sequence and TKpolyA was amplified by PCR with specific primers:

- preCMVNheIfor: 5' AAGCTAGCTGCTTCGCGATGTACGG 3'
- TKpolyASphIrev 5' ATGCATGCGAACAAACGACCCAACCG 3'

including the NheI (Forward) and SphI (Reverse) cloning site.

This amplicon was inserted into the pre-digested NheI – SphI sites of the adeno associated viral backbone vector pAAV-2.1 provided by InnovaVector (Pozzuoli, Italy). The AAV production was done in collaboration with the InnovaVector CDMO (https://www.innovavector.eu/our-products/research-grade-production/). The AAV vectors were produced using a transient transfection of three plasmids in HEK293 cells: pAd helper, pAAV rep-cap (packaging), pAAV Cis (including our insert, cloned in the pAAV2.1 Multi Cloning Site (MCS)). The vectors were purified by CsC1 centrifugation and underwent quality control such as Real Time PCR and Dot Blot analysis for physical titer, or Coomassie staining of SDS PAGE to evaluate the presence and purity of capsid proteins, the infectivity (eGFP+ cells/ml) and the sterility. The service sent us a viral preparation in PBS with a total yield of 1 x 1013 genome copies/ml (GC/ml). All AAV stocks were frozen at -80°C in single vials and thawed during the experiments.

3.3.14 Growth and maintenance of C2C12 cell line

C2C12 is an immortalized mouse myoblast cell line. These cells follow an anchorage-dependent growth mode at 37°C and 5% CO2. The recommended complete medium required to grow this cell line includes D-MEM high glucose, 10 % of fetal bovine serum

(Euroclone), 2mM of L-glutamine (Euroclone), 1% of penicillin (Euroclone). Cells are divided when they reach 50 - 70% of confluence (generally every 3-4 days) by enzymatic dissociation, Trypsin (Euroclone) and mechanical means. The maintenance of the cells was performed in 10 cm dishes with 10 ml of complete medium.

3.3.15 Transient transfection procedure

The transfection was performed by using Lipofectamine® 2000 Reagent (Invitrogen). According to the manufacturer's instructions, cells were transiently transfected at 70% of confluence. After 5-6 hours the medium was replaced with a complete medium. 48 hours after transfection, cells were harvested.

3.3.16 RNA processing

In order to get information about the Expression of the exogenous plasmid inserted for simulate the silencing of VDAC2 channel, RNA was purified from harvested C2C12 cells and processed by Real Time PCR.

3.3.16.1 RNA purification from transiently transfected C2C12 cells

Purification of total RNA was performed by using RNeasy® Mini Kit (Qiagen). Transiently transfected C2C12 cells were washed in PBS and then scraped after the addiction of 300 µl of 1% β-mercaptoethanol (β-ME) Buffer RTL. Afterward, 1 volume of 70% ethanol was added to the homogenized lysate and the samples were transferred to an RNeasy spin column placed in a 2 ml collection tube. To allow RNA binding, the samples were centrifuged for 15 s at 9500 rpm. To discard cell debris, a subsequent wash with 350 µl of RW1 Buffer was performed. After this first washing step, each sample was treated, whilst still being in the column, with DNaseI incubation mix (containing RDD buffer) for 15 min at room temperature to avoid genomic DNA contamination. Subsequent washings were performed with 350 µl of RW1 and 500 µl RPE buffer by centrifugation at 9500 rpm. RNA was eluted by adding 50 µl of RNase-free water directly to the spin column and by centrifuging it for 1 min at 9500 rpm. Absorbance at 260 nm (A260) was collected for each RNA sample using the NanoDrop (ND-1000) spectrophotometer (NanoDrop Technologies, Wilmington, DE, USA).

3.3.16.2 Retrotranscription

A total amount of 1 µg of RNA per reaction was used to perform the retrotranscription. The reaction was performed with the iScript™ cDNA Synthesis kit (Bio-Rad) according to the manufacturer's instructions

3.3.16.3 Real-time PCR

Real-time PCR monitors the number of amplicons of a targeted DNA molecule during the amplification process in real-time, where the amount of product is directly related to the fluorescence of a reporter dye. The initial amount of template DNA is inversely proportional to a parameter measured for each reaction, the threshold cycle.

Real-time PCR was performed using the CFX96™ Touch Real-Time PCR Detection System (Bio-Rad Laboratories, Inc., USA) and analysed using the Bio-Rad CFX Manager software package (Bio-Rad Laboratories, Inc., USA). All samples were analysed in triplicate with SsoFastTM EvaGreen® Supermix (Bio-Rad) using a specific primer mix and 20 ng of cDNA template to amplify target sequences: Green fluorescence protein (GFP), VDAC2 and Glyceraldehyde 3-phosphate Dehydrogenase (GAPDH). GAPDH was used as an internal reference.

The Bio-Rad CFX Manager software 1.5 generated values for the threshold cycle (Ct) determination automatically and gene expression comparison was based on the comparative Ct method.

3.3.17 Protein processing

3.3.17.1 Extraction of proteins from C2C12 cells

Transiently transfected C2C12 cells at 70% of confluence, were washed with cold PBS, scraped and lysed with 200 µl per well of a solution containing RIPA buffer (25 mM Tris-HCl pH 7.6, 150 mM NaCl, 1% NP-40, 1% sodium deoxycholate, 0.1% SDS) and 10x Protease Inhibitor cocktail (SigmaFAST™ Protease Inhibitor Cocktail Tablet, EDTA Free, SIGMA-ALDRICH). The cell lysates were collected and sonicated for 10 sec on ice (Omni-Ruptor 250, OMNI International Inc.). Immediately after the homogenized samples were centrifuged at 10000 rpm for 10 min at 4°C and the supernatants, containing the proteins, was collected and stored at -20°C, while the pellet, corresponding to the cellular debris, was discarded.

3.3.17.2 Colorimetric detection and quantitation of extracted proteins

The proteins were quantified by the Pierce® BCA Protein Assay Kit (ThermoFischer Scientific) in accordance with the manufacturer's protocol. Protein concentrations were determined and reported in reference to a standard curve of increasing known concentrations of bovine serum albumin (BSA). The analysis of the samples was performed in the same conditions as the standards, adding the BCA Working Reagent and incubating for 15 min at 37°C. The resultant colorimetric reaction was measured at 560 nm and the quantification was derived from the comparison of the sample's wells with the standard curve. The standard curve was prepared by plotting the average blank-corrected 560 nm measurement for each BSA standard *vs* its concentration in µg/ml.

3.3.17.3 Sodium dodecyl sulphate Polyacrylamide gel electrophoresis (SDS-PAGE)

SDS-PAGE is a technique used to separate proteins according to their electrophoretic mobility. Proteins (30 µg/sample) were size-fractionated using precast TGX Stain-FreeTM Gel 4-15 % gradient gels (Bio-Rad). Samples were prepared by adding 4x Laemmli Sample Buffer (Bio-Rad) and dithiothreitol (DTT) as reducing agent and then denaturated at 90°C for 10 min. The samples, negatively charged by the presence of SDS, were loaded on the polyacrylamide gel and allowed to migrate from the negative electrode (cathode) toward the positive one (anode) at 200V in 1x TGS Buffer (Tris/Glycine/SDS Buffer, Bio-Rad). The Precision Plus ProteinTM Dual Color Standards (Bio-Rad) was used as a protein marker. It allowed the visualization of protein molecular weights ranging from 10 to 250 KDa. Stain-Free Gel images and blotting images were detected with ChemiDocTM Imaging system (Bio- Rad) and analysed by Image LabTM Software (Bio-Rad).

3.3.17.4 Immunoblotting

Immunoblotting is an analytical technique used to detect the expression of specific proteins in a tissue homogenate or cellular extract. Proteins separated by SDS-PAGE were transferred onto nitrocellulose membrane of the Tans-Blot® Turbo^{TM} Transfer Pack Nitrocellulose Mini format (Bio-Rad) by using Tran-Blot® Turbo^{TM} Transfer System (Bio-Rad). Afterwards, the membrane was saturated with 5% milk in TBS-T 1x (0.05 M Tris-HCl, 0.138 M NaCl, 0.0027 M KCl pH 8.0, 0.05% Tween 20) and subsequently washed three times with TBS-T at room temperature.

Antibodies (Table 3.13) were diluted in 3% BSA TBS-T. Samples were incubated with primary antibodies for 3 hours at room temperature. Terminated the incubation, the membrane was washed three times with TBS-T. Afterwards, an incubation with a

secondary antibody, diluted in TBS-T 3% BSA (Table 3.13), for 1 hour at room temperature was performed. Following this step, three washing steps, of 5 min each, using TBS-T were performed. Bound antibodies were detected via chemiluminescence with Clarity™ Western ECL Substrate (Bio-Rad) by digital imaging with ChemiDoc™ Imaging system (Bio-Rad) and analysed by Image Lab™ Software (Bio-Rad).

Antibodies for immunoblotting		
Primary antibodies	Anti-SOD1	monoclonal, mouse, dilution 1:1000, Abcam
	Anti-SOD2	monoclonal, mouse, dilution 1:1000, Abcam
	Anti-DNP	Protein Carbonyl Assay Kit, 1:5000, Abcam
	Anti-HKII	Polyclonal, rabbit, dilution 1:1000, Abcam
	Anti-VDAC2	monoclonal, mouse, dilution 1:1000, Sigma-Aldrich
	Anti–MFN1	monoclonal, rabbit, dilution 1:1000, Invitrogen
	Anti–MFN2	monoclonal, rabbit, dilution 1:1000, Abcam
	Anti–DRP1	monoclonal, mouse, dilution 1:1000, Abcam

	Anti–GAPDH	monoclonal, mouse, dilution 1:1000, Sigma-Aldrich
	Anti-Actin	monoclonal, mouse, dilution 1:1000, Sigma-Aldrich
	Anti-Actinin	monoclonal, mouse, dilution 1:2500, Sigma-Aldrich
Secondary antibodies	Anti-Rabbit	anti-rabbit IgG HRP-conjugate, polyclonal goat, 1:5000, Promega
	Anti-Mouse	anti-mouse IgG HRP-conjugate, polyclonal goat 1:5000, Promega

Table 3.13 Western-Blot analysis. Primary and secondary antibodies employed and relative dilutions

3.3.18 Statistical methods

Analyses were performed with GraphPad Prism (version 9.00 for Windows; La Jolla, CA). Data are reported as mean ± SD or percentage. Continuous variables were compared by either Mann–Whitney test or Kurskal-Wallis test.

All tests were 2-tailed. P values <0.05 were considered significant.

4. Results

Catecholaminergic polymorphic ventricular tachycardia is a genetic arrhythmia syndrome associated with a high risk of sudden death. It is caused by mutations of genes involved in myocardial Ca^{2+} handling.

To mimic dominant CPVT, different transgenic animal models have been created over the years. Among these, the heterozygous mutation R4496C/WT in the RyR2 gene that encodes for the cardiac ryanodine receptor is the most suitable for the study of CPVT's pathophysiological condition. This model has a clear and reproducible phenotype and allows us a quick and simple genotyping screening.

We subjected alive CPVT mice (R4496C/WT mice) to two conditions prior to any experiment:

- Baseline condition

- Adrenergic activation was obtained with the delivery of norepinephrine and caffeine since this is the standard approach to elicit arrhythmias in genetically modified mice with dominant CPVT. This pharmacologic alteration triggers abnormal diastolic calcium release from CPVT mice but not from WT animals leading to arrhythmic events. In these experiments, mice were sacrificed 15 minutes post-administration of norepinephrine and caffeine

Being two different conditions, we set out to evaluate through different morphological and physiological analyses the changes that the acute and punctual phenomenon of adrenergic stimulation induces in our CPVT model.

4.1 Confirmation of structural abnormalities of CPVT mitochondria

Based on the findings obtained in the previous work performed by our group we set out to evaluate more in depth the mitochondrial structural abnormalities found in our model. The analysis of electron micrographs was conducted on $RyR2^{WT/WT}$ mice and on $RyR2^{R4496C/WT}$ mice, with and without the adrenergic stimulus.

We first performed an analysis of mitochondrial damage in our model and the controls by evaluating the ratio of mitochondria whose cristae were disrupted over the number of mitochondria in the field. We found that, as previously reported by our group, $RyR2^{R4496C/WT}$ mice in baseline condition have an increased ratio of disrupted mitochondria. We also observed that, while the adrenergic activation elicited an increase in this percentage in both groups, the $RyR2^{R4496C/WT}$ mice continued to show a greater

amount of damaged mitochondria. This finding suggests that adrenergic activation evokes a greater change in our CPVT model compared to the Wild Type (Figure 4.1)

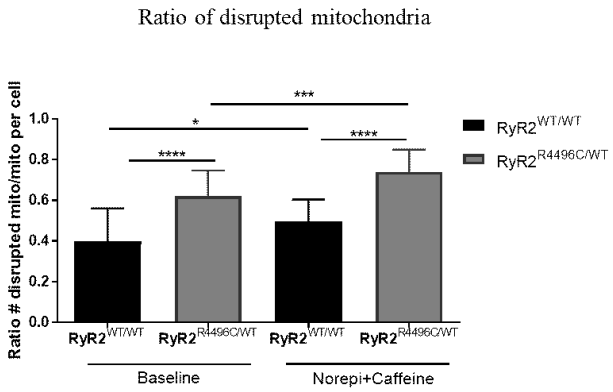

Figure 4.1. Analysis of disrupted mitochondria. Analysis of mitochondrial disruption in $RyR2^{WT/WT}$ and $RyR2^{R4496C/WT}$ in baseline condition and upon adrenergic activation (n=3, 10 images per sample, P-value= *, p< 0.5, P-value= ***, p< 0.001, P-value= ****, p< 0.0001, Kurskal-Wallis)

We then performed a morphological evaluation of mitochondria and we found that in the case of the CPVT phenotype, there are no significant differences in the baseline condition. However, we discovered that acute adrenergic stimulation increased the number of mitochondria per unit area. It was also found that mitochondria post stimulation are smaller and therefore the space occupied by single mitochondria and the ratio of mitochondrial area/total field area are reduced (Figure 4.2 A, B, C). We discovered that the observed changes in mitochondrial size and number occur only in $RyR2^{R4496C/WT}$ mice after adrenergic activation and are therefore genotype-related. (Figure 4.2 A, B, C) This result provides additional information on the structural alterations observed at the mitochondrial level by Bongianino et al., and suggests an alteration in mitochondrial dynamics in $RyR2^{R4496C/WT}$ mice. It would appear as if beta-adrenergic stimulation increases mitochondrial fission in our model.

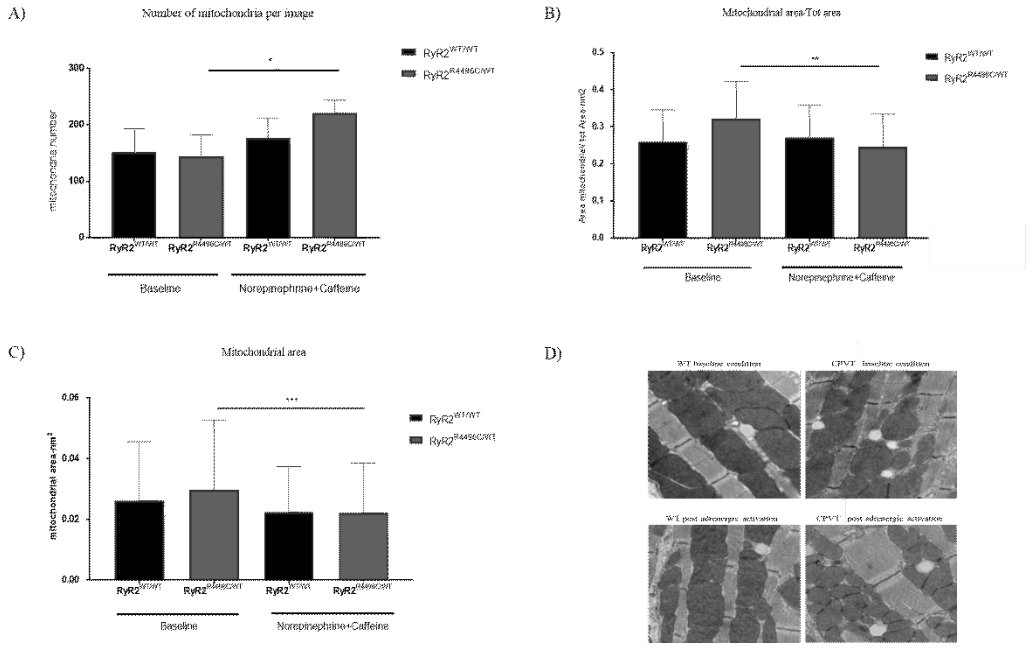

Figure. 4.2. Transmission electron microscopy images and analysis. A) Analysis of mitochondrial number, B) mitochondrial area/total area, C) single mitochondrial area, D) Cardiomyocyte interfibrillar area of $RyR2^{WT/WT}$ and $RyR2^{R4496C/WT}$ in baseline condition and upon adrenergic activation (n=3, 10 images per sample, P-value= *, p< 0.5, P-value= **, p< 0.1, P-value= ***, p< 0.001, Kurskal-Wallis)

To further investigate the pathways involved in mitochondrial dynamics and to verify the hypothesis that beta-adrenergic stimulation enhances mitochondrial fission (i.e., ratio of fusion vs. fission), we conducted a Western Blot analysis of the major fusion pathway proteins, MFN1 and MFN2, and of the fission factor DRP1. The results were normalized using GAPDH or RLP6, as an internal loading control, to correct for unavoidable sample-to-sample and lane-to-lane variations.

In comparison to $RyR2^{WT/WT}$ mice, we discovered that $RyR2^{R4496C/WT}$ animals had a significant reduction in the expression of the fusion proteins MFN1 and MFN2. Which therefore confirmed that, both at baseline and after the adrenergic stimulus, mitochondria in $RyR2^{R4496C/WT}$ mice do not activate the fusion process to mitigate the effects of environmental stress by mixing the contents of partially damaged mitochondria with other healthier mitochondria. (Figure 4.3 A and B)

Furthermore, compared to $RyR2^{R4496C/WT}$ baseline and $RyR2^{WT/WT}$ mice, we discovered a significant increase in DRP1 protein amount, in adrenergically stimulated CPVT mice. (Figure 4.3 C). Given the fact that the active form of DRP1 translocates to the mitochondrial outer membrane, we performed an analysis of the ratio between the cytosolic and mitochondrial fraction of the protein and found that, as expected, the quantity of the mitochondrial fraction compared to the cytosolic fraction in stimulated $RyR2^{R4496C/WT}$ mice was increased (Figure 4.3 D). Therefore, we proved that in $RyR2^{R4496C/WT}$ mice, mitochondria during the adrenergic stimulus activate the fission process, thus preferring the creation of new mitochondria in order to compensate for the damaged ones. In other works, it was reported that DRP1 is phosphorylated (i.e., activated) by CAMKII, whose activity is known to be augmented in our system [130]. This phenomenon could be an adaptation of our system to better buffer Ca^{2+} ions in the cytosol and to face the greater energy needs.

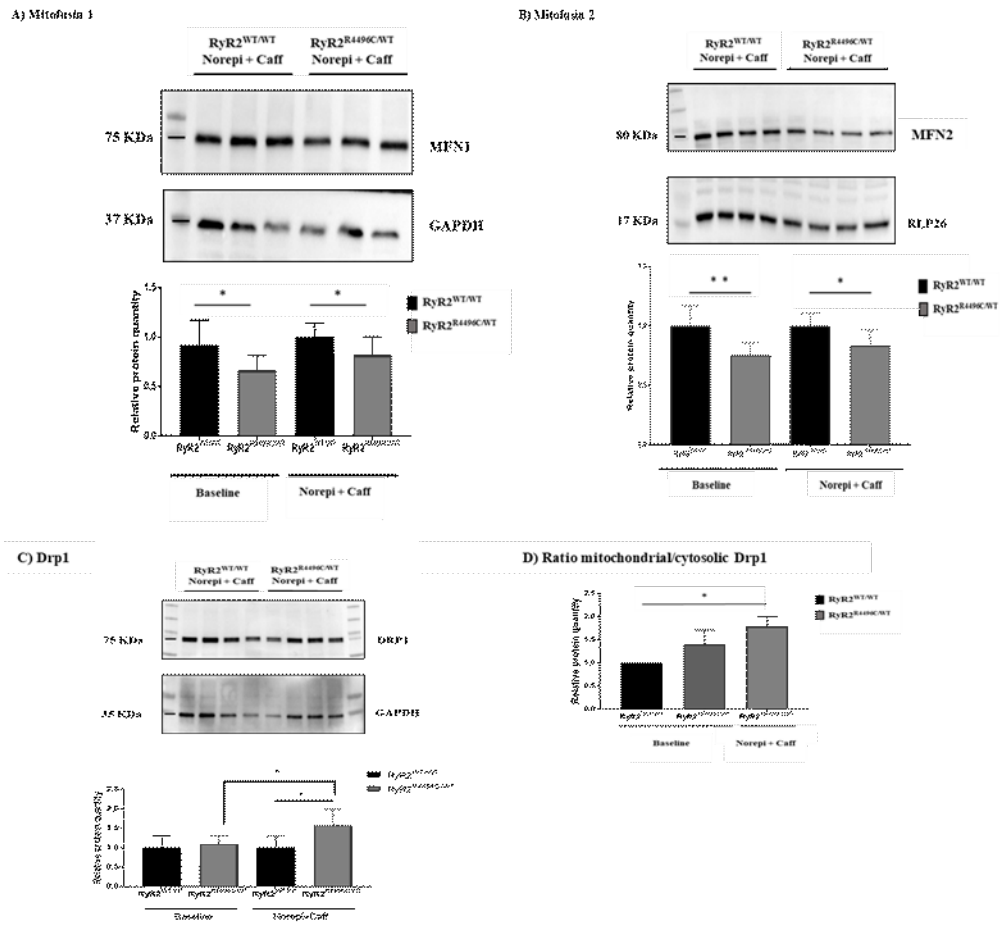

Figure. 4.3. Western blot analysis of fission/fusion proteins. Immunoblot and protein quantification analysis of A) Mitofusin 1 B) Mitofusin 2 C) Drp1 D) Ratio of mitochondrial to cytosolic Drp1 in baseline and stimulated $RyR2^{WT/WT}$ and $RyR2^{R4496C/WT}$ mice (n=8, P-value= *, $p< 0.05$, P-value=**, $p<0.001$, Mann-Whitney)

4.2 Mitochondrial physiology in CPVT and potential relationship to mitochondrial stress and structural abnormalities

Our main hypothesis to account for the mitochondrial alterations that we report in this thesis is the concept that given the presence of abnormal RyR2 channels that lead to diastolic calcium release, the mitochondria upregulate the uptake of calcium thus triggering a cascade of events that ultimately result in mitochondrial stress and alteration of its physiology and/or structure.

To test this hypothesis, we performed a thorough biophysical, molecular and structural dissection of those aspects of mitochondrial physiology directly or indirectly regulated by Ca^{2+}. These are:

- The assessment of Ca^{2+} entry pathways and mitochondrial membrane potential
- The measure of mitochondrial free Ca^{2+} levels
- The measure of mitochondrial reactive oxygen species (ROS) levels
- The assessment of mitochondrial energetics: ATP production, electron transport chain complexes activities and mitochondrial respiration
- The evaluation of mitochondrial metabolism due to incidental finding of an increased presence of lipid droplets (an indicator of metabolism [131])

4.2.1 Assessment of Ca^{2+} entry pathways and mitochondrial membrane potential.

Western Blot experiments revealed no differences in the expression of MCU and its regulators (EMRE, MICU1 and MICU2) or the different isoforms of the VDAC (data not shown). Given the fact that the maintenance of a proper mitochondrial membrane potential is one of the major contributors in mitochondrial wellbeing, we set out to assess it. We loaded resting isolated ventricular myocytes with the ratiometric mitochondrial potential indicator JC-1 [132], which localizes to mitochondria and presents 2 emission peaks, one when in monomeric form (in green) and another in J-aggregate form (in red) when mitochondria are highly polarized. Thus, the ratio between J-aggregate and monomeric signals serves as a semi-quantitative indicator of mitochondrial membrane potential. We found that 5% higher ratio of the J-aggregate over the monomer form of the probe at baseline in $RyR2^{R4496C/WT}$ mice, meaning a hyperpolarization of the mitochondrial membrane potential. After isoproterenol perfusion, a condition that is supposed to emulate the adrenergic activation performed in vivo, we found no differences between the two groups (Figure 4.4). What should also be noted is that Isoproterenol induces a similar response among phenotypes. Given the strong relation between the complexes of the electron transport chain and the mitochondrial membrane potential, we can interpret these data in light of the respiratory changes we observed in our model that will be discussed in the section 4.2.4 (page 63).

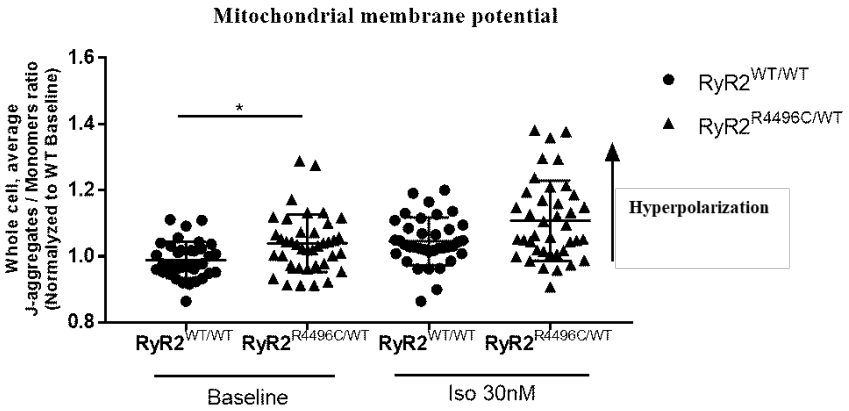

Figure 4.4. JC-1 measurement of mitochondrial membrane potential. Analysis of the ratio between J-aggregates and monomers of the JC-1 probe in cells deriving from $RyR2^{R4496C/WT}$ mice and $RyR2^{WT//WT}$ mice (n=4, 10 cells per sample, P-value *, $p<0.05$, Kurskal-Wallis)

4.2.2 Measure of mitochondrial free Ca^{2+} levels.

Given our hypothesis that the extra calcium released by RyR2s may pathologically increase the Ca^{2+} concentration inside the mitochondrion, we set out to investigate whether $RyR2^{R4496C/WT}$ mice have higher free mitochondrial Ca^{2+} levels in comparison to WT mice. If the results were to be supportive of our hypothesis, we would have the final confirmation that mitochondria in CPVT increase their uptake of Ca^{2+}.

Mitochondria were loaded with the Ca^{2+} indicator Rhod2 in isolated intact myocytes. Then, the external solution was replaced by a mock cytosol of known ionic composition, and the sarcolemma was permeabilized with saponin. Cells thus treated exchanged their soluble cytosolic contents by the mock cytosol, in which Fluo 4, a second calcium indicator, was included. Mitochondrial Rhod 2 loading was not affected by the above procedure, whereas a large majority of cytosolic Rhod 2 traces were removed and therefore did not interfere with mitochondrial measurements. Likewise, Fluo 4 remained in the cytosol without affecting the mitochondrial measurement. Local calcium release events (i.e., the so-called Ca2+ sparks) were measured (Fluo 4 signal) alongside the mitochondrial Ca2+ signal (Rhod 2).

We found that, in fact, $RyR2^{R4496C/WT}$ mitochondria both in baseline condition and upon in vivo adrenergic stimulation counterpart accumulate more calcium in comparison to the WT (Figure 4.5).

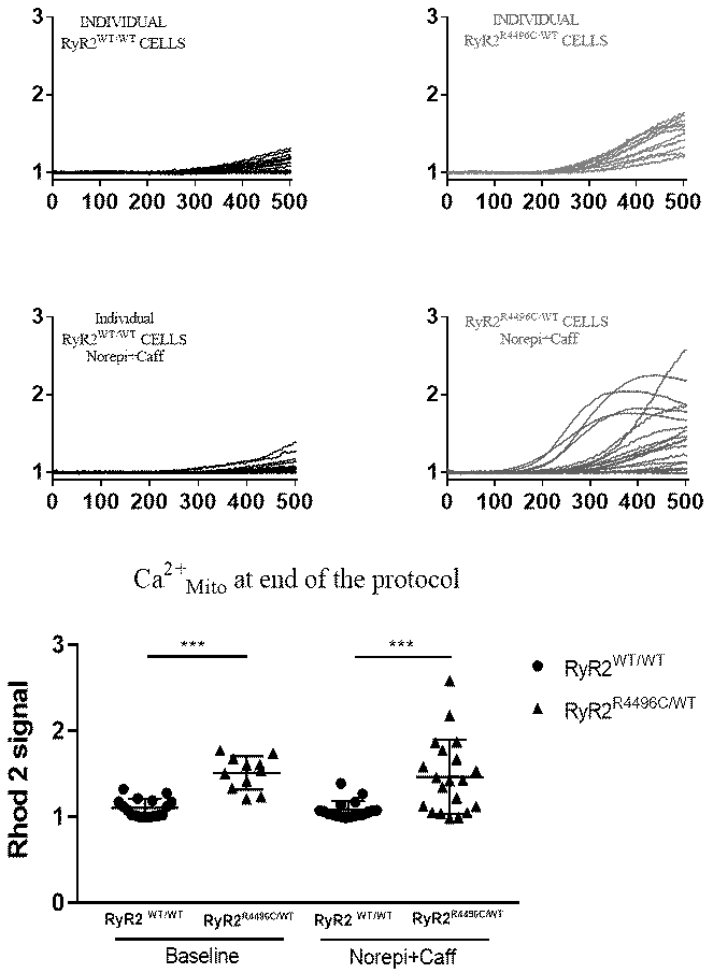

Figure 4.5. Global mitochondrial Ca^{2+} measurements. We show the behaviour of the signal of each cell from analyzed groups. We then show the analysis of the Rhod2 signal at the end of the collection protocol in $RyR2^{WT/WT}$ and $RyR2^{R4496C/WT}$ mice in baseline condition and upon adrenergic stimulation (n=4, P-value=*** $p < 0.001$, Two-way ANOVA)

Given the finding of increased Ca^{2+} content in $RyR2^{R4496C/WT}$ mice mitochondria, we set out to investigate whether this would lead to its precipitation in the form of Calcium-Phosphate precipitates of the ion's surplus as reported in the literature [133]. First, as an initial assessment, we analyzed the electron microscopy images we previously took and found that the area of the Calcium-Phosphate precipitates was increased in $RyR2^{R4496C/WT}$ mice in baseline condition compared to the baseline WT. We also found that upon adrenergic stimulation in the mutants the area of the precipitates, whilst still being significantly greater than in the WT counterpart, decreased markedly compared to $RyR2^{R4496C/WT}$ mice in baseline condition. In light of this preliminary result, we further investigated this aspect by performing a more sensitive experiment that relies on the intrinsic characteristic of the precipitates to be sensitive to pH changes in the mitochondrial matrix [133].

To obtain a quantitative estimation of the amount of Ca^{2+} that can be mobilized from precipitates, we measured Ca^{2+} concentration in mitochondrial preparations at both pH 7.5 and pH 6.8[134]. We observed that the Ca^{2+}concentration was higher in $RyR2^{R4496C/WT}$ mice when the measurement was performed at pH 6.8 than at pH 7.5, indicating that we were indeed able to measure the acid-sensitive Ca^{2+} stored in mitochondrial precipitates. We also found that upon adrenergic stimulation, the amount of insoluble Ca^{2+} in $RyR2^{R4496C/WT}$ mice does not change in comparison to the WT. (Figure 4.6)

This data concerning the baseline condition strengthens our previously reported data of an increased Ca^{2+} content in $RyR2^{R4496C/WT}$ mitochondria. While the situation concerning the adrenergically stimulated condition gives us an interesting starting point for considering the Ca^{2+} homeostasis in $RyR2^{R4496C/WT}$ mice after the physiological changes (increase in mitochondrial fission, etc.) induced by the adrenergic activation, such as a possible over activation of the NCLX channel as a protective mechanism against calcium overload [135].

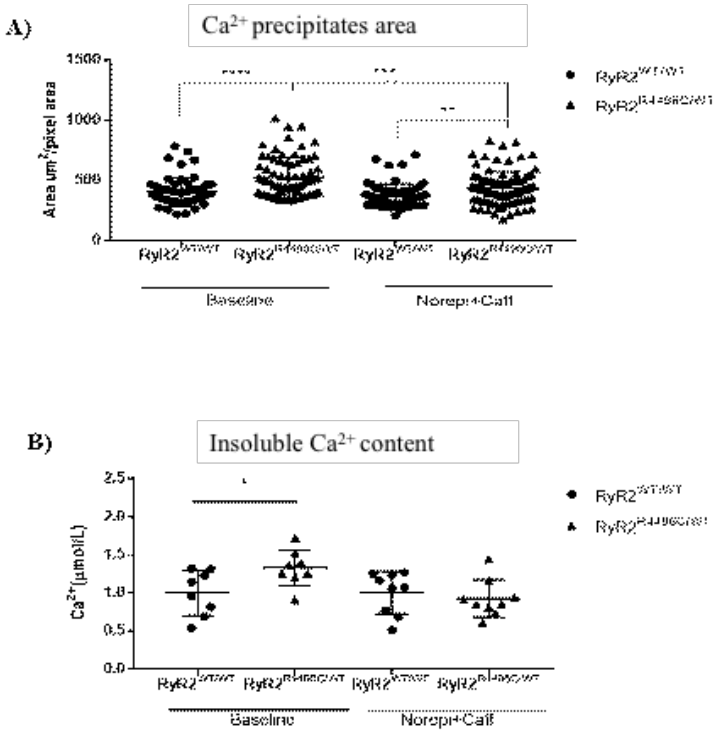

Figure 4.6. Insoluble Calcium analysis. A) We show the analysis of Electron microscopy images of Calcium precipitates in $RyR2^{WT/WT}$ and $RyR2^{R4496C/WT}$ mice both in baseline condition and post adrenergic stimulation (n=3, 10 images per sample P-value=** $p < 0.01$, P-value=***$p < 0.001$, P-value=**** $p < 0.0001$ Mann-Whitney). B) We show the analysis of the quantity of insoluble calcium in $RyR2^{WT/WT}$ and $RyR2^{R4496C/WT}$ mice both in baseline condition and post adrenergic stimulation (n=8, P-value=* $p< 0.05$, Mann-Whitney)

4.2.3 Measure of mitochondrial reactive oxygen species (ROS) levels.

We next investigated whether the increase in free calcium that we observed, may lead to ROS/RNS production. It has been reported how an excessive formation of mitochondrial ROS such as superoxide and hydrogen peroxide can be caused by a disruption in the RyR2 SR Ca^{2+} release complex, which has a significant impact on mitochondrial function [136]. Moreover, their close proximity to the dyad suggests that mitochondria can influence the local environment of redox-sensitive proteins involved in excitation-contraction coupling, such as RyR2. We performed flow cytometry experiments to evaluate the oxidative status of mitochondria in isolated cardiomyocytes loaded with fluorescent indicators. We were able to detect an increase in mitochondrial and cellular ROS and in $RyR2^{R4496C/WT}$ mice after adrenergic stimulation in comparison to both the WT and $RyR2^{R4496C/WT}$ mice in baseline condition (Figure 4.7).

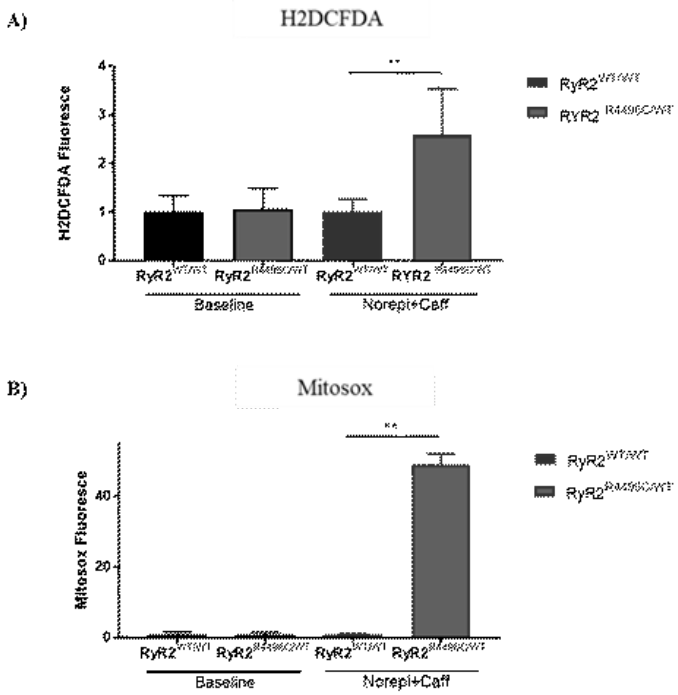

Figure 4.7. Cyto-fluorimetry analysis with ROS probes. We show the fluorescence intensity analysis of cardiomyocytes from $RyR2^{WT/WT}$ and $RyR2^{R4496C/WT}$ mice loaded

with the cellular ROS probe H2DCFDA (A) and with the mitochondrial ROS probe Mitosox (B) (n=3, P-value= ** $p<0.01$, Mann-Whitney)

The aforementioned data were later confirmed by confocal imaging of isolated cardiomyocytes loaded with the same probes. (Figure 4.8 A-F)

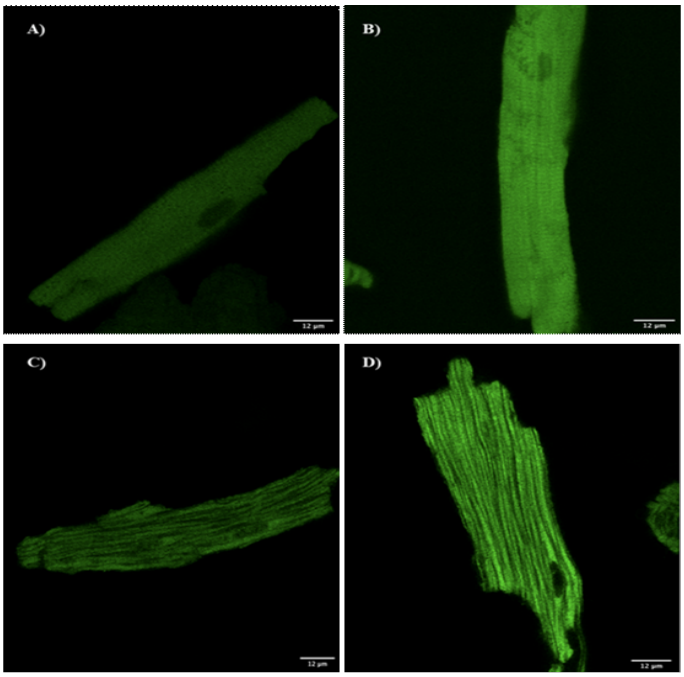
A)
B)
C)
D)

E)

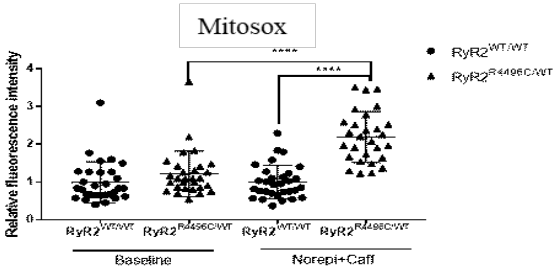
Mitosox
Relative fluorescence intensity
RyR2WT/WT
RyR2R4496C/WT
Baseline
Norepi+Caff

F)

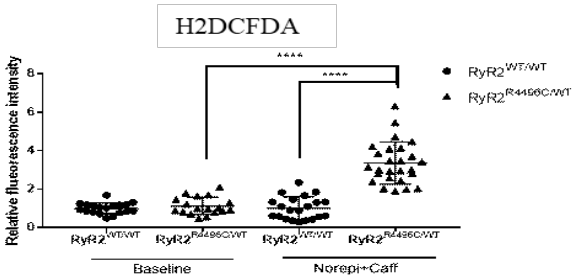
H2DCFDA
Relative fluorescence intensity
RyR2WT/WT
RyR2R4496C/WT
Baseline
Norepi+Caff

Figure 4.8. MitoSOX and H2DCFDA confocal images and analysis. A) $RyR2^{WT/WT}$ and B) $RyR2^{R4496C/WT}$ cells stained with H2DCFDA; C) WT and D) $RyR2^{R4496C/WT}$ cells stained with MitoSOX. We show the fluoresce intensity analysis of the probes Mitosox (E) and HDCFDA (F) in $RyR2^{WT/WT}$ and $RyR2^{R4496C/WT}$ mice in baseline condition and upon adrenergic stimulation (n=3, 10 images per animal, P-value= ****, $p< 0.0001$, Mann-Whitney)

We tested whether the observed increase in ROS could be associated with a decrease in the quantity of the superoxide dismutases SOD1 and SOD2. The data found confirmed our hypothesis by showing a decrease in $RyR2^{R4496C/WT}$ mice of, respectively, about 1.2 and 1.7-fold in the expression levels of superoxide dismutase 1 and 2 (Figure 4.9)

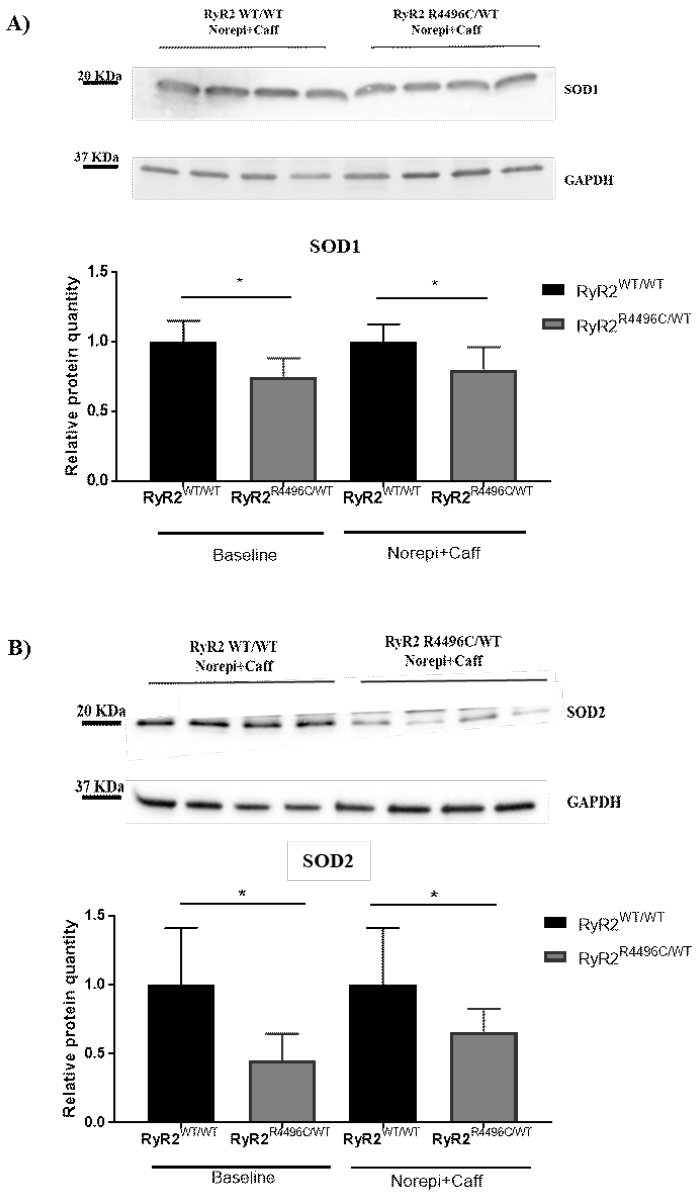

Figure 4.9. Western blot analysis of SODs. Immunoblot and protein quantification analysis of A) SOD1 B) SOD2 in $RyR2^{WT/WT}$ and $RyR2^{R4496C/WT}$ mice in baseline condition and upon adrenergic stimulation (n=8, P-value= *, $p < 0.05$, Mann-Whitney)

Given the evident finding of an increased ROS production in our model post adrenergic stimulation, we decided to evaluate the downstream effects it could provoke. Following a previously reported method, we assessed the oxidation status of proteins in $RyR2^{R4496C/WT}$ mice upon activation. To do this, the Oxidized Protein Western Blot Kit was used, whereby carbonyl groups of extracted proteins were derivatized to 2,4 dinitrophenylhydrazone (DNPH) by reaction with 2,4 dinitrophenylhydrazine and subsequently revealed by Western Blot [136]. We found that indeed stimulated $RyR2^{R4496C/WT}$ mice have an increased quantity of oxidized proteins compared to the WT counterpart (Figure 4.10).

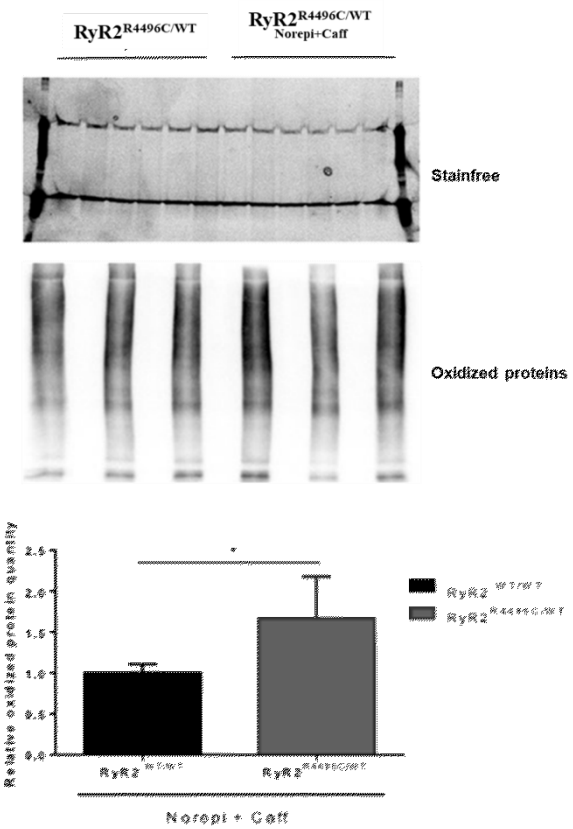

Figure 4.10. Western blot analysis of oxidized proteins. Immunoblot and protein quantification analysis of the relative quantity oxidized proteins in $RyR2^{WT/WT}$ and $RyR2^{R4496C/WT}$ mice upon adrenergic stimulation (n=5, P-value= * $p < 0.05$, Mann-Whitney)

In light of these results, we investigated whether RyR2 itself was more oxidized since it has been reported that this modification would lead to an increased "leakiness", and therefore exacerbate the, already present, extra release of Ca from the SR [136]. We found that immunoprecipitated RyR2 from adrenergically stimulated $RyR2^{R4496C/WT}$ mice is, in fact, more oxidized than in baseline $RyR2^{R4496C/WT}$ mice (Figure 4.18). In parallel, we performed the same experiment on $RyR2^{R4496C/WT}$ mice post adrenergic stimulation, treated in vitro with the antioxidant drug MitoTempo [136], and found that treatment does indeed reduce, although not statistically significant, the oxidation level of the immunoprecipitated RyR2. (Figure 4.11)

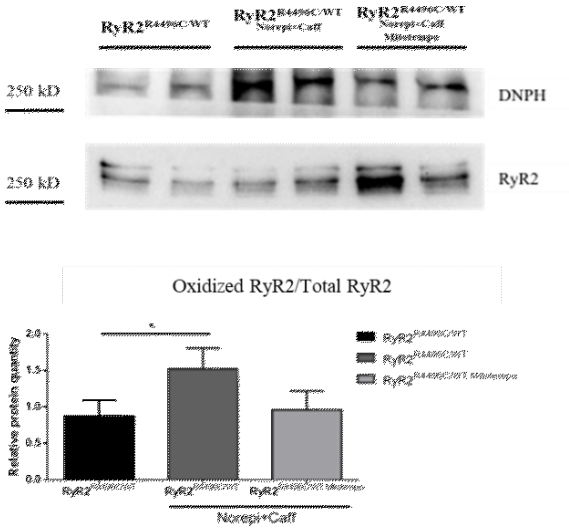

Figure 4.11. Western Blot analysis of oxidized immunoprecipitated RyR2. Immunoblot and protein quantification analysis of the relative quantity oxidized immuniprecipitated RyR2 from $RyR2^{R4496C/WT}$ mice baseline, $RyR2^{R4496C/WT}$ mice upon adrenergic stimulation and $RyR2^{R4496C/WT}$ mice upon adrenergic stimulation and treatment with MitoTempo (n=7, P-value= * $p< 0.05$, Kurskal-Wallis)

4.2.4 Assessment of mitochondrial energetics: ATP production, mitochondrial respiration and complexes activities.

It has been published very recently that the respiratory chain complexes are regulated both by mitochondrial free Ca^{2+} and Na^{+} [134], which itself depends on Ca^{2+} (via mitochondrial sodium/calcium exchange) and that also the TCA enzymes and glycolytic enzymes are directly regulated by Ca^{2+} [137]. Therefore, we expect that the increase in free mitochondrial Ca^{2+} in CPVT should translate into differences in mitochondrial physiology.

We first measured the ATP content in heart tissue homogenates in WT and $RyR2^{R4496C/WT}$ mice both at baseline and upon adrenergic stimulation by treating the samples with a commercial kit that relies on colorimetric quantification. We found a significant increase in the content of ATP in $RyR2^{R4496C/WT}$ mice upon adrenergic stimulation compared to the Wild type (Figure 4.12). We found that APT production significantly increases in CPVT mice upon adrenergic stimulation, which is a datum we expected considering the marked reaction our system has to adrenergic stimulation.

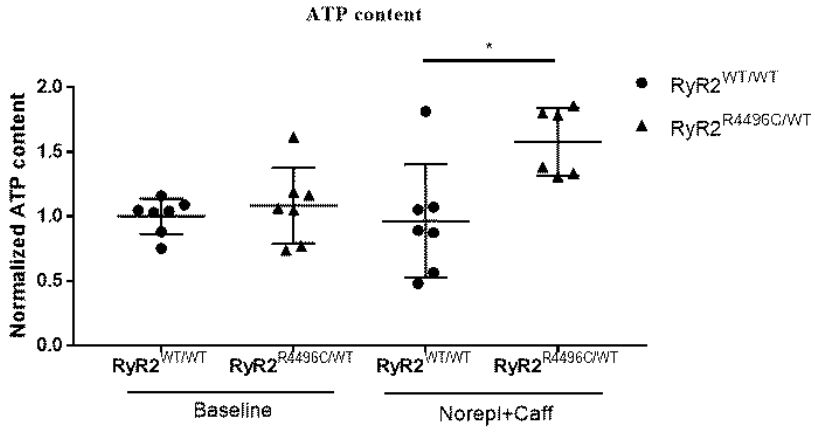

Figure 4.12. Measurement of ATP content. We show the normalized amount of ATP in tissue homogenates from $RyR2^{WT/WT}$ and $RyR2^{R4496C/WT}$ mice in baseline and upon adrenergic stimulation (n=7, P-value= * $p < 0.05$, Mann-Whitney).

Given ATP's production reliance on the Electron Transport Chain, we then performed a highly precise evaluation of mitochondrial respiration in our model using the Oroboros2k respirometry system. Upon standard mitochondrial isolation, respirometry experiments were performed in a closed chamber by sequentially adding substrates of the electron transport chain complexes and their specific inhibitor. The respiration was derived from the rate of oxygen concentration, which declines as the biological sample consumes oxygen. We found a significant decrease in $RyR2^{R4496C/WT}$ mice in respiration through complex I and II in baseline condition that upon adrenergic stimulation significantly increases (Figure 4.13).

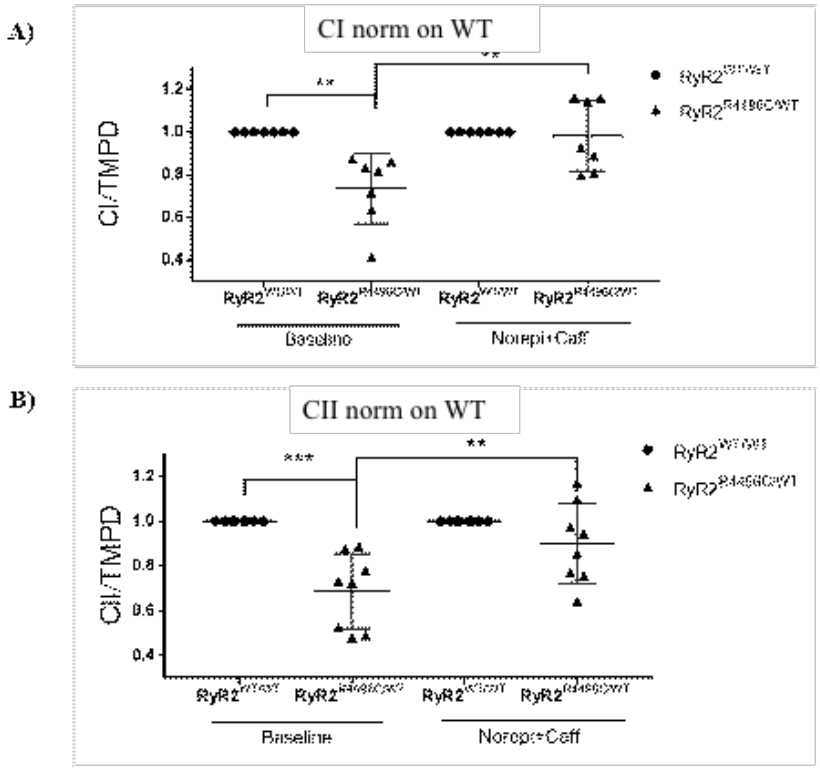

Figure 4.13. Mitochondrial respiration assessment. A) We show the respiration through complex I of the ETC normalized with the respiration through complex IV of $RyR2^{WT/WT}$ $RyR2^{R4496C/WT}$ mice both in baseline condition and post adrenergic stimulation (n=7, P-value= ** $p < 0.01$, Mann-Whitney). B) We show the respiration through complex II of the ETC normalized with the respiration through complex IV of $RyR2^{WT/WT}$ $RyR2^{R4496C/WT}$ mice both in baseline condition and post adrenergic stimulation (n=8, P-value= *** $p < 0.001$, Mann-Whitney).

These data prove to be quite interesting not only for the diminished respiratory capacity of the complexes in baseline condition, which could be an adaptation to the higher mitochondrial Ca^{2+} concentration found in our model but also for the extraordinary response to adrenergic activation that $RyR2^{R4496C/WT}$ mice have. For this reason, we set out to perform an additional spectrophotometric assay to evaluate the activity of each complex of the electron transport chain by supplying the direct substrate of each complex and then measuring the absorbance emitted by the reaction. We found significant differences only in the activity of complex I in baseline $RyR2^{R4496C/WT}$ mice compared to the WT counterpart. Of interest is how upon adrenergic stimulation the activity of the complex in $RyR2^{R4496C/WT}$ mice significantly increases (n=6; P-value= **) (Figure 4.14).

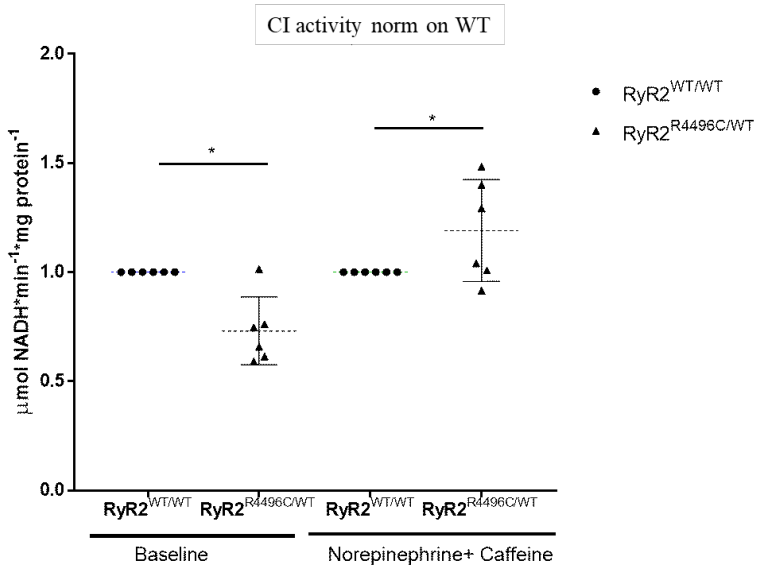

Figure 4.14. Analysis of complex I activity. We show the activity of complex I of isolated mitochondria from $RyR2^{WT/WT}$ and $RyR2^{R4496C/WT}$ mice both in baseline condition and post adrenergic stimulation (n=6, P-value= * $p < 0.05$, P-value=** $p< 0.01$, Mann-Whitney)

The present data regarding complex I is consistent with the results found by respirometry, and it could be an indicator of an adaptive mechanism employed by mitochondria in our model to better face the stimulus that the increased calcium entrance induces. In fact, it

would seem that through an unknown mechanism the enzyme is reversibly maintained in the deactivated form. Similarly, we performed complex activity assays on complex II, and we found that the single complex is not itself affected but the supercomplex II+III, the reportedly major contributor to respiration in the presence of succinate [138], displays the same pattern of reduced activity in baseline condition that increases upon adrenergic activation. (Figure 4.15)

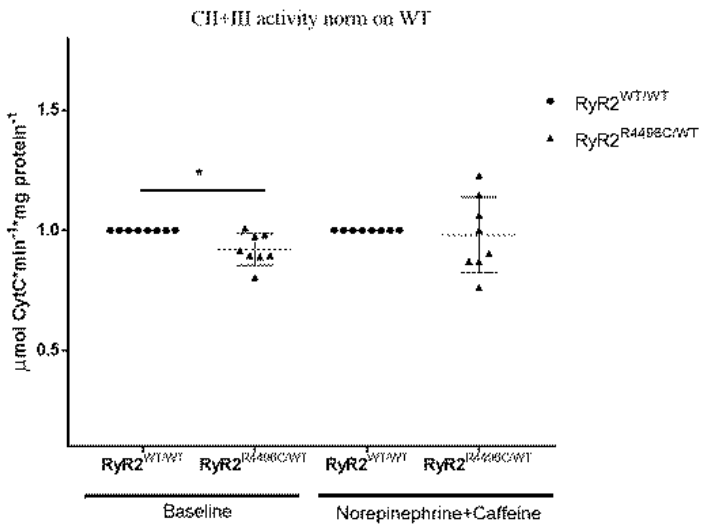

Figure 4.15. Analysis of complex II+III activity. We show the activity of supercomplex II+III of isolated mitochondria from $RyR2^{WT/WT}$ and $RyR2^{R4496C/WT}$ mice both in baseline condition and post adrenergic stimulation (n=8, P-value= * $p < 0.05$, Mann-Whitney)

Taken together these data suggest and adaptation of $RyR2^{R4496C/WT}$ mice to better handle the constant Ca^{2+} entrance in mitochondria in the baseline condition. Even though this adaptation seems to be overridden by an intense adrenergic stimulation.

4.2.5 Evaluation of mitochondrial metabolism

As part of our electron microscopy studies, we found an increase in the lipid droplet's area in $RyR2^{R4496C/WT}$ mice compared to the WT in baseline condition and instead, upon

adrenergic activation, we see an average value that is not significantly different from the control. (Figure 4.16).

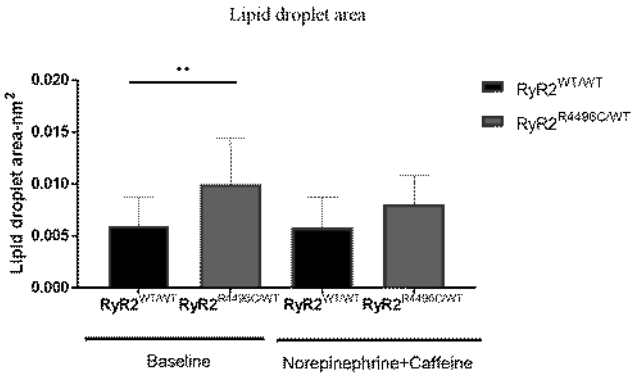

Figure 4.16. Electron microscopy analysis. We show the analysis of the area of lipid droplets in electron microscopy micrographs from $RyR2^{WT/WT}$ and $RyR2^{R4496C/WT}$ mice in baseline condition and upon adrenergic stimulation (n=3, 10 images per sample, P-value= **, Kurskal-Wallis)

Based on the literature from other cell types [14], our finding could be related to a potential substrate preference, by which cells would preferentially rely on glycolysis due to internal factors, such as an increase in cytosolic calcium and a reduction in mitochondrial respiration. Within the heart, lipid droplets represent either a stored form of energy or an indicator of defective fatty acid oxidation, coupled to nonregulated lipid uptake or associated with reduced heart function [139].

Moreover, changes in mitochondrial dynamics, such as an increase in mitochondrial fission, as we saw in $RyR2^{R4496C/WT}$ mice, have been shown in some cases to dictate the mitochondrial substrate preference for the energy requirements of the cell [140].

Furthermore, in the context of ischemia-reperfusion injury, lipid droplets have been shown to accumulate calcium, thus acting as a protective mechanism against cellular calcium overload [141].

However, noteworthy is the fact that the lipid droplets' areas in $RyR2^{R4496C/WT}$ mice upon adrenergic activation show a decreasing trend (not statistically significant) when compared to the areas of those found in baseline $RyR2^{R4496C/WT}$ mice. This could indicate a change in the metabolism induced by the adrenergic stimulation.

In light of these findings, we set out to perform a metabolic analysis of our model; we used the Seahorse extracellular flux (XF) to measure mitochondrial bioenergetics in isolated adult mouse cardiomyocytes. XF measures the extracellular acidification rate (ECAR) of the assay medium as a surrogate for the estimation of the glycolytic flux [142]. We performed this experiment on mice in baseline condition and found that $RyR2^{R4496C/WT}$ mice had higher levels of glycolysis compared to the WT, which could be an adaptation to better face stress of our model as it has been reported in cardiac hypertrophy [143]. The same experiment performed on mice post adrenergic stimulation shows an opposite result; in fact, $RyR2^{R4496C/WT}$ mice had a significant reduction in the glycolysis pathway than the control. (Figure 4.17)

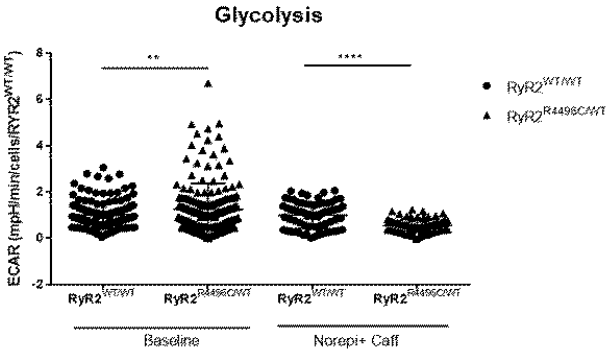

Figure 4.17. Glycolysis assessment. We show the ECAR parameter used to evaluate glycolysis levels in isolated cardiomyocytes from $RyR2^{WT/WT}$ and $RyR2^{R4496C/WT}$ mice in baseline and post adrenergic stimulation condition (n=5, P-value=** $p< 0.01$, P-value=****, $p<0.0001$ Mann-Whitney)

This datum can be explained by the changes in mitochondrial dynamics we found in our model upon adrenergic stimulation, meaning the increase of mitochondrial (i.e., active) Drp1 protein. In fact, it has been reported that there is a competition between Drp1's binding to mitochondria and the binding (i.e., activation) of the first rate-limiting enzyme of the glycolytic pathway, Hexokinase II (HK II) [144].

We, therefore, performed a Western Blot analysis to quantify the total protein levels of HK II and found no significant differences. However, since it is known that the active form of the enzyme translocates to the mitochondrial membrane we performed a fractionation of mitochondrial-bound proteins and cytosolic proteins. We found a decrease in the ratio of mitochondrial (i.e., active) and cytosolic (i.e., inactive) fraction of the protein in our model compared to the WT, both in the baseline condition and more so in the adrenergically stimulated condition. As mentioned before, we instead found a reversed situation when performing an analysis of the mitochondrial/cytosolic ratio of DRP, where we saw a distinct increase in the ratio of the mitochondrial/cytosolic fraction in $RyR2^{R4496C/WT}$ mice upon adrenergic activation. (Figure 4.18).

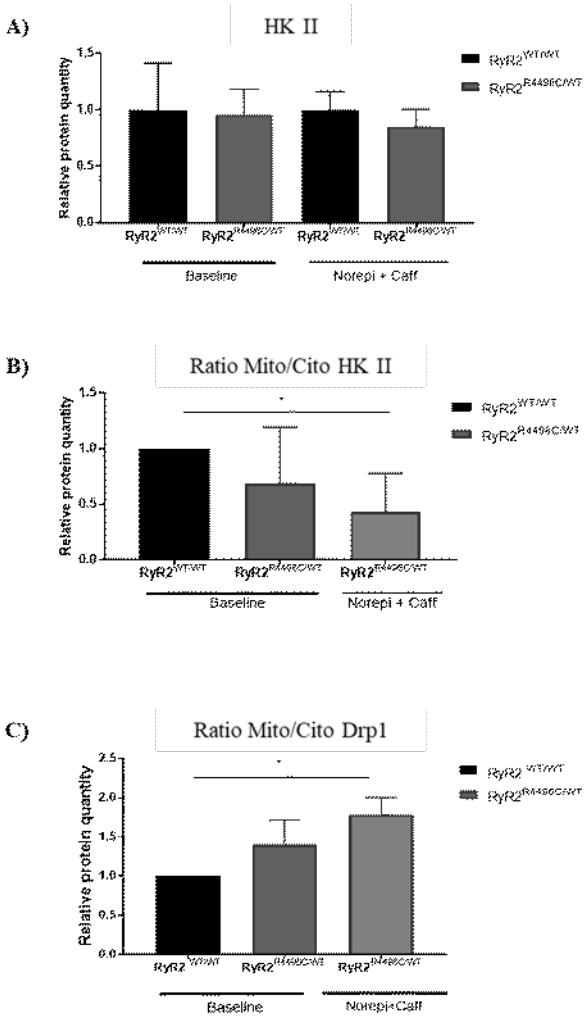

Figure 4.18. Western blot analysis of HKII. Immunoblot and protein quantification analysis of A) HKII B) the ratio of mitochondria/cytosolic HKII C) the ratio of mitochondrial/cytosolic DRP1 in heart extracts from $RyR2^{WT/WT}$ and $RyR2^{R4496C/WT}$ mice in baseline condition and upon adrenergic stimulation (n=4, P-value= *, $p < 0.05$, Mann-Whitney)

Given the findings concerning the glycolytic pathway we set out to evaluate the state of fatty acids beta-oxidation (FAO), especially taking into consideration what is reported in the literature regarding the stimulatory effect adrenergic stimulation has on FAO [145]. We found that while in the baseline condition there are no major changes between $RyR2^{R4496C/WT}$ mice and WT mice, we see, as expected, a marked increase in the activity of beta-oxidation in our model as a response to adrenergic activation. (Figure 4.19)

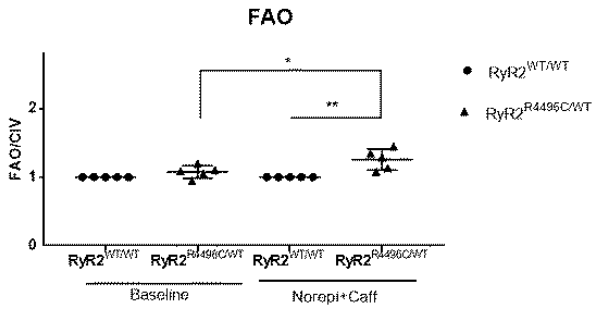

Figure 4.19. Beta-oxidation assessment. We show the analysis of the activity of beta-acid oxidation (normalized over the activity of ETC complex IV) from isolated mitochondria from $RyR2^{WT/WT}$ and $RyR2^{R4496C/WT}$ mice in baseline and post adrenergic stimulation condition (n=5, P-value=* $p< 0.05$, P-value=** $p< 0.01$, Mann-Whitney)

4.3 Identification of the channels implicated in mitochondrial Calcium uptake in CPVT mice

In order to identify the main channels implicated in mitochondrial Calcium uptake in CPVT mice we used RNA-interference strategies to silence the gene encoding for VDAC2, an OMM ion channel implicated in calcium uptake into mitochondria. Our goal was to see whether silencing the channel would impair the development of the mitochondrial alterations we have seen in our CPVT model and if it might increase the risk of arrhythmic episodes due to mitochondria's Ca^{2+} buffering role.

4.3.1 Generation of the miRNA molecule

RNA interference induces the degradation of an mRNA with a sequence complementary to a double-stranded RNA. It is a powerful, reversible, inexpensive, fast gene expression control system that has several applications in the field of scientific research and the therapeutic field, in particular gene therapy. After being processed by cellular enzymes, this small interfering RNA, initially called micro-RNA (miRNA), hybridizes with the mRNA produced by the target gene and inactivates it. The inactivation of the gene is the inactivation of the mRNA, so it is better to talk about the down-regulation of the gene. The construct was intended to selectively reduce VDAC2 expression. The recombinant plasmid was created when the dsRNA was inserted into the vector backbone as the final step in creating the recombinant plasmid. It was a 23 bp dsRNA of which 19 paired and 2 protruding nucleotides at each 3'OH end. (Figure 4.20) We were able to generate one dsRNA, called: mirVDAC2 544.

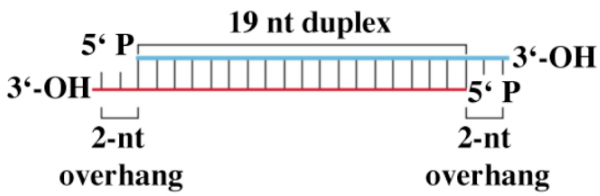

Figure 4.20. Theoretical display of the miRNA structure.

The encoded pre-miRNA ds oligo was ligated with the linearized pcDNATM6.2-GW/EmGFP-miR vector, which has 4-nucleotide 5′ overhangs on each strand to allow directional cloning. This vector permits the designed miRNA to be expressed under the control of the thymidine kinase (TK) polyadenylation signal and the Pol II human CMV (cytomegalovirus) promoter. Through the co-cistronic expression of EmGFP, we have the ability to visibly select the cells producing the miRNA. In order to obtain a larger quantity of our desired plasmid, we transformed the ligated vector into competent bacterial cells. We used the TOP10 E. coli cells (Invitrogen), which have been transformed using the “heat shock” procedure.

4.3.2 Evaluation of *in vitro* RNA and proteins silencing by pcDNAmirVDAC2_544 on C2C12 cell line

Since miRNAs cause mRNA degradation, the efficacy and specificity of miRNA-mediated transfection were assessed at both the mRNA and protein level.

Total RNA was obtained 48 hours after transfection from transfected C2C12 cells. The effect of the miRNA on the expression of the gene of interest was investigated using quantitative Real-Time PCR, which amplified the GFP and VDAC2 coding sequences for each sample (one transfected and the control) using specified primers. We found that the miRNA was able to significantly suppress VDAC2 mRNA expression when compared to the control. In parallel, we verified the effectiveness and specificity of miRNA-mediated silencing at the protein level. Total proteins were obtained 48 hours after transfection of C2C12 cells and the miRNA effect on the proteins of interest was investigated by Western Blot analysis.

Similarly to the Real Time-PCR data, the results showed the ability of the miRNA VDAC2 544 to knockdown the protein quantity of VDAC2 in the transfected cells in comparison to the non-transfected control. We, therefore, carried on with the preparation of our silencing molecule.

4.3.3 Cloning in pAAV2.1

Wild-type AAV contains a 4.7 kb genome made up of the rep and cap genes encoding 4 replication and 3 capsid proteins, respectively, flanked by two 145-bp inverted terminal repeats (ITRs). Recombinant AAV (rAAV) vectors retain only the AAV ITRs, thus leaving up to 4.7 kb for the packaging of therapeutic DNA.

From the obtained plasmids, a fragment consisting of the CMV promoter, EmGFP, pre-miRNA sequence, and TKpolyA was amplified by PCR with specific primers, which included the NheI (Forward), and SphI (Reverse) cloning sites. This amplicon was ligated into the pre-digested NheI – SphI sites of the adeno-associated viral backbone vector pAAV-2.1 provided by InnovaVector (Pozzuoli, Italy). The correct insertion of the mirVDAC2 544 amplicon inside the AAV2.1 backbone vector was confirmed by analytic digestion of the ligation with the restriction enzymes NheI and SphI. The pattern of bands visualized on the agarose gel allows the identification of the clones carrying the correct construct.

4.3.4 Evaluation of RNA and proteins silencing by pAAV2.1_CMV-GFP-mirVDAC2_544-TKpolyA on C2C12 cell line

As we performed before with the pcDNAmirVDAC2, we tested the pAAV2.1_CMV-GFP-mirVDAC2-TKpolyA *in vitro* in order to evaluate the efficacy and efficiency of the viral construct. We transfected C2C12 cell lines and assessed the efficacy of our construct both at the RNA and protein level. We found that our previous data were confirmed.

The construct was later cultured, and the DNA extracted up to the quantity requested by the external production facility.

4.3.5 *In vivo* screening results

We injected 150 µl (~ 9,7 x10^{11} GC) of AAV 2/9 CMV-GFP-miR VDAC2-TK polyA, in $RyR2^{R4496C/WT}$ mice at day 8 after birth via intraperitoneal injection. The mice were intended for ECG analysis and subsequently for the extraction of mRNA and proteins, and for enzymatic isolation of cardiomyocytes.

The mice were studied at 12 weeks of age and divided into two groups: one, which underwent infection and adrenergic stimulus, and the control group, which underwent adrenergic stimuli but was not infected. Before all the experiments, the mice also underwent an echocardiographic examination to evaluate possible cardiac morphological alterations; we did not find any structural alterations.

4.3.5.1 ECG

With the ECG recordings we evaluated the arrhythmogenic phenotype of the $RyR2^{R4496C/WT}$ +mir VDAC2 in correlation to the phenotype of $RyR2^{R4496C/WT}$ mice.

The $RyR2^{R4496C/WT}$ mutation allows the opening of RyR2 at reduced cytosolic Ca^{2+} levels; it is regarded as a gain of function that, by lowering the SR threshold, promotes spontaneous calcium release and facilitates the development of ventricular tachycardia.

ECG radiotelemetry transmitters were implanted subcutaneously under general anesthesia to measure ECG data in mice (heterozygous $RyR2^{R4496C/WT}$ and infected heterozygous $RyR2^{R4496C/WT}$ +mir VDAC2 mice). After 72 h of recovery from surgery, not infected and mirVDAC2 infected mice phenotype characterization was performed. First, basal ECG was recorded for 10 minutes since it is our baseline condition to which we compare the results of the stimulated condition. Subsequently, mice were adrenergically stimulated and the ECG was recorded for 15 minutes.

The result was an incidence of ventricular tachycardia in 5 out of 7 infected mice, compared with 4 out of 7 in not infected mice. (Figure. 4.21)

We believe this datum is related to the fact that the construct is able to diminish the entry of Ca^{2+} into the mitochondria (therefore preventing mitochondrial alterations and excessive ROS production) and limit the buffering function that mitochondria have on the cytosolic Ca^{2+}, consequently increasing the cytosolic concentration of these ions that it is the main trigger of arrhythmic events in the context of CPVT. However, we believe that the almost identical result in the two samples is because VDAC2 is not the only mitochondrial channel involved in the pathophysiology of the CPVT mouse, so its silencing is not able to drastically change the occurrence of the arrhythmogenic phenotype.

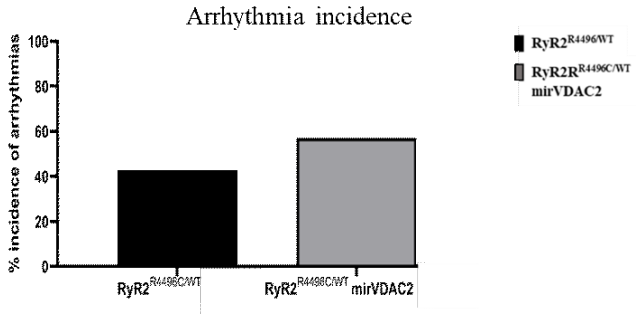

Figure. 4.21. Arrhythmia incidence chart. Incidence of arrhythmic events in $RyR2R^{R4496C/WT}$ and infected $RyR2R^{R4496C/WT}$ mirVDAC2 mice (n=7).

4.3.5.2 mRNA and proteins expression

Total RNA was obtained from the hearts of control mice and the infected mirVDAC2 mice; reverse transcription was utilized to convert RNA into cDNA. The effect of the viral targeting on the expression of the gene of interest was investigated using quantitative Real-Time PCR, amplifying the GFP and the VDAC2 sequences for each sample using specified primers.

The results of the Real Time-PCR experiment show a significant relative mRNA knockdown. The virus suppressed roughly 60% of VDAC2 mRNA expression when compared to the controls. We, therefore, obtained the first *in vivo* confirmation that this construct is able to knockdown the mRNA expression. (Figure 4.22).

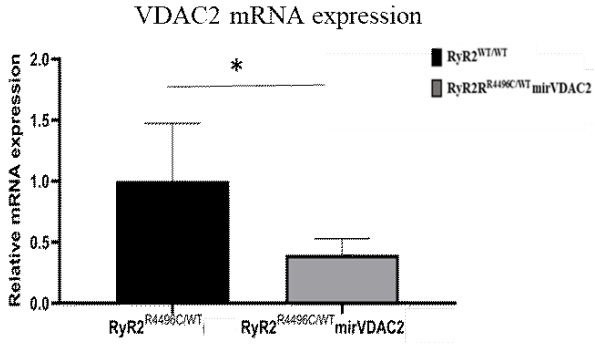

Figure. 4.22. Real Time analysis of VDAC2 expression. Analysis of VDAC2 relative mRNA expression in mice infected with mirVDAC2 relative to $RyR2^{R4496C/WT}$ mice. (n=4, P-value=*, $p<0.05$, Mann-Whitney test)

We also verified the effectiveness of the viral construct at the protein level. Total proteins were obtained from the hearts of both control mice and the infected mirVDAC2 mice. The viral targeting effect on VDAC2 was investigated by Western Blot analysis, incubating the Western Blot membrane with the VDAC2 antibody.

Similarly to the Real Time-PCR experiment, the results of the immunoblotting experiment show the capacity of this silencing molecule to reduce VDAC2 protein quantity. The mirVDAC2 suppressed about 80% VDAC2 protein expression in comparison to the controls. (Figure 4.23)

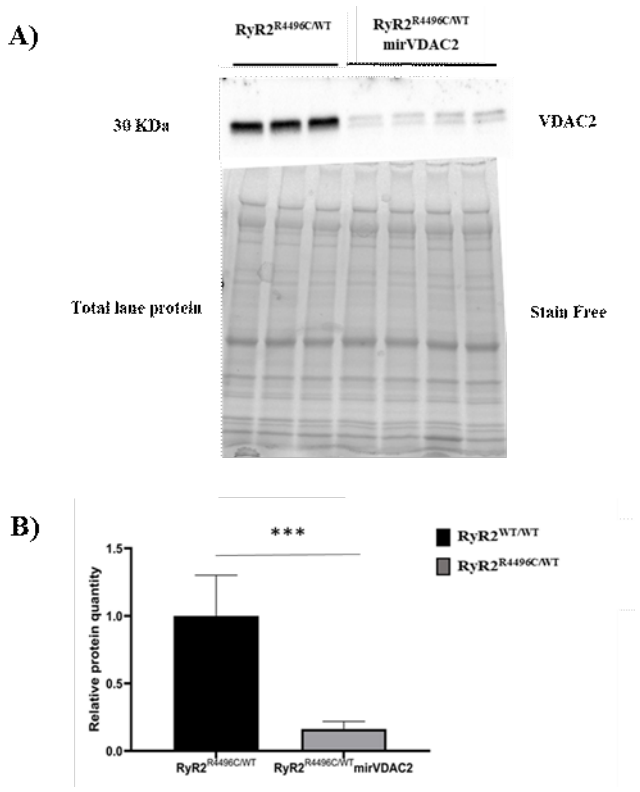

Figure. 4.23. Western Blot analysis of VDAC2 expression. Immunoblot and protein quantification analysis of VDAC2 relative protein expression in mice infected with mirVDAC2 relative to $RyR2^{R4496C/WT}$ mice. (n=7, P-value= ***, $p < 0.001$, Mann-Whitney test)

4.3.6 Mitochondrial Ca^{2+} evaluation

As was mentioned before, the closeness of mitochondria to Ca^{2+} release sites is critical to facilitate fast mitochondrial Ca^{2+} absorption during SR Ca^{2+} release; especially in CPVT. We previously proved that in our model mitochondria uptake a greater quantity of calcium. Given the efficacy of our silencing molecule, we set out to evaluate whether its administration to $RyR2^{R4496C/WT}$ mice would revert the observed increase in mitochondrial calcium content. In fact, if the VDAC2 channel is majorly involved in Ca^{2+} entry into $RyR2^{R4496C/WT}$ mitochondria and its silencing should prevent excess Ca^{2+} to enter.

Following the same protocol reported before, we discovered that after the infection with mirVDAC2 the amount of mitochondrial calcium in treated $RyR2^{R4496C/WT}$ mice was reduced, reaching levels comparable to those of WT mice. (Figure 4.24). With these experiments, we can therefore confirm the involvement of VDAC in the increase in free mitochondrial Ca^{2+} in CPVT.

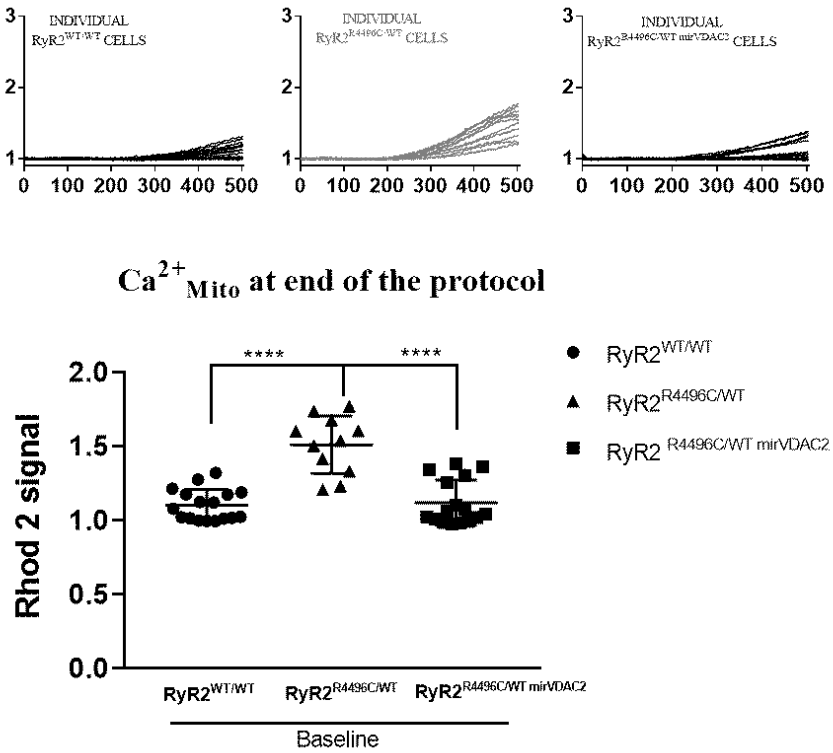

Figure. 4.24. Mitochondrial calcium post infection with mirVDAC2. We show the behaviour of the signal of each cell from the analyzed groups. We then show the analysis of the Rhod2 signal at the end of the collection protocol in $RyR2^{WT/WT}$ $RyR2^{R4496C/WT}$ mice, $RyR2^{R4496C/WT}$ +mir VDAC2 (n=4, P-value=****, p<0.0001, One-way ANOVA).

4.3.7 Mitochondrial reactive oxygen species (ROS) levels in pAAV2.1_CMV-GFP-mirVDAC2_544-TKpolyA infected mice

Given our findings of a correlation between an excessive calcium uptake by mitochondria and ROS production in our model, we set out to evaluate whether VDAC2 silencing would revert the increase in reactive species we previously observed.

With the same experimental settings we previously described, we analyzed isolated cardiomyocytes from $RyR2^{R4496C/WT}$ +mir VDAC2, versus $RyR2^{R4496C/WT}$ cardiomyocytes both in the baseline condition and upon adrenergic stimulation (given the fact that is the stimulus that induces ROS production in our model).

We were not able to analyze with the H2DCFDA probe due to the emission interference of the GFP tag present in our viral construct.

We found that infected mice in both conditions showed a significantly reduced mitochondrial ROS production compared to baseline $RyR2^{R4496C/WT}$ mice (n=5). We performed the analysis in comparison to baseline $RyR2^{R4496C/WT}$ mice since adrenergic stimulation significantly increased the production of ROS in our model (Figure. 4.25, 4.26)

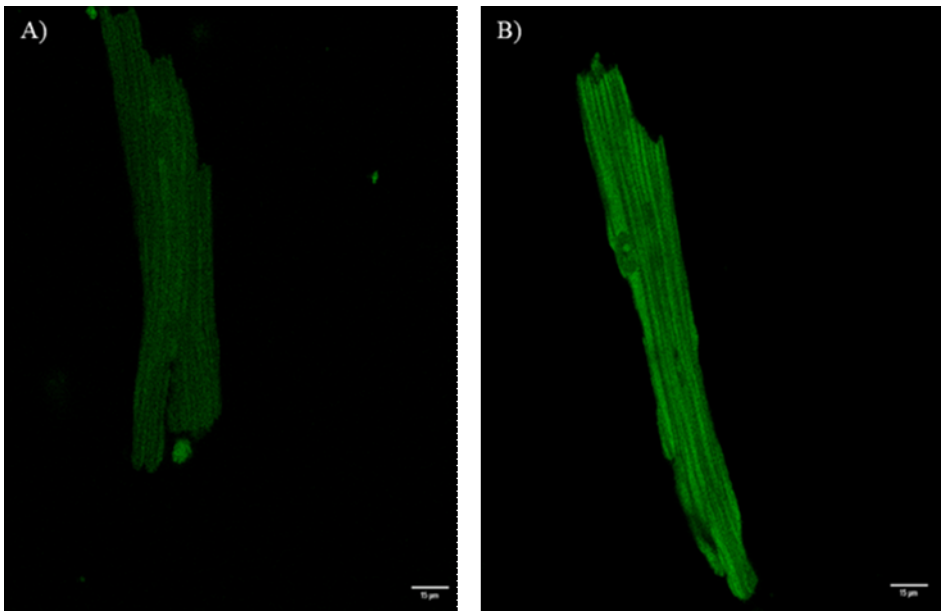

Figure.4.25. Mitosox confocal images post infection with mirVDAC2. A) $RyR2^{WT/WT}$ and B) $RyR2^{R4496C/WT}$ cells stained with MitoSOX post infection with mirVDAC2

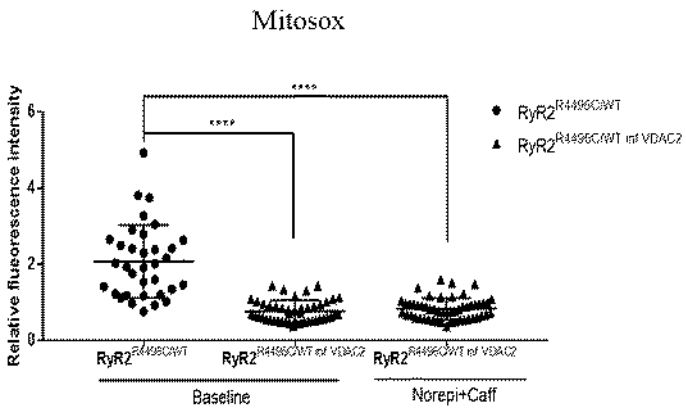

Figure. 4.26. Mitosox fluorence analysis post infection with mirVDAC2. We show the fluoresce intensity analysis of cardiomyocytes labeled with Mitosox (n=4, P-value= ****, p< 0.0001, Mann-Whitney)

This result is further proof of our hypothesis that correlates the increase of mitochondrial Ca^{2+} content and the cascade of events that leads to physiological and structural alterations in the mitochondrion.

5. Discussion

In cardiomyocytes, mitochondria occupy almost 35% of cell volume and the ATP that they generate allows heart excitation-contraction, a high-energy demanding process [146]. The release of Ca^{2+} from the sarcoplasmic reticulum by ryanodine receptors (RyR2s) initiates muscle contraction and the local transfer of Ca^{2+} to the mitochondrial matrix activates enzymes of the tricarboxylic acid cycle to drive the electron transport chain (ETC) in order to accelerate ATP production [147], thereby providing a link between Ca^{2+} -dependent contraction and mitochondria metabolic output.

Leakage of Ca^{2+} from the SR can cause triggered activity and life-threatening cardiac arrhythmias. This is the basic pathologic mechanism in Catecholaminergic Polymorphic Ventricular Tachycardia (CPVT), an inherited arrhythmic disease characterized by mutations in the Ryanodine receptor type 2 [148] gene or in the other proteins of its macromolecular complex. CPVT is characterized by ventricular tachycardia and fibrillation that occur in patients after exercise or stress. Of relevance, it has been observed that during β-adrenergic stimulation, increased energy demand directly accelerates oxidative phosphorylation and electron flux at the electron transport chain to produce more ATP but this can result in enhanced mito-ROS emission, leading to oxidation of RyR2 channel and thus augmenting Ca^{2+} leak [149, 150]. It has also been reported how massive increases in mitochondrial Ca^{2+} lead to calcium overload, and this is a known mechanism for substantial increases in electron-transport-chain-generated superoxide [151].

Taken together, the observations reported in the literature point toward a direct relation between calcium homeostasis and mitochondria. What still needs to be understood is what changes, besides an increase in ROS production, calcium-handling aberrations can induce in mitochondrial physiology.

In 2017 our group observed, through electron microscopy studies, that $RyR2^{R4496C/WT}$ mice ventricular myocytes have damaged mitochondria in terms of morphological features such as a marked disruption of the crista, a condition that, in the long-term, could severely impair the cardiac function [129].

In the present study, we test the hypothesis that augmented RyR2-mediated SR Ca^{2+} leak through increased mitochondrial Ca^{2+} uptake induces mitochondrial disruption, metabolic alterations, and mito-ROS production. We also hypothesize that these changes can be prevented by modulation of the expression of mitochondrial channels involved in Ca^{2+} uptake from the cytosol. Our investigation is inserted into a larger project aimed at better understanding the molecular basis of the interaction between the SR calcium release units and the cardiac mitochondria in CPVT.

The mechanism that induces the arrhythmic event in both patients and our CPVT mouse model is the adrenergic stimulation, for this reason, we studied and characterized mitochondrial morphology and physiology both in the baseline condition and upon adrenergic activation.

In the **baseline condition** we proved that the pillar of our hypothesis is confirmed; in fact, by data obtained in live cell imaging of mitochondrial Ca2+ dynamics, we showed that the enhanced RyR2-mediated Ca2+ leak in our model results in a higher ability of mitochondria to accumulate and retain Ca2+. Of importance in the context of ion balance, are the data found concerning the presence of insoluble calcium in the form of precipitates in cardiomyocytes from RyR2R4496C/WT mice, which show the necessity in our model to find alternative ways to clear the excess calcium and store it.

As an unexpected finding, we observed that in our model the mitochondrial membrane potential is mildly hyperpolarized in comparison to the control, which might partially contribute to the mitochondrial calcium uptake. It was reported in a different model that a CI and CII inhibition induces a proton-based $\Delta\psi$ hyperpolarization. This hyperpolarization was associated with low levels of CI and CII-driven O_2 consumption and was prevented by co-inhibition of CII, CIII, or CIV activity. CI- and CII-inhibition similarly reduced free matrix ATP levels and increased the cell dependence on extracellular glucose to maintain cytosolic free ATP [152]. It was also reported that a mitochondrial hyperpolarization of the membrane potential was demonstrated to precede an excessive generation of ROS [153].

With these reported pathways in mind, we set out to evaluate mitochondrial respiration and complexes' activities in our RyR2R4496C/WT mice. We found that, as expected, there are changes in our model at the respiratory level, meaning a decrease in respiration through complex I and II, confirmed by a decreased activity of isolated complex I and supercomplex II+III. We hypothesize that these alterations are driven by an adaptation of the system in the baseline condition in order to avoid excessive ROS production induced by an increase in mitochondrial calcium, which is known to stimulate electron transport chain transfer and therefore increase the probability of reverse electron transport, which is the main source of ROS [154].

Given these findings of alterations in mitochondrial physiology, we set out to evaluate whether this would induce major changes in our model's cardiac metabolism. In fact, we found an increase in glycolysis, which could be an adaptation to better face the stress in our model, as it has been reported in cardiac hypertrophy [143]. We attribute the first phenomenon to the reported increase of cytosolic calcium in our model, as it is reported that an increase in cytosolic calcium can stimulate glycolysis [137]. This data concerning the metabolism and the substrate preference in our model is actually in line with the

electron microscopy data we found concerning the area of lipid droplets, which is increased in the baseline condition (due to an increased use of glucose as a fuel source).

Upon **adrenergic activation**, we, once again, confirmed that also in this condition, our main hypothesis of increased mitochondrial calcium uptake in our model due to the enhanced RyR2-mediated Ca2+ leak was proven correct. We, in fact, saw that in RyR2R4496C/WT mice, this results in a higher ability of mitochondria to accumulate and retain Ca2+. This datum is all the more obvious in this stimulated condition, in comparison to the baseline condition, since the mitochondrial Ca2+ concentration is not only greater than that of the Wild type but is also uptaken at a faster rate.

We also found that there is a decreasing trend of the quantity in insoluble calcium and the area of the calcium phosphate precipitates. We speculate that this is due to an acidification of the matrix due to the increase in respiration, which solubilizes the calcium, which is then extruded by the NCLX transporter in order to avoid mitochondrial calcium overload [155].

We then observed by electron microscopy that adrenergic stimulation by norepinephrine and caffeine increases the number of mitochondria and reduces their size. These data were confirmed by an increase in the fission/fusion ratio noted as a higher DRP1 protein expression in RyR2R4496C/WT mice compared to controls. This phenomenon is likely to occur due to the reported mechanism in which DRP1 is phosphorylated (i.e., activated) by CAMKII [156], whose activity is reported to be augmented in our CPVT model [130]. It is unknown if this occurrence offers beneficial or detrimental consequences. We also found that in our model fusion proteins Mitofusin 1 and 2 are decreased in quantity. This phenomenon could be attributed to the fact that, as it was reported, Mitofusins can be degraded by the cysteine protease calpain pathway, which is activated at relatively high ambient Ca2+ concentrations of about 1 μmol/L [157]. A reduction in the quantity of these fusion proteins has been reported to increase ER and mitochondria coupling, given Mitofusin's tethering role in the cell [158]. Taken together, these data suggest that calcium has a dual role in inducing the degradation of fusion proteins and the activation of fission proteins, possibly in order to increase the mitochondrial buffering capacity.

We then moved on to evaluate once again the respiratory capability of our system and the metabolic status, since it has been reported that changes in mitochondrial dynamics can induce alterations in mitochondrial function. We found that mitochondrial respiration and consequently the complexes' activities are increased in comparison to the RyR2R4496C/WT mice in the baseline condition, reaching the same levels as the control group. We believe that, while in baseline there seems to be an adaptation of the system to avoid excessive ROS production, this condition is overridden by the intense adrenergic stimulus that induces a massive calcium entrance and therefore an increase in

mitochondrial respiration which leads to both an increase in ATP production and also, as a detrimental effect, an increase in ROS production.

We, in fact, found that in our model there is a marked increase in ATP production upon adrenergic activation. Given this finding, we set out to perform a more thorough metabolic assessment. We discovered that there is a decrease in the glycolytic pathway activity, which we ascribe to the known competition of the binding site between the fission protein Drp1 and the rate-limiting glycolytic enzyme HKII. In fact, it has been reported that increased recruitment of fission protein Drp1 to the mitochondrial membrane inhibits the binding of HKII and therefore the glycolytic pathway [144]. Specularly, we also observe a marked increase in fatty acid oxidation upon adrenergic stimulation, which has been reported to occur both in healthy hearts [159] and in Heart Failure [160]. In this instance, it has been demonstrated how in models of HF, it was found that β_2-adrenergic receptor stimulation shifts substrate preference towards free fatty acids (FFA) oxidation which in turn is associated with greater and deleterious myocardial oxygen requirement [161]. This data is in line with the electron microscopy data we found concerning the area of lipid droplets, which moderately decreased upon adrenergic stimulation, we speculate due to the increase in fatty acid oxidation driven by the excessive response to the adrenergic pathway stimulus.

It is known that in some cardiac diseases such as heart failure (HF), an abnormal mitochondrial function could be paralleled by increased emission of reactive oxygen species (ROS) [150]. Excessive mitochondria-derived ROS (mitoROS) may cause significant changes in intracellular Ca^{2+} homeostasis [128]. It was demonstrated that increased activity of the electron transport chain results in enhanced mito-ROS production, which can overcome intracellular antioxidant defenses and produce cell-wide deleterious effects. In our CPVT model, we found a reduced ability of the system to clear ROS due to a reduction in protein quantity of the enzymes superoxide dismutases SOD1 and SOD2 and an increase in ROS production upon adrenergic stimulation.

Importantly, it has been reported that in CPVT mito-ROS could mediate an increased activity of RyR2 that is reflected by an augmented propensity to aberrant Ca^{2+} leak from the sarcoplasmic reticulum leading to an increased incidence of pro-arrhythmic diastolic Ca^{2+} waves [163]. It was also reported that in a different model of CPVT prolonged exposure to β-adrenergic agonists evoked deleterious effects on Ca^{2+} cycling due to enhanced RyR2 oxidation (thereby its activity) by mito-ROS [136]. We have confirmed this data by showing how in our CPVT model there is an increase in total oxidized proteins and an increase in oxidized RyR2. Consequently, we indirectly confirmed that increased Ca^{2+} leak via hyperactive RyR2 channels drives further SR Ca^{2+} leak via mito-ROS, in an indirect, positive feedback process that is detrimental to intracellular Ca^{2+} handling. We have also shown how treatment with the antioxidant drug Mitotempo partially reverses this phenomenon by mildly reducing the oxidative level of RyR2. Our

data suggest that it exists a deleterious loop between SR and mitochondria in which SR Ca^{2+} leak triggers mitochondrial damage and increases ROS production, which in turn further oxidizes RyR2 and enhances intracellular Ca^{2+} leak, contributing to the maintenance of impaired cardiac function in CPVT.

To better characterize the specific contribution of single protein players in Ca^{2+} release from SR and Ca^{2+} uptake by mitochondria, we decided to silence VDAC2 in CPVT cardiomyocytes. In a previous work on our CPVT model, it was demonstrated how the stimulation of VDAC2 activity drove an augmented Ca^{2+} -buffering activity of mitochondria and therefore lead to an arrhythmic phenotype rescue [7]. In this work mitochondrial physiology was not explored, therefore we cannot conclude that this therapeutic approach would not be detrimental in the long term. We designed an opposite approach in order to prove that the event responsible for the mitochondrial alterations we observe is the excess in mitochondrial Ca^{2+} deriving from an aberrant Ca^{2+} leak from the SR.

VDACs play a key role in calcium homeostasis, particularly in cardiac cells, by transporting Ca^{2+} from the cytosol through the outer mitochondrial membrane towards the inside of the organelle, thus rapidly decreasing cytosolic Ca^{2+} [76]. With the aim of inducing RNA interference toward VDAC2 we generated an artificial miRNA targeted to the VDAC2 gene. The silencing construct was tested *in vitro* in order to verify the knockdown efficiency (about 80% of protein expression is suppressed) and inserted into an adeno-associated viral vector that was used to infect young $RyR2^{R4496C/WT}$ mice. We were able to document that VDAC2 is one of the main mediators, although not the only, of the buffering activity that mitochondria exert on cytosolic Ca^{2+} released during adrenergic stimulation in CPVT settings. Indeed, myocytes with VDAC2 knockdown presented lower mitochondrial Ca^{2+} levels (that returned to almost physiological levels) and lower mito-ROS production when compared to $RyR2^{R4496C/WT}$ non-treated animals.

Importantly, despite VDAC2 silencing being able to prevent mito-Ca^{2+} overload, it did not have any effect on arrhythmic events in CPVT. Our idea is that if on one hand, diminishing the entry of Ca^{2+} into the mitochondria prevents excessive cellular oxidation, on the other hand, it limits the buffering function that the mitochondria have on the cytosolic Ca^{2+}, consequently increasing the cytosolic concentration of these ions that it is the main trigger of arrhythmic events in the context of CPVT.

Taken together, our experimental findings demonstrate that SR Ca^{2+} leak via RyR2 channels plays a crucial role in the pathophysiology of mitochondrial Ca^{2+} overload and dysfunction in CPVT. The different conditions observed in the baseline state and upon adrenergic activation show the phasic nature of these events, where an intense stimulus induces major changes that, over time, revert to the baseline condition.

Our work tackles the long-lasting question of whether mitochondria act as a calcium buffer or not [164] and whether this is a protective mechanism or a detrimental occurrence for the cell. We have finally demonstrated how, in our disease model, mitochondria do in fact uptake the excess of the ion that is released by the mutated RyR.

In this study, it was possible to characterize the role of mitochondria in the physiopathology in CPVT. Besides reporting their calcium-buffering role, we characterized the molecular/metabolical changes this role induces in their physiology.

Mitochondria, in fact, implement a series of pathways that enable the organelle to not be damaged by the excess calcium that is known to be dangerous for the cell. It is a mechanism developed in order to cope with the molecular manifestation of CPVT that renders the excessive calcium nontoxic and therefore not able to severely impair mitochondrial function.

Mitochondria, while acting as calcium buffers, are not unbalanced by the entrance of excess ions, in fact, they develop a coping mechanism that allows them to not be terminally damaged, both in the baseline condition and in the adrenergically stimulated one. Upon adrenergic activation, we see that the effect on mitochondrial physiology is greater but also not so severe as to induce mitochondrial death or long-lasting detrimental consequences (such as calcium overload).

Our data of mild mitochondrial alteration is consistent with what is observed in the clinics, since of all the CPVT patients present in our group's database (over 250), none of them has any substantial mitochondrial dysfunction.

What we discovered in our model of dominant CPVT we can expect to be able to replicate in different models of this disease, including also the recessive forms. We expect to do so since these pathways are connected to the underlying mechanism of the disease (meaning the abnormal release of calcium from the SR) and are not dependent on the specific mutation or protein involved.

References

1. Priori SG, Napolitano C, Memmi M, Colombi B, Drago F, Gasparini M, et al. Clinical and Molecular Characterization of Patients With Catecholaminergic Polymorphic Ventricular Tachycardia. Circulation. 2002;106:69–74.

2. Imberti JF, Underwood K, Mazzanti A, Priori SG. Clinical Challenges in Catecholaminergic Polymorphic Ventricular Tachycardia. Heart Lung Circ. 2016;25:777–83.

3. Lahat H, Pras E, Olender T, Avidan N, Ben-Asher E, Man O, et al. A Missense Mutation in a Highly Conserved Region of CASQ2 Is Associated with Autosomal Recessive Catecholamine-Induced Polymorphic Ventricular Tachycardia in Bedouin Families from Israel. The American Journal of Human Genetics. 2001;69:1378–84.

4. Lahat H, Eldar M, Levy-Nissenbaum E, Bahan T, Friedman E, Khoury A, et al. Autosomal Recessive Catecholamine- or Exercise-Induced Polymorphic Ventricular Tachycardia. Circulation. 2001;103:2822–7.

5. Saks V, Dzeja P, Schlattner U, Vendelin M, Terzic A, Wallimann T. Cardiac system bioenergetics: metabolic basis of the Frank-Starling law. J Physiol. 2006;571:253–73.

6. Bongianino R, Denegri M, Mazzanti A, Lodola F, Vollero A, Boncompagni S, et al. Allele-Specific Silencing of Mutant mRNA Rescues Ultrastructural and Arrhythmic Phenotype in Mice Carriers of the R4496C Mutation in the Ryanodine Receptor Gene (RYR2). Circ Res. 2017;121:525–36.

7. K SM, Fabiola W, Simon S, Lisa D, J DN, Qinghai T, et al. Suppression of Arrhythmia by Enhancing Mitochondrial Ca2+ Uptake in Catecholaminergic Ventricular Tachycardia Models. JACC Basic Transl Sci. 2017;2:737–47.

8. Castano Paolo, Artico Marco. Anatomia umana : principi. Edi. Ermes; 2005.

9. Castano Paolo, Artico Marco. Anatomia umana : principi. Edi. Ermes; 2005.

10. Hall JE, Hall ME, Guyton AC. Guyton and Hall textbook of Medical Physiology. 2021.

11. Perriard J-C, Hirschy A, Ehler E. Dilated cardiomyopathy: a disease of the intercalated disc? Trends Cardiovasc Med. 2003;13:30–8.

12. Perriard J-C, Hirschy A, Ehler E. Dilated cardiomyopathy: a disease of the intercalated disc? Trends Cardiovasc Med. 2003;13:30–8.

13. Gallicano GI, Kouklis P, Bauer C, Yin M, Vasioukhin V, Degenstein L, et al. Desmoplakin is required early in development for assembly of desmosomes and cytoskeletal linkage. J Cell Biol. 1998;143:2009–22.

14. Oosthoek PW, Viragh S, Lamers WH, Moorman AFM. Immunohistochemical delineation of the conduction system: II: The atrioventricular node and Purkinje fibers. Circ Res. 1993;73:482–91.

15. Keith A, Flack M. The Form and Nature of the Muscular Connections between the Primary Divisions of the Vertebrate Heart. J Anat Physiol. 1907;41 Pt 3:172–89.

16. Franzini-Armstrong C, Protasi F, Tijskens P. The assembly of calcium release units in cardiac muscle. In: Annals of the New York Academy of Sciences. New York Academy of Sciences; 2005. p. 76–85.

17. Joseph Feher. Quantitative Human Physiology An Introduction Book. Second Edition. 2017.

18. D. A. Eisner JLCKK and AWT. Calcium and Excitation-Contraction Coupling in the Heart. Circ Res. 2017.

19. D. M. Bers. Cardiac excitation-contraction coupling. Nature. 2002;415:198–205.

20. Stern MD, Pizarro G, Ríos E. Local control model of excitation-contraction coupling in skeletal muscle. Journal of General Physiology. 1997;110:415–40.

21. Ríos E, Stern MD. Calcium in close quarters: microdomain feedback in excitation-contraction coupling and other cell biological phenomena. Annu Rev Biophys Biomol Struct. 1997;26:47–82.

22. Sommer JR. The anatomy of the sarcoplasmic reticulum in vertebrate skeletal muscle: its implications for excitation contraction coupling. Z Naturforsch [c]. 1982;37:665–78.

23. Takeshima H, Nishimura S, Matsumoto T, Ishida H, Kangawa K, Minamino N, et al. Primary structure and expression from complementary DNA of skeletal muscle ryanodine receptor. Nature. 1989;339:439–45.

24. Hakamata Y, Nakai J, Takeshima H, Imoto K. Primary structure and distribution of a novel ryanodine receptor/calcium release channel from rabbit brain. FEBS Lett. 1992;312:229–35.

25. Efremov RG, Leitner A, Aebersold R, Raunser S. Architecture and conformational switch mechanism of the ryanodine receptor. 2014. https://doi.org/10.1038/nature13916.

26. Swan H, Piippo K, Viitasalo M, Heikkilä P, Paavonen T, Kainulainen K, et al. Arrhythmic disorder mapped to chromosome 1q42-q43 causes malignant polymorphic ventricular tachycardia in structurally normal hearts. J Am Coll Cardiol. 1999;34:2035–42.

27. Dhindwal S, Lobo J, Cabra V, Santiago DJ, Nayak AR, Dryden K, et al. A cryo-EM-based model of phosphorylation- and FKBP12.6-mediated allosterism of the cardiac ryanodine receptor. Sci Signal. 2017;10.

28. Meissner G. Regulation of mammalian ryanodine receptors. Front Biosci. 2002;7:d2072--d2080.

29. Priori SG, Blomström-Lundqvist C, Mazzanti A. 2015 ESC Guidelines for the management of patients with ventricular arrhythmias and the prevention of sudden cardiac death. Eur Heart J. 2015;8:746–837.

30. Eisner DA, Caldwell JL, Kistamás K, Trafford AW. Calcium and Excitation-Contraction Coupling in the Heart. Circ Res. 2017. https://doi.org/10.1161/CIRCRESAHA.117.310230.

31. Marx SO, Reiken S, Hisamatsu Y, Jayaraman T, Burkhoff D, Rosemblit N, et al. PKA phosphorylation dissociates FKBP12.6 from the calcium release channel (ryanodine receptor): Defective regulation in failing hearts. Cell. 2000;101:365–76.

32. Lehnart SE, Wehrens XHT, Marks AR. Calstabin deficiency, ryanodine receptors, and sudden cardiac death. Biochem Biophys Res Commun. 2004;322:1267–79.

33. Wehrens XHT, Lehnart SE, Huang F, Vest JA, Reiken SR, Mohler PJ, et al. FKBP12.6 deficiency and defective calcium release channel (ryanodine receptor) function linked to exercise-induced sudden cardiac death. Cell. 2003;113:829–40.

34. Ikemoto N, Bhatnagar GM, Nagy B, Gergely J. Interaction of Divalent Cations with the 55,000-Dalton Protein Component of the Sarcoplasmic Reticulum: STUDIES OF

FLUORESCENCE AND CIRCULAR DICHROISM. Journal of Biological Chemistry. 1972;247:7835–7.

35. Volpe P, Martini A, Furlan S, Meldolesi J. Calsequestrin is a component of smooth muscles: the skeletal- and cardiac-muscle isoforms are both present, although in highly variable amounts and ratios. Biochemical Journal. 1994;301:465–9.

36. Biral D, Volpe P, Damiani E, Margreth A. Coexistence of two calsequestrin isoforms in rabbit slow-twitch skeletal muscle fibers. FEBS Lett. 1992;299:175–8.

37. Jones LR, Suzuki YJ, Wang W, Kobayashi YM, Ramesh V, Franzini-Armstrong C, et al. Regulation of Ca2+ signaling in transgenic mouse cardiac myocytes overexpressing calsequestrin. Journal of Clinical Investigation. 1998;101:1385–93.

38. Wang S, Trumble WR, Liao H, Wesson CR, Dunker AK, Kang C. Crystal structure of calsequestrin from rabbit skeletal muscle sarcoplasmic reticulum. Nat Struct Biol. 1998;5:476–83.

39. Ikemoto N, Antoniu B, Kang JJ, Meszaros LG, Ronjat M. Intravesicular calcium transient during calcium release from sarcoplasmic reticulum. Biochemistry. 1991;30:5230–7.

40. O'Brian JJ, Ram ML, Kiarash A, Cala SE. Mass spectrometry of cardiac calsequestrin characterizes microheterogeneity unique to heart and indicative of complex intracellular transit. J Biol Chem. 2002;277:37154–60.

41. Zhang L, Kelley J, Schmeisser G, Kobayashi YM, Jones LR. Complex Formation between Junctin, Triadin, Calsequestrin, and the Ryanodine Receptor. Journal of Biological Chemistry. 1997;272:23389–97.

42. Furukawa Y, Wallick DW, Martin PJ, Levy MN. Chronotropic and dromotropic responses to stimulation of intracardiac sympathetic nerves to sinoatrial or atrioventricular nodal region in anesthetized dogs. Circ Res. 1990;66:1391–9.

43. Levy MN. Cardiac sympathetic-parasympathetic interactions. Fed Proc. 1984;43:2598–602.

44. Santana LF, Cheng EP, Lederer WJ. How does the shape of the cardiac action potential control calcium signaling and contraction in the heart? Journal of Molecular and Cellular Cardiology. 2010;49:901–3.

45. Marban E, Kusuoka H, Yue DT, Weisfeldt ML, Wier WG. Maximal Ca2+-activated force elicited by tetanization of ferret papillary muscle and whole heart: mechanism and characteristics of steady contractile activation in intact myocardium. Circ Res. 1986;59:262–9.

46. di Barletta MR, Viatchenko-Karpinski S, Nori A, Memmi M, Terentyev D, Turcato F, et al. Clinical Phenotype and Functional Characterization of CASQ2 Mutations Associated With Catecholaminergic Polymorphic Ventricular Tachycardia. Circulation. 2006;114:1012–9.

47. Martin WF, Garg S, Zimorski V. Endosymbiotic theories for eukaryote origin. Phil Trans R Soc B. 2015;370:20140330.

48. Reichert AS, Neupert W. Contact sites between the outer and inner membrane of mitochondria-role in protein transport.

49. Siegmund SE, Grassucci R, Carter SD, Barca E, Farino ZJ, Juanola-Falgarona M, et al. Three-Dimensional Analysis of Mitochondrial Crista Ultrastructure in a Patient with Leigh Syndrome by In Situ Cryoelectron Tomography. iScience. 2018;6:83–91.

50. Mannella CA, Lederer WJ, Jafri MS. The connection between inner membrane topology and mitochondrial function. Journal of Molecular and Cellular Cardiology. 2013;62:51–7.

51. Kasahara A, Cipolat S, Chen Y, Dorn GW, Scorrano L. Mitochondrial fusion directs cardiomyocyte differentiation via calcineurin and notch signaling. Science (1979). 2013;342:734–7.

52. Sun N, Finkel T. Cardiac mitochondria: A surprise about size. Journal of Molecular and Cellular Cardiology. 2015;82:213–5.

53. Taegtmeyer H, de Villalobos D. Metabolic support for the postischaemic heart. The Lancet. 1995;345:1552–5.

54. Lopaschuk GD, Ussher JR, Folmes CDL, Jaswal JS, Stanley WC. Myocardial Fatty Acid Metabolism in Health and Disease. Physiol Rev. 2010;90:207–58.

55. Lemieux H, Hoppel CL. Mitochondria in the human heart. J Bioenerg Biomembr. 2009;41:99–106.

56. Elrod JW, Wong R, Mishra S, Vagnozzi RJ, Sakthievel B, Goonasekera SA, et al. Cyclophilin D controls mitochondrial pore–dependent Ca2+ exchange, metabolic flexibility, and propensity for heart failure in mice. J Clin Invest. 2010;120:3680–7.

57. Manninen AH. Metabolic Effects of the Very-Low-Carbohydrate Diets: Misunderstood "Villains" of Human Metabolism. J Int Soc Sports Nutr. 2004;1:7.

58. BRINKMANN JFF, ABUMRAD NA, IBRAHIMI A, vanderVUSSE GJ, GLATZ JFC. New insights into long-chain fatty acid uptake by heart muscle: a crucial role for fatty acid translocase/CD36. Biochemical Journal. 2002;367:561–70.

59. Heinrich T. Metabolism—the lost child of cardiology∗. J Am Coll Cardiol. 2000;36:1386–8.

60. Hoeks J, van Baak MA, Hesselink MKC, Hul GB, Vidal H, Saris WHM, et al. Effect of β1- and β2-adrenergic stimulation on energy expenditure, substrate oxidation, and UCP3 expression in humans. American Journal of Physiology-Endocrinology and Metabolism. 2003;285:E775–82.

61. Nevzorova J, Evans BA, Bengtsson T, Summers RJ. Multiple signalling pathways involved in β2-adrenoceptor-mediated glucose uptake in rat skeletal muscle cells. Br J Pharmacol. 2006;147:446–54.

62. Carafoli E. The interplay of mitochondria with calcium: An historical appraisal. Cell Calcium. 2012;52:1–8.

63. Berridge MJ, Lipp P, Bootman MD. The versatility and universality of calcium signalling. Nature Reviews Molecular Cell Biology. 2000;1:11–21.

64. Rapizzi E, Pinton P, Szabadkai G, Wieckowski MR, Vandecasteele G, Baird G, et al. Recombinant expression of the voltage-dependent anion channel enhances the transfer of Ca2+ microdomains to mitochondria. Journal of Cell Biology. 2002;159:613–24.

65. Kirichok Y, Krapivinsky G, Clapham DE. The mitochondrial calcium uniporter is a highly selective ion channel. Nature. 2004;427:360–4.

66. Finkel T, Menazza S, Holmström KM, Parks RJ, Liu J, Sun J, et al. The ins and outs of mitochondrial calcium. Circulation Research. 2015;116:1810–9.

67. Bravo-Sagua R, Parra V, López-Crisosto C, Díaz P, Quest AFG, Lavandero S. Calcium transport and signaling in mitochondria. Compr Physiol. 2017;7:623–34.

68. Yu F, Abdelwahid E, Xu T, Hu L, Wang M, Li Y, et al. The role of mitochondrial fusion and fission in the process of cardiac oxidative stress. Histol Histopathol. 2020;35:541–52.

69. Colombini M. The VDAC channel: Molecular basis for selectivity. Biochim Biophys Acta Mol Cell Res. 2016;1863:2498–502.

70. Kayser H, Kratzin HD, Thinnes FP, Götz H, Schmidt WE, Eckart K, et al. [Identification of human porins. II. Characterization and primary structure of a 31-lDa porin from human B lymphocytes (Porin 31HL)]. Biol Chem Hoppe Seyler. 1989;370:1265–78.

71. De Pinto V, Messina A, Lane DJR, Lawen A. Voltage-dependent anion-selective channel (VDAC) in the plasma membrane. FEBS Lett. 2010;584:1793–9.

72. Sampson MJ, Lovell RS, Craigen WJ. The murine voltage-dependent anion channel gene family. Conserved structure and function. Journal of Biological Chemistry. 1997;272:18966–73.

73. de Stefani D, Bononi A, Romagnoli A, Messina A, de Pinto V, Pinton P, et al. VDAC1 selectively transfers apoptotic Ca2+ signals to mitochondria. Cell Death Differ. 2012;19:267–73.

74. Schredelseker J, Paz A, López CJ, Altenbach C, Leung CS, Drexler MK, et al. High resolution structure and double electron-electron resonance of the zebrafish voltage-dependent anion channel 2 reveal an oligomeric population. Journal of Biological Chemistry. 2014;289:12566–77.

75. Shoshan-Barmatz V, De Pinto V, Zweckstetter M, Raviv Z, Keinan N, Arbel N. VDAC, a multi-functional mitochondrial protein regulating cell life and death. Molecular Aspects of Medicine. 2010;31:227–85.

76. Maurya SR, Mahalakshmi R. Mitochondrial VDAC2 and cell homeostasis: highlighting hidden structural features and unique functionalities. Biological Reviews. 2017;92:1843–58.

77. Min CK, Yeom DR, Lee KE, Kwon HK, Kang M, Kim YS, et al. Coupling of ryanodine receptor 2 and voltage-dependent anion channel 2 is essential for Ca2+ transfer from the sarcoplasmic reticulum to the mitochondria in the heart. Biochemical Journal. 2012;447:371–9.

78. Zhuo W, Zhou H, Guo R, Yi J, Zhang L, Yu L, et al. Structure of intact human MCU supercomplex with the auxiliary MICU subunits. Protein and Cell. 2021;12:220–9.

79. Fan M, Zhang J, Tsai C-W, Orlando BJ, Rodriguez M, Xu Y, et al. Structure and mechanism of the mitochondrial Ca 2+ uniporter holocomplex. Nature |. 2020;582:129.

80. Gambardella J, Sorriento D, Ciccarelli M, del Giudice C, Fiordelisi A, Napolitano L, et al. Functional role of mitochondria in arrhythmogenesis. In: Advances in Experimental Medicine and Biology. Springer New York LLC; 2017. p. 191–202.

81. Imberti JF, Underwood K, Mazzanti A, Priori SG. Clinical Challenges in Catecholaminergic Polymorphic Ventricular Tachycardia. 2016. https://doi.org/10.1016/j.hlc.2016.01.012.

82. Saks V, Dzeja P, Schlattner U, Vendelin M, Terzic A, Wallimann T. Cardiac system bioenergetics: metabolic basis of the Frank-Starling law. J Physiol. 2006;571 Pt 2:253–73.

83. Priori SG, Napolitano C, Tiso N, Memmi M, Vignati G, Bloise R, et al. Mutations in the cardiac ryanodine receptor gene (hRyR2) underlie catecholaminergic polymorphic ventricular tachycardia. Circulation. 2001;103:196–200.

84. Györke I, Hester N, Jones LR, Györke S. The Role of Calsequestrin, Triadin, and Junctin Conferring Cardiac Ryanodine Receptor Responsiveness to Luminal Calcium. Biophys J. 2004;86:2121–8.

85. Lahat H, Eldar M, Levy-Nissenbaum E, Bahan T, Friedman E, Khoury A, et al. Autosomal recessive catecholamine- or exercise-induced polymorphic ventricular tachycardia: Clinical features and assignment of the disease gene to chromosome 1p13-21. Circulation. 2001;103:2822–7.

86. Lahat H, Pras E, Olender T, Avidan N, Ben-Asher E, Man O, et al. A missense mutation in a highly conserved region of CASQ2 is associated with autosomal recessive catecholamine-induced polymorphic ventricular tachycardia in Bedouin families from Israel. Am J Hum Genet. 2001;69:1378–84.

87. Venetucci L, Denegri M, Napolitano C, Priori SG. Inherited calcium channelopathies in the pathophysiology of arrhythmias. Nature Reviews Cardiology. 2012;9:561–75.

88. Jiang D, Xiao B, Yang D, Wang R, Choi P, Zhang L, et al. RyR2 mutations linked to ventricular tachycardia and sudden death reduce the threshold for store-overload-induced Ca2+ release (SOICR). Proc Natl Acad Sci U S A. 2004;101:13062–7.

89. Jiang D, Wang R, Xiao B, Kong H, Hunt DJ, Choi P, et al. Enhanced store overload-induced Ca2+ release and channel sensitivity to luminal Ca2+ activation are common defects of RyR2 mutations linked to ventricular tachycardia and sudden death. Circ Res. 2005;97:1173–81.

90. Yamamoto T, Yano M, Xu X, Uchinoumi H, Tateishi H, Mochizuki M, et al. Identification of target domains of the cardiac ryanodine receptor to correct channel disorder in failing hearts. Circulation. 2008;117:762–72.

91. Valle G, Arad M, Volpe P. Molecular adaptation to calsequestrin 2 (CASQ2) point mutations leading to catecholaminergic polymorphic ventricular tachycardia (CPVT): comparative analysis of R33Q and D307H mutants. J Muscle Res Cell Motil. 2020. https://doi.org/10.1007/s10974-020-09587-2.

92. Priori SG, Chen SRW. Inherited dysfunction of sarcoplasmic reticulum Ca2+ handling and arrhythmogenesis. Circulation Research. 2011;108:871–83.

93. Jiang D, Xiao B, Yang D, Wang R, Choi P, Zhang L, et al. RyR2 mutations linked to ventricular tachycardia and sudden death reduce the threshold for store-overload-induced Ca2+ release (SOICR). Proc Natl Acad Sci U S A. 2004;101:13062–7.

94. Bongianino R, Priori SG. Gene therapy to treat cardiac arrhythmias. Nature Publishing Group. 2015;12:531–46.

95. Bongianino R, Priori SG. Gene therapy to treat cardiac arrhythmias. Nature Publishing Group. 2015;12:531–46.

96. Nyegaard M, Overgaard MT, Sondergaard MT, Vranas M, Behr ER, Hildebrandt LL, et al. Mutations in calmodulin cause ventricular tachycardia and sudden cardiac death. Am J Hum Genet. 2012;91:703–12.

97. Roux-buisson N, Cacheux M, Fourest-lieuvin A, Fauconnier J, Brocard J, Denjoy I, et al. Absence of triadin, a protein of the calcium release complex, is responsible for cardiac arrhythmia with sudden death in human. Hum Mol Genet. 2012;21:2759–67.

98. Rooryck C, Kyndt F, Bozon D, Roux-Buisson N, Sacher F, Probst V, et al. New Family with Catecholaminergic Polymorphic Ventricular Tachycardia Linked to the Triadin Gene. J Cardiovasc Electrophysiol. 2015;26:1146–50.

99. Cacheux M, Fauconnier J, Thireau J, Osseni A, Brocard J, Roux-Buisson N, et al. Interplay between Triadin and Calsequestrin in the Pathogenesis of CPVT in the Mouse. Molecular Therapy. 2019;28.

100. Knollmann BC, Chopra N, Hlaing T, Akin B, Yang T, Ettensohn K, et al. Casq2 deletion causes sarcoplasmic reticulum volume increase, premature Ca2+ release, and catecholaminergic polymorphic ventricular tachycardia. Journal of Clinical Investigation. 2006;116:2510–20.

101. Kalscheur MM, Vaidyanathan R, Orland KM, Abozeid S, Fabry N, Maginot KR, et al. KCNJ2 mutation causes an adrenergic-dependent rectification abnormality with calcium sensitivity and ventricular arrhythmia. Heart Rhythm. 2014;11:885–94.

102. Devalla HD, Gélinas R, Aburawi EH, Beqqali A, Goyette P, Freund C, et al. TECRL , a new life-threatening inherited arrhythmia gene associated with overlapping clinical features of both LQTS and CPVT . EMBO Mol Med. 2016;8:1390–408.

103. Kalscheur MM, Vaidyanathan R, Orland KM, Abozeid S, Fabry N, Maginot KR, et al. KCNJ2 mutation causes an adrenergic-dependent rectification abnormality with calcium sensitivity and ventricular arrhythmia. Heart Rhythm. 2014;11:885–94.

104. Devalla HD, Gélinas R, Aburawi EH, Beqqali A, Goyette P, Freund C, et al. TECRL , a new life-threatening inherited arrhythmia gene associated with overlapping clinical features of both LQTS and CPVT . EMBO Mol Med. 2016;8:1390–408.

105. Priori SG, Napolitano C, Memmi M, Colombi B, Drago F, Gasparini M, et al. Clinical and molecular characterization of patients with catecholaminergic polymorphic ventricular tachycardia. Circulation. 2002;106:69–74.

106. Hayashi M, Denjoy I, Extramiana F, Maltret A, Buisson NR, Lupoglazoff JM, et al. Incidence and risk factors of arrhythmic events in catecholaminergic polymorphic ventricular tachycardia. Circulation. 2009;119:2426–34.

107. Cerrone M, Colombi B, Santoro M, Raffale di Barletta M, Scelsi M, Villani L, et al. Bidirectional Ventricular Tachycardia and Fibrillation Elicited in a Knock-In Mouse Model Carrier of a Mutation in the Cardiac Ryanodine Receptor (RyR2). Circ Res. 2005;96:e77--e82.

108. Lahat H, Eldar M, Levy-Nissenbaum E, Bahan T, Friedman E, Khoury A, et al. Autosomal recessive catecholamine- or exercise-induced polymorphic ventricular tachycardia: Clinical features and assignment of the disease gene to chromosome 1p13-21. Circulation. 2001;103:2822–7.

109. Reid DS, Tynan M, Braidwood L, Fitzgerald GR. Bidirectional tachycardia in a child. A study using His bundle electrography. Br Heart J. 1975;37:339–44.

110. Leenhardt A, Lucet V, Denjoy I, Grau F. Catecholaminergic polymorphic ventricular tachycardia in children. A 7-year follow-up of 21 patients. Circulation. 1995;:1512–9.

111. Priori SG, Blomström-Lundqvist C, Mazzanti A. 2015 ESC Guidelines for the management of patients with ventricular arrhythmias and the prevention of sudden cardiac death. Eur Heart J. 2015;8:746–837.

112. Ruan Y, Liu N, Napolitano C, Priori SG. Therapeutic Strategies for Long-QT Syndrome: Does the Molecular Substrate Matter? Circ Arrhythm Electrophysiol. 2008;1:290–7.

113. Priori SG, Napolitano C, Memmi M, Colombi B, Drago F, Gasparini M, et al. Clinical and molecular characterization of patients with catecholaminergic polymorphic ventricular tachycardia. Circulation. 2002;106:69–74.

114. Sumitomo N, Harada K, Nagashima M, Yasuda T, Nakamura Y, Aragaki Y, et al. Catecholaminergic polymorphic ventricular tachycardia: Electrocardiographic characteristics and optimal therapeutic strategies to prevent sudden death. Heart. 2003;89:66–70.

115. Hasdemir C, Priori SG, Overholt E, Lazzara R. Catecholaminergic polymorphic ventricular tachycardia, recurrent syncope, and implantable loop recorder. J Cardiovasc Electrophysiol. 2004;15:729.

116. Ruan Y, Liu N, Napolitano C, Priori SG. Therapeutic Strategies for Long-QT Syndrome: Does the Molecular Substrate Matter? Circ Arrhythm Electrophysiol. 2008;1:290–7.

117. Leenhardt A, Lucet V, Denjoy I, Grau F. Catecholaminergic polymorphic ventricular tachycardia in children. A 7-year follow-up of 21 patients. Circulation. 1995;:1512–9.

118. Rosen MR, Danilo P. Effects of tetrodotoxin, lidocaine, verapamil, and AHR-2666 on ouabain-induced delayed afterdepolarizations in canine purkinje fibers. Circ Res. 1980;46:117–24.

119. Liu N, Napolitano C, Venetucci LA, Priori SG. Flecainide and Antiarrhythmic Effects in a Mouse Model of Catecholaminergic Polymorphic Ventricular Tachycardia. Trends Cardiovasc Med. 2012;22:35–9.

120. Amoni M, Dries E, Ingelaere S, Vermoortele D, Roderick HL, Claus P, et al. cells Ventricular Arrhythmias in Ischemic Cardiomyopathy-New Avenues for Mechanism-Guided Treatment. 2021. https://doi.org/10.3390/cells10102629.

121. Sumitomo N, Harada K, Nagashima M, Yasuda T, Nakamura Y, Aragaki Y, et al. Catecholaminergic polymorphic ventricular tachycardia: Electrocardiographic characteristics and optimal therapeutic strategies to prevent sudden death. Heart. 2003;89:66–70.

122. Swan H, Laitinen P, Kontula K, Toivonen L. Calcium channel antagonism reduces exercise-induced ventricular arrhythmias in catecholaminergic polymorphic ventricular tachycardia patients with RyR2 mutations. J Cardiovasc Electrophysiol. 2005;16:162–6.

123. Wilde A a M, Bhuiyan Z a, Crotti L, Facchini M, De Ferrari GM, Paul T, et al. Left cardiac sympathetic denervation for catecholaminergic polymorphic ventricular tachycardia. N Engl J Med. 2008;358:2024–9.

124. Boncompagni S, Rossi AE, Micaroni M, Beznoussenko G v, Polishchuk RS, Dirksen RT, et al. Mitochondria Are Linked to Calcium Stores in Striated Muscle by Developmentally Regulated Tethering Structures. Mol Biol Cell. 2008;20:1058–67.

125. Boncompagni S, Rossi AE, Micaroni M, Hamilton SL, Dirksen RT, Franzini-Armstrong C, et al. Characterization and temporal development of cores in a mouse model of malignant hyperthermia. Proceedings of the National Academy of Sciences. 2009;106:21996–2001.

126. Ferrantini C, Coppini R, Scellini B, Ferrara C, Pioner JM, Mazzoni L, et al. R4496C RyR2 mutation impairs atrial and ventricular contractility. Journal of General Physiology. 2015;147:39–52.

127. Bers DM. Cardiac excitation–contraction coupling. Nature. 2002;415:198–205.

128. Murphy DB, Davidson MW. Fundamentals of Light Microscopy and Electronic Imaging. Hoboken, NJ, USA: John Wiley & Sons, Inc.; 2012.

129. Bongianino R, Denegri M, Mazzanti A, Lodola F, Vollero A, Boncompagni S, et al. Allele-specific silencing of mutant mRNA rescues ultrastructural and arrhythmic phenotype in mice carriers of the R4496C mutation in the ryanodine receptor gene (RYR2). Circ Res. 2017;121:525–36.

130. Liu N, Ruan Y, Denegri M, Bachetti T, Li Y, Colombi B, et al. Calmodulin kinase II inhibition prevents arrhythmias in RyR2R4496C+/− mice with catecholaminergic polymorphic ventricular tachycardia. J Mol Cell Cardiol. 2011;50:214–22.

131. Goldberg IJ, Trent CM, Schulze PC. Lipid Metabolism and Toxicity in the Heart. Cell Metab. 2012;15:805–12.

132. di Lisa F, Blank PS, Colonna R, Gambassi G, Silverman HS, Stern MD, et al. Mitochondrial membrane potential in single living adult rat cardiac myocytes exposed to anoxia or metabolic inhibition. J Physiol. 1995;486:1–13.

133. Greenawalt JW, Rossi CS, Lehninger AL. EFFECT OF ACTIVE ACCUMULATION OF CALCIUM AND PHOSPHATE IONS ON THE STRUCTURE OF RAT LIVER MITOCHONDRIA. Journal of Cell Biology. 1964;23:21–38.

134. Hernansanz-Agustín P, Choya-Foces C, Carregal-Romero S, Ramos E, Oliva T, Villa-Piña T, et al. Na+ controls hypoxic signalling by the mitochondrial respiratory chain. Nature. 2020;586:287–91.

135. Assali EA, Jones AE, Veliova M, Acín-Pérez R, Taha M, Miller N, et al. NCLX prevents cell death during adrenergic activation of the brown adipose tissue. Nat Commun. 2020;11:3347.

136. Hamilton S, Terentyeva R, Martin B, Perger F, Li J, Stepanov A, et al. Increased RyR2 activity is exacerbated by calcium leak-induced mitochondrial ROS. Basic Res Cardiol. 2020;115:38.

137. Camille Dejos DG and ARC. The Two-Way Relationship Between Calcium and Metabolism in Cancer. Front Cell Dev Biol. 2020;8.

138. King TE. Preparation of succinate dehydrogenase and reconstitution of succinate oxidase. In: Methods in Enzymology. Academic Press; 1967. p. 322–31.

139. Goldberg IJ, Reue K, Abumrad NA, Bickel PE, Cohen S, Fisher EA, et al. Deciphering the Role of Lipid Droplets in Cardiovascular Disease. Circulation. 2018;138:305–15.

140. Nan J, Zhu W, Rahman MS, Liu M, Li D, Su S, et al. Molecular regulation of mitochondrial dynamics in cardiac disease. Biochimica et Biophysica Acta (BBA) - Molecular Cell Research. 2017;1864:1260–73.

141. Barba I, Chavarria L, Ruiz-Meana M, Mirabet M, Agulló E, Garcia-Dorado D. Effect of intracellular lipid droplets on cytosolic Ca2+ and cell death during ischaemia–reperfusion injury in cardiomyocytes. J Physiol. 2009;587:1331–41.

142. Readnower RD, Brainard RE, Hill BG, Jones SP. Standardized bioenergetic profiling of adult mouse cardiomyocytes. Physiol Genomics. 2012;44:1208–13.

143. Tran DH, Wang Z v. Glucose Metabolism in Cardiac Hypertrophy and Heart Failure. J Am Heart Assoc. 2019;8:e012673.

144. Yang Y-L, Li J, Liu K, Zhang L, Liu Q, Liu B, et al. Ginsenoside Rg5 increases cardiomyocyte resistance to ischemic injury through regulation of mitochondrial hexokinase-II and dynamin-related protein 1. Cell Death Dis. 2017;8:e2625–e2625.

145. Zhou L, Huang H, Yuan CL, Keung W, Lopaschuk GD, Stanley WC. Metabolic response to an acute jump in cardiac workload: effects on malonyl-CoA, mechanical efficiency, and fatty acid oxidation. American Journal of Physiology-Heart and Circulatory Physiology. 2008;294:H954–60.

146. Page E, McCallister LP. Quantitative electron microscopic description of heart muscle cells. Application to normal, hypertrophied and thyroxin-stimulated hearts. Am J Cardiol. 1973;31:172–81.

147. Mammucari C, Raffaello A, Vecellio Reane D, Gherardi G, de Mario A, Rizzuto R. Mitochondrial calcium uptake in organ physiology: from molecular mechanism to animal models. Pflugers Archiv European Journal of Physiology. 2018;470:1165–79.

148. Priori SG, Mazzanti A, Santiago DJ, Kukavica D, Trancuccio A, Kovacic JC. Precision Medicine in Catecholaminergic Polymorphic Ventricular Tachycardia: JACC Focus Seminar 5/5. J Am Coll Cardiol. 2021;77:2592–612.

149. Bovo E, Lipsius SL, Zima A v. Reactive oxygen species contribute to the development of arrhythmogenic Ca^{2+} waves during β-adrenergic receptor stimulation in rabbit cardiomyocytes. J Physiol. 2012;590:3291–304.

150. Bertero E, Maack C. Calcium Signaling and Reactive Oxygen Species in Mitochondria. Circ Res. 2018;122:1460–78.

151. Brookes PS, Yoon Y, Robotham JL, Anders MW, Sheu S-S. Calcium, ATP, and ROS: a mitochondrial love-hate triangle. American Journal of Physiology-Cell Physiology. 2004;287:C817–33.

152. Forkink M, Manjeri GR, Liemburg-Apers DC, Nibbeling E, Blanchard M, Wojtala A, et al. Mitochondrial hyperpolarization during chronic complex I inhibition is sustained by low activity of complex II, III, IV and V. Biochimica et Biophysica Acta (BBA) - Bioenergetics. 2014;1837:1247–56.

153. Dzeja PP, Holmuhamedov EL, Ozcan C, Pucar D, Jahangir A, Terzic A. Mitochondria. Circ Res. 2001;89:744–6.

154. Hernansanz-Agustín P, Enríquez JA. Generation of Reactive Oxygen Species by Mitochondria. Antioxidants. 2021;10.

155. Assali EA, Jones AE, Veliova M, Acín-Pérez R, Taha M, Miller N, et al. NCLX prevents cell death during adrenergic activation of the brown adipose tissue. Nat Commun. 2020;11:3347.

156. Bo T, Yamamori T, Suzuki M, Sakai Y, Yamamoto K, Inanami O. Calmodulin-dependent protein kinase II (CaMKII) mediates radiation-induced mitochondrial fission

by regulating the phosphorylation of dynamin-related protein 1 (Drp1) at serine 616. Biochem Biophys Res Commun. 2018;495:1601–7.

157. Dewenter M, von der Lieth A, Katus HA, Backs J. Calcium Signaling and Transcriptional Regulation in Cardiomyocytes. Circ Res. 2017;121:1000–20.

158. Filadi R, Greotti E, Turacchio G, Luini A, Pozzan T, Pizzo P. Mitofusin 2 ablation increases endoplasmic reticulum–mitochondria coupling. Proceedings of the National Academy of Sciences. 2015;112:E2174–81.

159. Michele Ciccarelli GSVPBT and GI. Adrenergic receptors and metabolism: role in development of cardiovascular disease. Front Physiol. 2013;4.

160. Zhou L, Huang H, Yuan CL, Keung W, Lopaschuk GD, Stanley WC. Metabolic response to an acute jump in cardiac workload: effects on malonyl-CoA, mechanical efficiency, and fatty acid oxidation. American Journal of Physiology-Heart and Circulatory Physiology. 2008;294:H954–60.

161. Nikolaidis LA, Hentosz T, Doverspike A, Huerbin R, Stolarski C, Shen Y-T, et al. Catecholamine stimulation is associated with impaired myocardial O2 utilization in heart failure. Cardiovasc Res. 2002;53:392–404.

162. Liu T, O'Rourke B. Regulation of mitochondrial Ca2+ and its effects on energetics and redox balance in normal and failing heart. J Bioenerg Biomembr. 2009;41:127–32.

163. Cooper LL, Li W, Lu Y, Centracchio J, Terentyeva R, Koren G, et al. Redox modification of ryanodine receptors by mitochondria-derived reactive oxygen species contributes to aberrant Ca2+ handling in ageing rabbit hearts. J Physiol. 2013;591:5895–911.

164. Williams GSB, Boyman L, Chikando AC, Khairallah RJ, Lederer WJ. Mitochondrial calcium uptake. Proceedings of the National Academy of Sciences. 2013;110:10479–86.